UTILIZATION OF CARBIDE LIME FOR THE SYNTHESIS OF HYDROXYAPETITE AND STUDY OF ITS BIOCOMPATIBILITY

Thesis Submitted for the Award of the Degree of

DOCTOR OF PHILOSOPHY

in

Biotechnology

By

Navneet Kaur

Registration Number: 12014137

Supervised By

Dr. Anjuvan Singh (15950)

Department of Biotechnology (Professor)

Lovely Professional University

LOVELY PROFESSIONAL UNIVERSITY, PUNJAB
2026

DECLARATION

I, hereby declared that the presented work in the thesis entitled **"Utilization of Carbide Lime for the Synthesis of Hydroxyapatite and Study of its Biocompatibility"** in fulfillment of degree of **Doctor of Philosophy (Ph. D.)** is outcome of research work carried out by me under the supervision of **Dr. Anjuvan Singh**, working as Professor in the Department of Biotechnology, school Bioengineering & Biosciences of **Lovely Professional University, Punjab, India**. In keeping with general practice of reporting scientific observations, due acknowledgements have been made whenever work described here has been based on findings of other investigator. This work has not been submitted in part or full to any other University or Institute for the award of any degree.

(Signature of scholar)

Name of the scholar: Navneet Kaur

Registration No: 12014137

Department/School: Biotechnology/ Bioengineering & Biosciences

University: Lovely Professional University, Phagwara, Punjab, INDIA

CERTIFICATE

This is to certify that the work reported in the Ph. D. thesis entitled **"Utilization of Carbide Lime for the Synthesis of Hydroxyapatite and Study of its Biocompatibility"** submitted in fulfillment of the requirement for the award of degree of **Doctor of Philosophy (Ph.D.)** in the Department of Biotechnology, School Bioengineering & Biosciences of **Lovely Professional University, Punjab, India**, is a research work carried out by **Navneet Kaur**, registration number **12014137**, is bonafide record of his/her original work carried out under my supervision and that no part of thesis has been submitted for any other degree, diploma or equivalent course.

(Signature of the supervisor)

Name of supervisor: Dr. Anjuvan Singh

Designation: Professor

Department/school:Biotechnology/ Bioengineering & Biosciences

University: Lovely Professional University, Phagwara, Punjab(INDIA)

Abstract

Industrial pollution is a rising concern, impacting the environment and human health through harmful emissions and waste. While traditional biomaterials are often expensive, transforming industrial waste into low-cost biomaterials offers a sustainable and economical solution. This approach helps reduce pollution, minimize waste, and promote eco-friendly practices. This research undertakes a detailed examination of a novel approach with the goal of developing cost-effective, nontoxic, biocompatible, and biodegradable biomaterials. Hydroxyapetite biomaterial synthesized from carbide lime, an industrial waste product of the acetylene industry. The study also focuses on enhancing the mechanical strength of the synthesized hydroxyapetite, aiming to improve their performance and suitability for a range of applications while promoting sustainability and waste reduction. Carbide lime, an industrial waste, is accumulating rapidly, and its detrimental impact on ecosystems and human health underscores the urgent need for a shift toward more environmentally sustainable alternatives. Carbide lime can be converted into a hydroxyapetite biomaterial suitable for use in biomedical applications. hydroxyapetite biomaterials have gained popularity in the biomedical field, and combining them with sintering additives could enhance their mechanical properties, making them more suitable for load bearing implantation. The primary aim of this study is to synthesize a hydroxyapetite biomaterial from carbide lime, an industrial byproduct of the acetylene industry, with enhanced mechanical properties. The synthesized hydroxyapetite will be suitable for implantation and will possess non-toxic, biocompatible, and biodegradable characteristics. The study starts with a comprehensive review of existing literature, offering an overview of the current use of industrial waste in biomaterial synthesis and exploring their potential for creating biomaterials suitable for load-bearing implants. This study examines the purification of calcium hydroxide, the main component of carbide lime, and the optimal weight percentage for adding sintering additives like aluminium oxide and titanium dioxide. Key factors such as mechanical strength, biocompatibility, toxicity, and biodegradability are also carefully considered. The literature review facilitated the selection of industrial waste materials, which was followed by the initiation of

the experimental section. Carbide lime, a byproduct of the acetylene industry, is used as the starting material for synthesizing hydroxyapetite due to its high calcium hydroxide content, which is the key component in hydroxyapetite synthesis. The high calcium hydroxide content in carbide lime has recently garnered significant interest for its potential use in synthesizing hydroxyapetite.

Initially, carbide lime, a byproduct of the acetylene industry and a primary source of calcium hydroxide, was extracted using the dilution method. The extracted calcium hydroxide was then purified by calcining it at 800°C for 2 hours to obtain calcium oxide, which served as a precursor for hydroxyapetite (HAp) synthesis. Finally, the wet chemical precipitation method was employed to synthesize hydroxyapetite (HAp) with a stoichiometric Ca/P ratio of 1.67. Subsequently, two sintering additives, aluminium oxide and titanium dioxide, were selected based on literature and optimized using the Taguchi L25 orthogonal array, with the weight percentage of hydroxyapetite (HAp) kept constant at 70%. The HAp and sintering additives were then mixed using steel balls through a mechanical method. Various ratios of aluminium oxide and titanium dioxide were mixed with HAp, maintaining the HAp constant at 70%, as follows: 20% aluminum oxide: 10% titanium dioxide; 22% aluminum oxide: 8% titanium dioxide; 24% aluminum oxide: 6% titanium dioxide; 26% aluminum oxide: 4% titanium dioxide; and 28% aluminum oxide: 2% titanium dioxide. These mixtures were then fabricated into pellets. All ratios were optimized using the Taguchi L25 orthogonal array, incorporating five different temperatures (900, 950, 1000, 1050, and 1100°C) and five varying time durations (1, 2, 3, 4, and 5 hours). The sintering process was performed to improve the mechanical strength of the biomaterial, and its biological activity was also assessed.

All samples, including carbide lime, calcium hydroxide, calcium oxide, and HAp, were extensively characterized using various techniques such as X-ray diffraction (XRD), Fourier-transform infrared spectroscopy (FTIR), Field Emission Scanning Electron Microscopy (FESEM), Dynamic Light Scattering (DLS), and Thermo gravimetric Analysis (TGA) to verify phase purity, morphology, chemical composition, and thermal stability.

he XRD analysis of HAp revealed distinct sharp peaks, confirming its crystalline structure, while the FTIR spectrum of HAp showed the presence of calcium and phosphate functional groups at the phosphate (PO_4^{3-}) peaks, which appear at 564 cm^{-1} and 600 cm^{-1}. Additionally, a band at 962 cm^{-1} indicates the out-of-plane bending of carbonate (CO_3^{2-}) groups, indicating the successful synthesis of HAp from carbide lime.

The addition of sintering additives enhanced the mechanical strength of hydroxyapetite while maintaining controlled porosity, achieved through the sintering process. Sintering kinetics was used to analyze the material's densification behavior and porosity under different temperatures (900-1100°C) and time conditions (1, 2, 3, 4, 5 hours). The evolution of porosity and bulk density was examined using Archimedes' principle, and the morphology was analyzed using Field Emission Scanning Electron Microscopy (FESEM). Sintered density was assessed by measuring the diameter and height of the pellets after sintering. Relative density and linear shrinkage were calculated. The impact of sintering parameters, such as temperature and soaking time, on the material's densification was also investigated. The addition of 20% aluminum oxide, 10% titanium dioxide, and 70% HAp exhibited the highest mechanical strength of 42.25 MPa at 1100°C for 5 hours. The pores were minimized at this temperature and time, indicating that the material was successfully densified, aligning with the goal of the research. The synthesized ternary blend (20% aluminum oxide, 10% titanium dioxide, and 70% HAp) also showed the formation of an appatite layer on days 7, 14, and 21 after immersion in simulated body fluid (SBF), compared with synthesized HAp. MTT assay was conducted to assess the toxicity of the optimal ternary blend ratio and synthesized HAp as a control on MG-63 cell lines, revealing cell proliferation at lower concentrations and inhibition of proliferation at higher concentrations. The biodegradation rate of the ternary blend was 3.09%, while that of the synthesized hydroxyapetite was 1.8%.

This work emphasizes the potential of the ternary blend of hydroxyapetite as a sustainable biomaterial with enhanced mechanical strength and controlled porosity,

making it suitable for applications in orthopedics, dental implants, and load-bearing implants. The integration of industrial waste valorization with advanced biomaterial synthesis not only supports circular economy principles but also addresses significant challenges in healthcare and environmental sustainability. This study lays the foundation for further research into functionalized hydroxyapetite composites for various applications in the biomedical and environmental fields. Developing mechanically improved biomaterials with customized properties is essential for advanced tissue engineering and bone regeneration. Additionally, this research explores the sintering kinetics of the ternary blend, highlighting its improved mechanical strength and controlled porosity when additives are incorporated into hydroxyapetite synthesized from industrial waste.

Hydroxyapetite synthesized using calcium-rich industrial waste precursors provides a cost-effective and environmentally friendly solution. The results indicated that the optimized sintering conditions produced a material with a dense structure and controlled porosity, making it suitable for applications that require mechanical stability. This work highlights the potential of industrial waste-derived hydroxyapetite as a sustainable option for mechanically enhanced biomaterials, particularly in bone implants. By integrating industrial waste valorization, controlled porosity, and improved mechanical strength, this study presents a novel approach for designing advanced biomaterials with multifunctional properties, offering a sustainable path for biomaterial production.

Keywords: Carbide lime, Hydroxyapetite, Optimization, Sintering additives, Aluminium oxide, Titanium dioxide, Taguchi L25 orthogonal array, Biodegradability, Biocompatibility, Toxicity.

ACKNOWLEDGMENTS

I would like to express my deepest gratitude and heartfelt appreciation to everyone who contributed to the successful completion of my research work. This research would not have been possible without the unwavering support and encouragement of many individuals.

Above all, I offer my profound thanks to **Waheguru Ji**, the Most Gracious and Most Merciful, whose countless blessings have guided me throughout this journey. I am truly humbled by His divine grace, which granted me the strength, patience, and wisdom to navigate the challenges of this research and reach this significant milestone in my Ph.D. thesis. His benevolence has been a constant source of inspiration, illuminating my path every step of the way.

"Waheguru ji ka Khasla, Waheguru ji ki Fateh"

Thank you **Waheguru ji** for everything!!

I would like to extend my heartfelt gratitude and profound appreciation to my esteemed advisor, **Dr. Anjuvan Singh (Professor, LPU)**, for his unwavering guidance and support throughout every stage of this research journey. His constant encouragement and belief in my abilities have been instrumental in helping me achieve my goals.

I consider myself truly fortunate to have had the opportunity to work under his mentorship. His exceptional leadership not only enriched my academic growth but also inspired me to face challenges with resilience and an open mind. During moments of self-doubt, his encouragement uplifted my spirits and strengthened my confidence, reminding me of the importance of perseverance. His insightful feedback, constructive criticism, and patient guidance consistently directed me toward academic excellence, for which I will always be deeply grateful.

I would like to convey my heartfelt gratitude to **Dr. Swastik Pradhan (Professor, LPU)** for his unwavering support throughout my research journey. His profound knowledge and dedication played a pivotal role in shaping both my research and overall academic development. His mentorship went far beyond academic guidance, fostering a nurturing environment that encouraged intellectual growth. His constant support, valuable insights, and encouragement have been a source of inspiration, significantly contributing to the successful completion of this work and I also thank **Dr. Piyush Kumar Gupta,** Department of Life Sciences, Sharda School of Basic Sciences and Research, **Sharda University, Greater Noida,** for his support in my journey.

I would like to express my heartfelt gratitude to my precious baby girl, **Shereen Kaur**, who endured countless challenges during this journey. I am profoundly thankful for the sacrifices she unknowingly made, bearing long hours of my absence as I pursued my academic goals. I owe her more than words can express. Her innocent smile has been a constant source of comfort, easing my stress and reviving my spirit in moments of exhaustion. The thought that I could be an inspiration to her became my greatest motivation, giving me the strength to persevere and reminding me of the greater purpose behind this achievement.

This thesis is lovingly dedicated to my **Husband, Sandeep Singh**, whose unwavering support and encouragement has been a pillar of strength during the most challenging times of this journey. Words fall short in expressing the depth of my gratitude for everything he has done. I have learned countless life lessons from him, and his belief that education and hard work never go in vain has been a constant source of inspiration. This journey would not have been possible without his steadfast support. His willingness to create a nurturing home environment allowed me to fully dedicate myself to my research, while his shared responsibilities eased my burden, making this achievement possible. I am profoundly grateful for his unwavering faith in me, for standing by my side through every high and low, and for always encouraging me to dream big and giving me the wings to fly.

I would like to express my heartfelt gratitude to my **Family** my **Father Baljit Singh**, my **Mother Rajinder Kaur** and my **Brother Gurpartap Singh** for their unwavering support and encouragement throughout my PhD journey. Their constant motivation during my difficult times gave me the strength to pursue my goal. My **mother's endless prayers** and my **father's cherished dream** of seeing his daughter complete her PhD and become a **doctor** have been the driving forces behind this accomplishment. Their presence in every hardship and their unwavering belief in me played a crucial role in the successful completion of my PhD work. I am truly blessed to have them as my pillars of strength.

I would like to sincerely thank my **friends** and **lab mates** – **Priyanka Thakur**, **Lovepreet Kaur**, and everyone who contributed to my journey. Working and collaborating with them has been a truly enriching experience. I am genuinely grateful for their willingness to share their knowledge and for providing a supportive and positive environment. Their insightful discussions and interactions have greatly enhanced my learning experience and played a vital role in my research journey.

I extend my sincere gratitude to the **Central Instrumentation Facility, Lovely Professional University (CIF, LPU)** for providing access to essential analytical instruments, including Field Emission Scanning Electron Microscopy (FE-SEM)**,** Fourier Transform Infrared Spectroscopy (FTIR)**,** x- ray diffraction (XRD)**,** and Thermo gravimetric Analysis (TGA). I am also thankful to **Tri Biotech Pvt. Ltd.** for facilitating the **MTT assay**, which significantly contributed to the successful completion of my research work.

---- Navneet Kaur

TABLE OF CONTENT

LIST OF TABLES

LIST OF FIGURES

ABBREVIATIONS

Al	Aluminum
Al_2O_3	aluminum oxide
Al^{3+}	aluminum cations
AlNPs	Aluminium oxide nano particles
ANOVA	Analysis of Variance
α-Al_2O_3	Corundum
β-TCP	β-tricalcium phosphate
°C	Degree Celsius
Ca $(NO_3)_2$	Calcium Nitrate
Ca $(OH)_2$	calcium hydroxide
Ca_{10} $(PO_4)_6(OH)_2$,	Hydroxyapetite
Ca^{2+}	calcium ions
$CaAl_2O_4$	calcium aluminate
CaC_2	calcium carbide
$CaCl.2H_2O$	Calcium Chloride dehydrate
$CaCO_3$	Calcium Carbonate,
CaO	calcium oxide
$CaSO_4$	Calcium Sulfate
$CaSO_4 \cdot 2H_2O$	Calcium Sulfate Dihydrate
$CaSO_4 \bullet 2H_2O$	Gypsum
$CaTiO_3$	calcium titanate
$(CH_2OH)_3CNH_2$	Tris(hydroxymethyl)aminomethane
CNTs	Carbon Nanotubes
CO_2	Carbon dioxide
DLS	Dynamic Light Scattering
DMEM	Dulbecco's Modified Eagle Medium
DMSO	Dimethyl Sulfoxide
EDS	Energy Dispersive Spectroscopy
FBS	Fetal Bovine Serum
FESEM	Field Emission Scanning Electron Microscope
FTIR	Fourier Transformed Infrared
g/cm^3,	grams per centimeter cube
g/l	grams per liter
GO	Graphene Oxide
GPa	Giga pascel
γ-Al_2O_3	gamma aluminium oxide
H_3PO_4	orthophosphoric acid
H_3PO_4	Phosphoric Acid
HAp	Hydroxyapetite

Hcp	hexagonal close-packed
JCPDS	Joint Committee on Powder Diffraction Standards
KCl	Potassium chloride
mg/Ml	milligrams per milliliter
$MgCl_2.6H_2O$	Magnesium Chloride hexahydrate
Mm	Millimeter
MPa	Mega pascal
MTT	3-(4,5-dimethylthiazol-2-yl)-2,5-diphenyl tetrazolium Bromide
Na_2SO_4	Sodium Sulfate
NaCl	Sodium Chloride
$NaHCO_3$	Sodium Bicarbonate
NCCS	National Centre for Cell Science
NH_4OH	Ammonium hydroxide
$(Na_2HPO_4).2H_2O$	Sodium Phosphate dibasic dehydrate
$(NH_4)_3PO_4$	Ammonium Phosphate
NPs	Nanoparticles
O	Oxygen
O^{2-}	oxygen anion
OH^-	hydroxide ions
PCL	Polycaprolactone
PDI	polydispersity index
PGA	Polyglycolic acid
PLA	Polylactic acid
PMMA	polymethyl methacrylate
PO_4^{3-}	phosphate groups
S/N	signal-to-noise
SBF	Stimulated Body Fluid
SEM	Scanning Electron Microscope
SiO	Silica
SPS	Spark Plasma Sintering
SS	sum of squares
TGA	Thermo gravimetric analysis
TiO_2	Titanium dioxide
Tris-HCl	Tris hydrochloride
θ-Al_2O_3	theta aluminium oxide
UTM	universal testing machine
wt %	Weight percentage
XRD	X- Ray Diffraction
ZrO_2	Zirconia

Chapter I

INTRODUCTION

1. Introduction

Industrialization has played a pivotal role in shaping modern society, driving technological advancements, and improving quality of life. However, this progress has come at a significant environmental cost, primarily in the form of waste generation. Industries such as gas production, manufacturing, construction, chemical production, and mining generate vast quantities of waste, much of which is either hazardous or difficult to manage sustainably [1]. For example, the chemical and pharmaceutical industries release toxic byproducts and solvents that contaminate water and soil, while the mining sector produces slag, which contributes to heavy metal pollution and landscape disruption [2]. Similarly, construction and demolition activities produce large volumes of concrete, asphalt, and other debris, which strain existing waste management infrastructure [3].

The harmful effects of industrial waste are widespread [4]. Unmanaged waste contributes to air, water, and soil pollution, adversely impacting ecosystems and human health. For instance, hazardous chemical waste can lead to the bioaccumulation of toxins in aquatic and terrestrial ecosystems, while solid waste contributes to land degradation and the release of greenhouse gases. Additionally, inadequate waste management raises the possibility of groundwater pollution and decreases the amount of cultivation land available, creating long-term problems for environmental sustainability and food security [5]. These issues underscore the urgent need for innovative waste management strategies that go beyond disposal and focus on waste valorization—converting waste into valuable resources.

1.1 Novel valorization of carbide lime into a sustainable and valuable resource

Among the various types of industrial waste, carbide lime holds huge potential for repurposing. Carbide lime is a byproduct of acetylene gas production, which is widely, used in welding, cutting, and various chemical synthesis processes. The reaction of calcium carbide with water generates acetylene gas, leaving behind a solid byproduct primarily composed of calcium hydroxide ($Ca(OH)_2$) [6]. Historically, carbide lime has been used in low-value applications such as soil

stabilization, neutralization of acidic soils, and wastewater treatment. For instance, its alkaline nature makes it effective in adjusting pH levels in wastewater treatment plants and mitigating heavy metal contamination. In the construction industry, carbide lime has been employed as a binder for soil stabilization, enhancing the strength and durability of subgrade materials [7].

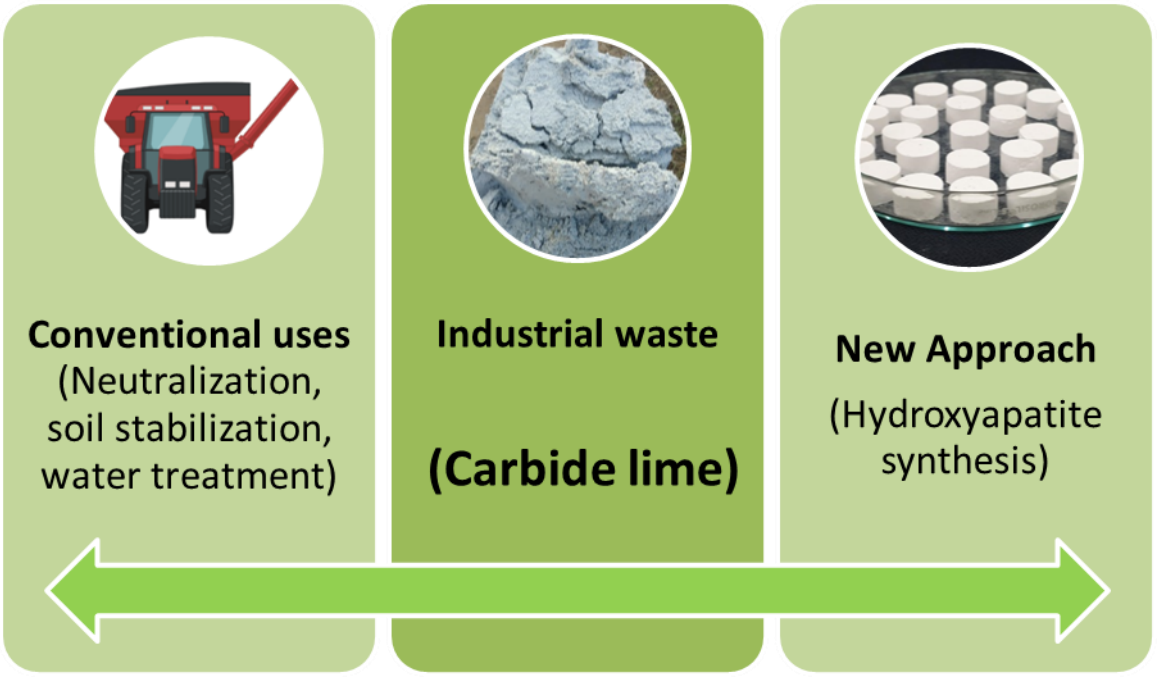

Figure 1.1: Novel approach of synthesizing Hydroxyapetite from an industrial waste.

While these conventional uses highlight the versatility of carbide lime, they do not fully exploit its chemical potential. The high calcium content of carbide lime makes it a promising precursor for synthesizing advanced materials, including hydroxyapetite (HAp). Hydroxyapetite, chemically represented as $Ca_{10}(PO_4)_6(OH)_2$, is a naturally occurring calcium phosphate mineral that forms the primary inorganic component of human bones and teeth. Its unique properties, such as biocompatibility, bioactivity, and osteoconductivity, have made it a basis of biomedical research and applications [8].

Hydroxyapetite is widely used in bone grafts, dental implants, and as a coating material for metallic implants to improve their integration with biological tissues. Its ability to promote cell attachment, proliferation, and differentiation makes it

particularly valuable in tissue engineering and regenerative medicine. Despite its extensive applications, the synthesis of hydroxyapetite remains a resource-intensive process. Conventional methods rely on high-purity precursors such as calcium nitrate and ammonium phosphate; they are not only costly but also add to the production's environmental impact because they generate chemical waste and energy-intensive procedures [9].

Given the limitations of traditional synthesis methods, there is a growing interest in developing alternative, sustainable, and cost-effective approaches for hydroxyapetite production [10]. This is where carbide lime emerges as a transformative solution. By repurposing this industrial byproduct as a precursor for hydroxyapetite synthesis, it is possible to address the dual challenges of waste management and sustainable material production. Carbide lime is a great option for calcium phosphate-based compounds, especially hydroxyapetite, due to its high calcium concentration. The synthesis of hydroxyapetite from carbide lime involves a series of chemical transformations. In general, the calcium hydroxide present in carbide lime reacts with phosphate sources under controlled conditions, such as wet precipitation or hydrothermal treatment, to form hydroxyapetite. These processes require precise control of parameters such as temperature, pH, and reactant concentrations to ensure the desired phase purity, crystallinity, and morphology of the final product. In order to alter the characteristics of hydroxyapetite for particular biomedical applications, it is essential to optimize these parameters, such as enhancing its mechanical strength for load-bearing applications or improving its bioactivity for faster osseo integration [11].

In addition to its technical feasibility, the use of carbide lime for hydroxyapetite synthesis offers significant environmental benefits. The disposal of carbide lime in landfills poses several environmental risks, including soil alkalinity, groundwater contamination, and the generation of greenhouse gases [12]. By converting this waste into a high-value biomaterial, these environmental risks can be mitigated, contributing to sustainable waste management practices. Furthermore, this approach aligns with the principles of the circular economy, which emphasize resource efficiency, waste reduction, and the development of closed-loop systems.

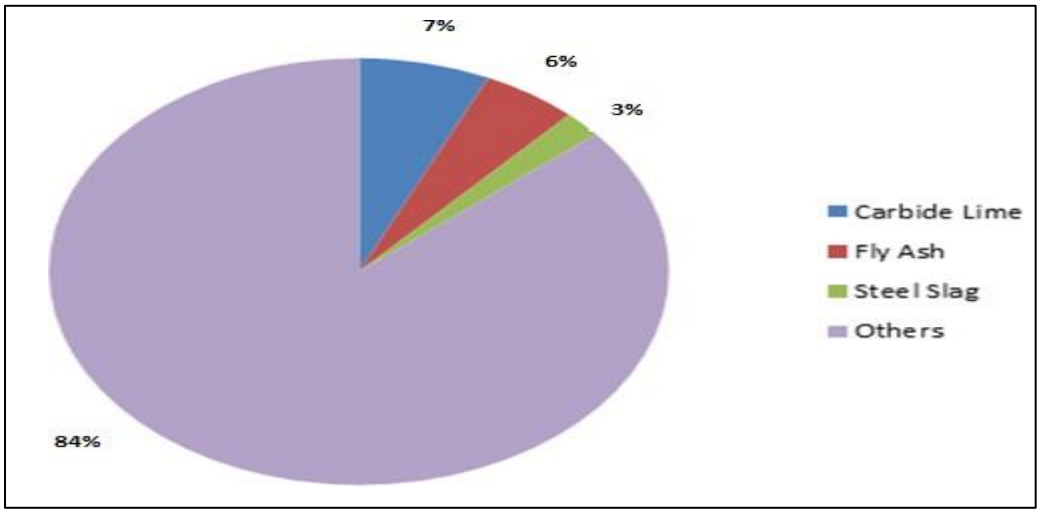

Fig 1.2: Industrial waste production (million tonnes/year)[211]

The valorization of carbide lime also has broader socio-economic implications. By reducing the reliance on high-purity chemical precursors, this approach lowers the production cost of hydroxyapetite, making it more accessible for widespread use in biomedical applications. This is particularly important in developing countries, where the high cost of imported biomaterials often limits access to advanced healthcare technologies [13]. Additionally, the repurposing of industrial waste into valuable materials creates new opportunities for economic growth and job creation, particularly in industries focused on sustainable materials and green chemistry.

This thesis aims to explore the feasibility of synthesizing hydroxyapetite from carbide lime, with a focus on optimizing the synthesis process and characterizing the resultant material. A comprehensive evaluation of the physical, chemical, and biological properties of the synthesized hydroxyapetite will be conducted to determine its suitability for biomedical applications. In this present research Hap powder with a Ca/P ratio of 1.67 will be synthesized utilizing the wet chemical precipitation method which uses carbide lime waste as a potent source of calcium hydroxide. There have been various methods used by numerous researchers to synthesize hydroxyapetite, including co-precipitation, hydrothermal synthesis, Sol-gel, chemical precipitation, and electrochemical deposition [14] and out of this wet chemical precipitation is widely used method [15]. The advantage of using the wet chemical precipitation method is that it is cost-effective, allows control over particle

size and morphology, has high purity, and is environmentally friendly

Pure hydroxyapetite is extremely expensive [16], so to overcome this problem, an attempt has been made for the synthesis of hydroxyapetite from an industrial waste with good mechanical properties as well as good biocompatibility. HAP was synthesized using the wet chemical precipitation method. To get a consistent particle size, the dry powder of the produced HAP was crushed into a powder using a mortar and pestle and then put into a sieve shaker. Following an hour of calcination at 800°C, the powder was combined with the proper weight percentage of titanium dioxide and aluminium oxide. The combined powder was then placed in a ball milling bottle with the stainless steel balls and ball milled for a 24 hours to ensure a thorough mixing of the mixture. This method of combining the powders is called the dry mix method.

The 13mm diameter cylindrical calcined mixed powder was compressed by uniaxial pressing at 750 MPa to form a pellet. The cylindrical pellets were then sintered in a muffle furnace for 1, 2, 3, 4, and 5 hours at various temperatures including 900, 950, 1000, 1050, and 1100°C, the sintering of the pellets were done according to the Taguchi L25 orthogonal array [17]. For every pellet, the sintered density was measured. The Archimedes Principle was used to calculate the bulk density and porosity. Relative density and shrinkage of the pellets were also calculated. Pure hydroxyapetite has poor mechanical characteristics; therefore, two additives, such as titanium dioxide (TiO_2) and aluminum oxide (Al_2O_3), were added to it to improve its mechanical qualities and make it suitable for use in biomedical applications. The weight percentages of titanium oxide (2-10%), aluminum oxide (20- 28%), and hydroxyapetite were kept constant at 70%, respectively. Mechanical tests like compressive strength were examined following the sintering process [18]. The phase decomposition of the HAp composite was determined by XRD analysis for the various temperatures at a scanning range of $2\theta = 20\text{-}80°$ and further characterization of the sample was done by using FTIR, TGA, and SEM analysis.

SBF (stimulated body fluid) was used to test the biocompatibility behavior of the synthesized hydroxyapetite composite. The results showed that SBF might serve as a

medium for the synthesis of hydroxyapetite with ion concentrations similar to those of the inorganic components of human blood plasma [19]. MTT assay was used to assess the toxicity and cell viability using MG63 cell lines and a biodegradation test was conducted to determine the percentage of degradation that took place that came out to be 3.09% [20]. In conclusion, the utilization of carbide lime for hydroxyapetite synthesis represents a novel approach to waste valorization and sustainable materials development. This research not only addresses the challenges associated with industrial waste disposal but also demonstrates the potential of carbide lime to serve as a high-value resource in the field of biomaterials. By bridging the gap between waste management and biomedical innovation, this study contributes to a more sustainable and resource- efficient future while advancing the frontiers of green chemistry and sustainable materials science.

1.2 An overview of the thesis

The complete thesis has been divided into the following five chapters: **Chapter I**: An overview of the research and its importance is presented. **Chapter II** discusses the review of literature regarding the history of carbide lime its earlier uses and the history of biomaterial. **Chapter III** elaborates the chemical, physical and biological characteristics of the materials and processes utilized to synthesize hydroxyapetite-based composites from carbide lime. **Chapter IV** elaborates the results and discussion of the experimental work, which has been compromised up into the following sections, each of which has a particular objective: **Part 1:** Discusses the isolation and characterization of carbide lime from the industrial waste. **Part 2:** Chemical synthesis and control of process parameters of the synthesized hydroxyapetite. **Part 3:** Characterization of synthesized hydroxyapetite from carbide lime. **Part 4:** Development of mechanical strength of the synthesized hydroxyapetite. **Part 5:** Invitro study of hydroxyapetite and study of its biocompatibility. In **Chapter V** the thesis work is briefly reviewed and concluded, along with future aspects for additional research

Chapter II

REVIEW OF LITRATURE

2. Review of literature

The increasing focus on sustainability has driven significant research into the utilization of waste materials for producing value-added biomaterials like hydroxyapetite (HAp). The utilization of waste materials for creating value-added products has roots in ancient practices, where communities repurposed natural by-products for practical applications. With the advancement of science, these waste streams have transitioned from rudimentary uses to sophisticated applications, such as the production of hydroxyapetite (HAp), a highly valued biomaterial. This biomaterial, renowned for its biocompatibility and similarity to human bone mineral, is now extensively used in orthopedics, dentistry, and regenerative medicine. The evolution of waste utilization reflects humanity's ingenuity in transforming natural by- products into high-value materials, contributing to sustainability and the advancement of modern biomaterial science. This approach not only supports circular economy principles but also provides an eco-friendly and economically viable alternative for developing biomaterials. The adaptation of waste-derived HAp for biomedical applications demonstrates the potential of waste valorization to contribute significantly to both sustainability and advancements in healthcare materials.

2.1 An outline of Hydroxyapetite

Hydroxyapetite (HAp), with the chemical formula $Ca_{10}(PO_4)_6(OH)_2$, is a calcium phosphate mineral that has a hexagonal crystal structure closely resembling the mineral phase of human bones and teeth [21].Its lattice arrangement, composed of calcium ions surrounded by phosphate and hydroxide groups, provides high biocompatibility and bioactivity, making it a critical material in medical applications[22]. Hydroxyapetite (HAp) plays a vital role in medical applications due to its exceptional biocompatibility, bioactivity, and structural similarity to the mineral component of human bones and teeth. Its ability to integrate seamlessly with biological tissues makes it an ideal material for orthopedic and dental applications, such as bone grafts, dental implants, and coatings for metallic implants [23]. HAp supports Osseo integration by promoting bone bonding and new tissue formation at

the implant site, enhancing implant stability and longevity. Furthermore, HAp serves as a carrier for controlled drug delivery, particularly for antibiotics and anticancer drugs, offering localized treatment with minimal side effects. Its versatility and compatibility with biological systems make hydroxyapetite an important material in regenerative medicine and biomedical innovation [24].

2.1.1 Biocompatible material's significance in biomedical applications

In biomedical applications, biocompatible materials are crucial because they can interact with biological systems safely and effectively without triggering unfavorable immune responses[25].These materials are essential for improving the effectiveness of medical devices and treatments because they facilitate the integration, replacement, or repair of damaged tissues. Biocompatible materials, such implants and scaffolds, facilitate cell adhesion and growth in orthopedic and dental applications, ensuring stability and promoting tissue regeneration. Their compatibility with the body reduces toxicity, rejection, and inflammation, which makes them essential in the development of pacemakers, stents, prosthesis, and drug delivery systems [26].

2.2 Importance of carbide lime synthesis

Carbide lime, a by-product of acetylene gas production, primarily contains calcium hydroxide ($Ca(OH)_2$), making it a viable precursor for calcium-based compounds [27]. As a sustainable and cost-effective alternative for producing valuable materials like hydroxyapetite (HAp), carbide lime synthesis is relevant because it reduces industrial waste and adheres to the principles of the circular economy by turning an environmental pollutant into a resource for biomedical and other applications [28].

In hydroxyapetite synthesis, the calcium in carbide lime can react with phosphate sources under controlled conditions to form high-purity HAp, which is essential for applications such as bone grafts, dental implants, and tissue engineering scaffolds. The approach offers economic advantages over conventional raw materials while addressing sustainability challenges. Moreover, the use of carbide lime in biomaterial synthesis contributes to resource conservation, waste management, and

environmental protection, enhancing its relevance in both industrial and biomedical contexts.

2.3 Hydroxyapetite: structure, Properties and applications

The chemical formula for hydroxyapetite (HAp) is $Ca_{10}(PO_4)_6(OH)_2$, and it is made up of hydroxide ions (OH^-), phosphate groups (PO_4^{3-}), and calcium ions (Ca^{2+}). The structure consists of two hydroxide ions that occupy interstitial spaces within the lattice, six phosphate groups that form the crystal lattice, and ten calcium ions that give strength and stability. This unique combination of calcium, phosphate, and hydroxide makes HAp chemically similar to the natural mineral found in bones and teeth, contributing to its excellent biocompatibility and bioactivity [29]. These properties enable hydroxyapetite to play a crucial role in biomedical applications such as bone grafts, dental implants, and tissue engineering scaffolds, where it supports Osseo integration and tissue regeneration [30].

2.3.1 Synthesis methods of hydroxyapetite

Hydroxyapetite (HAp) can be synthesized using several methods, each with its own set of advantages, depending on the desired properties and intended applications of the material.

1. **Wet precipitation method:** The most common and straightforward method is wet precipitation**,** where calcium salts (e.g., calcium hydroxide or calcium carbonate) are reacted with phosphate solutions (such as phosphoric acid) under controlled conditions of pH, temperature, and stirring. This method typically yields a powder form of HAp and is favored for its simplicity and cost-effectiveness. By adjusting parameters like pH and temperature, the size, morphology, and crystallinity of the HAp can be controlled to some extent. However, the method may result in HAp with low crystallinity, which can be undesirable for certain applications that require highly crystalline forms [31, 32].

2. Sol- Gel method: Another popular technique for creating hydroxyapetite is the sol-gel method. This process involves dissolving calcium and phosphate precursors in a solvent, then allowing the solution to go through condensation and hydrolysis reactions to create a gel. HAp is then created by heating this gel. Producing high-purity HAp with a consistent composition requires precise control over the material's stoichiometry and homogeneity, which is one of the sol-gel process's key benefits. The technique also makes it possible to add other functional groups or dopants to the HAp structure, changing its characteristics for certain uses. To obtain the required phase purity, the procedure can take longer and might call for further processes like drying and calcination [33, 34].

3. Hydrothermal method: For the production of high-quality HAp, the hydrothermal method is another effective technology. HAp is synthesized using this process at high temperatures and pressures, usually in an autoclave. Better crystallization and particle growth are encouraged by the high temperature and high pressure environment, producing well-formed HAp with regulated crystallinity and homogeneity. This process is especially well-suited for producing HAp with enhanced mechanical qualities, which makes it perfect for uses like prosthetics and bone implants that call for great strength and stability. However, the hydrothermal process is more expensive than other approaches due to its high energy requirements and sophisticated equipment [35, 36].

4. Biomimetic Synthesis: This is a method that aims to replicate the natural process of bone mineralization, often in the presence of organic molecules like collagen, proteins, or lipids. This technique typically involves forming HAp under physiological conditions (e.g., at body temperature and neutral pH), which allows for the production of material that closely resembles the mineralized matrix found in natural bone. This method is particularly important for applications in tissue engineering and regenerative medicine, where the material’s biological activity and compatibility with surrounding tissues are crucial. Biomimetic methods can be used to create porous HAp scaffolds that facilitate cell growth and tissue regeneration. The primary challenge, however, is maintaining control over the synthesis conditions to

avoid undesirable impurities or phases [37, 38].

5. Solid state reaction method: In order to create HAp, the solid-state reaction process combines solid calcium and phosphate precursors and heats them to high temperatures. This process can be useful for creating HAp in huge amounts and is frequently employed for large-scale production. Nevertheless, the solid-state approach usually yields less control over the crystallinity and particle size of the finished product, and it could necessitate high temperatures to attain phase purity, which in certain situations could result in sintering and undesired grain growth [39, 40].

6. Microwave-assisted synthesis: This is more recent advancement in HAp synthesis that rapidly heats the reactants using microwave energy. When compared to traditional heating techniques, this approach is quite effective and can drastically cut down on synthesis times. Better control over the material's uniformity and particle size is made possible by microwave-assisted synthesis, which is essential for biomedical applications like bone tissue engineering and medication delivery. Additionally, the process tends to yield extremely homogeneous HAp with enhanced crystallinity, which makes it a viable strategy for advanced materials. However, the technique requires specialized equipment and may not be suitable for large-scale production [41, 42].

7. Co-precipitation Method: This technique is comparable to precipitation but entails the simultaneous precipitation of several substances from a solution, including phosphate and calcium ions. When mixed with other ions or additives to change the material's characteristics, the process is advantageous for creating HAp with a consistent composition. The synthesized HAp's phase and stoichiometry can be precisely controlled using this approach. It is especially helpful when doping HAp with ions such as fluoride, strontium, or magnesium to customize its bioactivity for dental or bone regeneration applications [43, 44].

8. Hydrolysis Method: The hydrolysis method involves the reaction of calcium precursors, such as calcium phosphates or calcium carbonate, with water under

controlled conditions to produce HAp. By carefully controlling the reaction temperature and pH, this method can yield highly pure, well-crystallized HAp. It is considered a straightforward approach and can be adapted to large-scale production for industrial applications. The hydrolysis method is particularly useful for synthesizing HAp in its pure form with minimal impurities, making it suitable for medical applications [45, 46].

9. Electrochemical Method: In this method, an electric field is applied to a solution containing calcium and phosphate precursors in order to synthesize HAp electrochemically. The nucleation and growth of HAp crystals are influenced by the electric field, which enables fine control over the material's shape and crystallinity. To improve the biocompatibility of implants, HAp can also be deposited using this technique onto metallic substrates like titanium or stainless steel. For the production of HAp coatings that can enhance implant Osseo integration, the electrochemical technique is beneficial [47, 48].

10. Spray Pyrolysis: This adaptable technique entails spraying a solution containing precursors of calcium and phosphate into a heated chamber, where the droplets break down and produce HAp particles. Large amounts of HAp with regulated particle sizes and morphologies can be produced using this quite easy and economical technique. This process is very helpful for creating fine HAp powders or thin films for use in coatings, medication delivery, and implant surface modification [49, 50].

11. Flame Synthesis: Flame synthesis is a high-temperature method that involves the combustion of a mixture of calcium and phosphate precursors in a flame, where rapid cooling results in the formation of HAp. This method offers the advantage of fast synthesis and can produce nanostructured HAp with high surface area, making it suitable for applications requiring high reactivity, such as in catalytic processes or as a substrate for bioactive coatings [51,52].

12. Ultrasonic-assisted synthesis: High-frequency sound waves are used in ultrasonic-assisted synthesis to facilitate reactant dispersion and accelerate the crystallization of HAp. High shear forces produced by the ultrasonic waves

disintegrate agglomerates, resulting in a more even particle distribution and lower crystallite sizes. This technique is useful for tissue engineering scaffolds and drug delivery applications where precise particle properties are required since it allows for exquisite control over particle size and shape [53, 54].

13. Peptide-Assisted Synthesis: This method involves the use of peptides or proteins to assist in the formation of HAp. Peptides can influence the nucleation and growth of hydroxyapetite crystals by providing templates or functional groups that promote specific interactions between calcium and phosphate ions. Peptide- assisted synthesis is useful for creating HAp with enhanced biological properties, as it can improve cellular interaction, osteoconductivity, and bioactivity. This technique is particularly relevant for applications in regenerative medicine, where HAp scaffolds are designed to mimic the natural bone environment [55, 56].

14. Microwave-Assisted Hydrothermal Synthesis: This hybrid technique, which combines hydrothermal processing and microwave radiation, enables faster heating and more consistent HAp crystallization. High-quality HAp can be produced more quickly via microwave-assisted hydrothermal synthesis, which also gives more control over the size, shape, and purity of the crystals. This technique is especially useful for applications requiring quick synthesis or for the creation of HAp with nanostructures [57, 58].

15. Solvothermal Method: The solvothermal method is similar to hydrothermal synthesis but uses organic solvents instead of water as the solvent. This method allows for the synthesis of HAp under different reaction conditions, including the incorporation of organic molecules or dopants into the structure, which can further tailor its properties for specific applications. The solvothermal method can produce highly crystalline HAp with unique structural features, making it suitable for a range of advanced applications [59, 60].

Table 2.1: Different types of synthesis methods for the synthesis of hydroxyapetite.

S No	Method	Description	Advantages	Applications	References
1.	Wet Precipitation Method	Calcium salts react with phosphate solutions to form HAp under controlled pH and temperature.	Simple, cost-effective, scalable.	Bone implants, dental applications.	[31,32]
2.	Sol-Gel method	Calcium and phosphate precursors form a gel, which is then heated to form HAp.	Allows for precise control over stoichiometry and homogeneity.	Drug delivery, coatings, bone regeneration.	[33,34]
3.	Hydrothermal method	Synthesis occurs under high temperature and pressure in an autoclave, producing well-crystallized HAp.	Produces highly crystalline HAp, improves mechanical properties.	Bone implants, prosthetics, bone tissue engineering.	[35,36]
4.	Biomimetic Synthesis method	Mimics the natural mineralization of bones under physiological conditions,often using organic molecules.	Produces HAp that closely resembles natural bone, promotes tissue regeneration.	Bone regeneration, tissue scaffolds.	[37,38]
5.	Solid-State Reaction method	Calcium and phosphate precursors are mixed and heated at high temperatures to form HAp.	Suitable for bulk production, cost-effective.	Large-scale production, industrial applications.	[39,40]
6.	Microwave Assisted Synthesis method	Uses microwave energy to rapidly heat reactants and synthesize HAp.	Fast synthesis, better particle uniformity, high crystallinity.	Nanostructured HAp, bone grafts coatings.	[41,42]
7.	Co-precipitation method	Simultaneous precipitation of calcium and phosphate ions to form HAp.	Allows for uniform composition, doping with ions.	Bone regeneration, dental implants, and coatings.	[43,44]
8.	Hydrolysis method	Calcium precursors react with water under controlled conditions to form HAp.	High purity, well-controlled synthesis.	Bone implants, dental applications.	[45,46]

9.	Spray Pyrolysis method	Calcium and phosphate solution is sprayed into a heated chamber where droplets decompose to form HAp.	Simple, cost-effective, and capable of producing large quantities of HAp.	Thin films, coatings, drug delivery.	[49,50]
10.	Flame Synthesis method	Combustion of calcium and phosphate precursors in a flame, rapidly cooling to form HAp.	Fast synthesis, produces nanostructured HAp with high surface area.	Nanostructured HAp, catalytic processes, bioactive coatings.	[51,52]
11.	Ultrasonic-Assisted Synthesis Method	High-frequency sound waves are used to disperse reactants and promote crystallization of HAp.	Improved particle dispersion, smaller crystal sizes, and uniformity.	Bone tissue engineering, drug delivery.	[53,54]
12.	Peptide-Assisted Synthesis method	Peptides or proteins assist in the formation of HAp by promoting nucleation and growth.	Enhances biological properties, promotes osteoconductiv ity.	Bone regeneration, tissue scaffolds.	[55,56]
13.	Microwave-Assisted Hydrothermal method	Combines microwave radiation with hydrothermal conditions to rapidly heat and crystallize HAp.	Rapid heating, uniform crystallization, short synthesis time.	Nanostructured HAp, biomedical applications, coatings.	[57,58]
14	Solvothermal method	Uses organic solvents instead of water to synthesize HAp under controlled conditions.	Allows incorporation oforganic molecules or dopants produces high-quality HAp.	Drug delivery, bone scaffolds, bioactive coatings.	[59,60]

2.4 Raw materials for hydroxyapetite synthesis

The synthesis of hydroxyapetite (HAp) relies on various raw materials, broadly classified into synthetic chemicals, natural sources, and industrial byproducts. Common synthetic precursors include calcium hydroxide, calcium nitrate, ammonium phosphate, and phosphoric acid, known for their high purity and reaction control. Natural sources such as limestone, eggshells, and seashells provide calcium carbonate, while bone ash and fish bones offer calcium phosphate, making them eco-friendly and renewable options. Industrial byproducts like gypsum, phosphogypsum,

and lime sludge from the paper and pulp industry serve as sustainable alternatives, promoting waste recycling and cost efficiency. The choice of raw material significantly influences the purity, crystallinity, and biocompatibility of the synthesized HAp, highlighting the importance of selecting suitable and sustainable precursors.

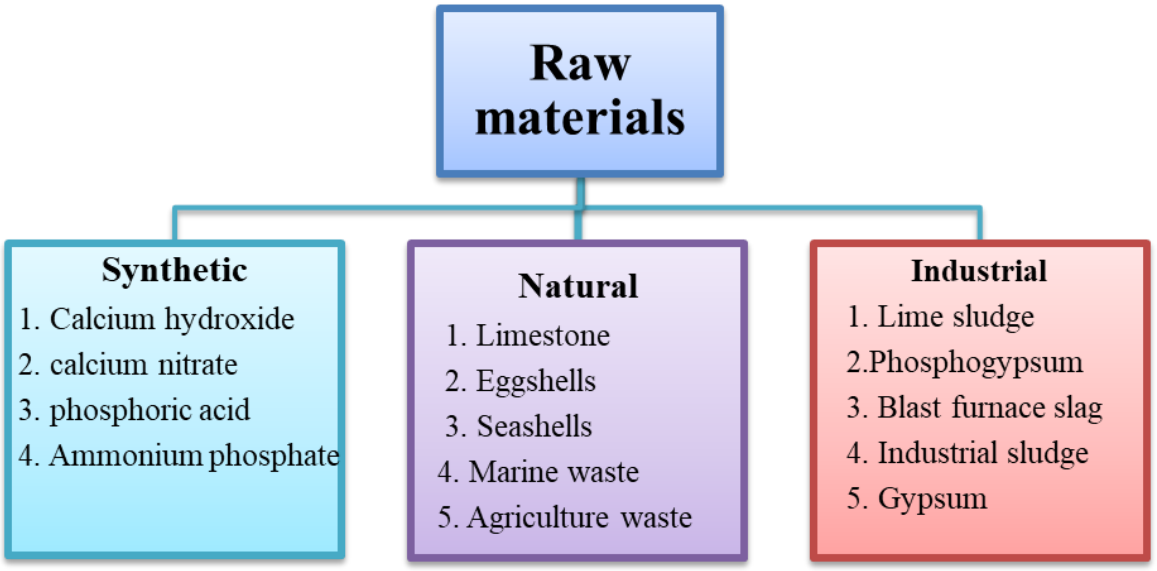

Figure 2.1: Different types of raw materials used for synthesis of hydroxyapetite.

2.4.1 Synthetic Raw Materials for Hydroxyapetite Synthesis:

1. **Calcium Hydroxide ($Ca(OH)_2$):** Calcium hydroxide is a commonly used synthetic precursor in hydroxyapetite (HAp) synthesis. It is a highly pure source of calcium ions that can readily react with phosphate sources like phosphoric acid to form hydroxyapetite. It is preferred in laboratory settings for its predictable composition and easy handling. However, its use requires precise control over reaction conditions, as it can sometimes produce impure or poorly crystalline HAp if the reaction is not carefully controlled [61, 62].

2. **Calcium Nitrate ($Ca(NO_3)_2$):** Calcium nitrate is another synthetic source of calcium ions used in HAp synthesis. It is highly soluble in water, making it easy to incorporate into the synthesis process, particularly in aqueous solutions. This allows for the production of highly homogeneous HAp.

Calcium nitrate is typically used in precipitation methods, where it is mixed with phosphate solutions to form HAp. However, careful washing and purification are necessary to remove any residual nitrate ions, which may affect the final material's properties [63, 64].

3. **Phosphoric Acid (H_3PO_4):** Phosphoric acid is often used in combination with calcium precursors to synthesize hydroxyapetite. It reacts with calcium hydroxide or calcium salts to form HAp. Phosphoric acid offers a high concentration of phosphate ions and allows for precise control over the stoichiometry of the reaction. This ensures that the resulting HAp has an ideal Ca/P ratio, which is critical for the material's bioactivity and structural integrity [65, 66].

4. **Ammonium Phosphate ($(NH_4)_3PO_4$):** Ammonium phosphate is a commonly used phosphate precursor in HAp synthesis. It provides phosphate ions that readily react with calcium sources to form hydroxyapetite. It is highly soluble and can be used in aqueous systems to form HAp through precipitation methods. The synthesis process typically involves mixing ammonium phosphate with calcium salts under controlled conditions to produce HAp with high crystallinity [67, 68].

2.4.2 Natural Raw Materials for Hydroxyapetite Synthesis:

1. **Limestone (Calcium Carbonate, $CaCO_3$):** Limestone is a natural and abundant source of calcium carbonate, making it a widely used precursor for hydroxyapetite synthesis. After calcination at high temperatures, limestone is converted into calcium oxide (CaO), which can be reacted with phosphate sources to form HAp. This method is cost-effective and environmentally friendly, but it requires energy- intensive processes to achieve the desired calcium compounds, such as calcination [69, 70].

2. **Eggshells (Calcium Carbonate):** Eggshells, a waste product of the poultry industry, are rich in calcium carbonate. They are an affordable and renewable

source of calcium for HAp synthesis. Eggshells need to undergo cleaning, grinding, and calcination to remove organic materials before they can be used in HAp production. The use of eggshells as a precursor not only reduces waste but also provides an eco-friendly route for HAp synthesis [71, 72].

3. **Seashells (calcium carbonate, such as clams and oysters):** Another sustainable supply of calcium carbonate is seashells, such as those found in clams and oysters. They have been investigated more and more as a raw material for HAp synthesis, and they are especially frequent in coastal areas. Seashells can be cleaned and calcined to produce calcium oxide, which can subsequently react with phosphate sources to produce hydroxyapetite. The recycling of marine waste and sustainable material manufacture are supported by the use of seashells in HAp synthesis [73, 74].

4. **Fish Scales and Bones (Calcium Phosphate):** Fish scales and bones, which are often discarded as waste in the fishing industry, are rich in calcium phosphate. After cleaning, drying, and calcining, they can serve as a calcium and phosphate source for HAp synthesis. The use of fish-derived materials not only reduces waste in the fishing industry but also provides an eco-friendly alternative for producing high-quality hydroxyapetite [75, 76].

2.4.3 Industrial raw materials

1. **Lime Sludge (From Paper and Pulp Industry, Calcium Carbonate and Hydroxide):** Lime sludge, a byproduct of the paper and pulp industry, is rich in calcium carbonate and calcium hydroxide, both of which are essential for HAp synthesis. By processing and purifying lime sludge, it can be used as a low-cost and sustainable precursor for producing hydroxyapetite. This approach contributes to reducing industrial waste and supports circular economy principles [77, 78].

2. **Phosphogypsum (Calcium Sulfate, $CaSO_4$)**: However, it contains more trace contaminants, such as heavy metals. Upon proper purification and

treatment, phosphogypsum can serve as a useful calcium source for the synthesis of HAp. Its use promotes sustainable material production and lowers environmental pollution associated to its disposal [79, 80].

3. **Blast Furnace Slag (Calcium Silicates and Aluminates):** Blast furnace slag, generated during steel production, is a byproduct rich in calcium silicates and aluminates. These compounds can be processed to extract calcium for HAp synthesis. The use of blast furnace slag in HAp production not only contributes to waste recycling but also provides an alternative, cost-effective calcium source for biomedical applications [81, 82].

4. **Industrial Sludge (Calcium and Phosphate Compounds):** Calcium and phosphate compounds found in industrial sludge from a variety of industries, such as the dairy and chemical sectors, can be used repeatedly for HAp production. The components required for the creation of HAp can be extracted by cleaning and purifying this sludge, which helps to reduce waste and source materials sustainably [83, 84].

5. **Gypsum (Calcium Sulfate Dihydrate, $CaSO_4 \cdot 2H_2O$):** Gypsum, a byproduct of the phosphate fertilizer industry, contains calcium sulfate. It can be processed to extract calcium ions, which can then be used in HAp synthesis. Gypsum is a readily available and low-cost alternative to traditional calcium sources, although its use may require additional chemical treatments to remove impurities before it can be effectively utilized [85, 86].

Table 2.2: Different sources of raw material for the synthesis of hydroxyapetite.

S No	Category	Raw Material	Composition	Source	Biomedical Applications	References
1.	Synthetic	Calcium Hydroxide ($Ca(OH)_2$)	Calcium	Laboratory-grade	Bone grafts, dental implants, drug delivery systems	[61,62]
		Calcium Nitrate ($Ca(NO_3)_2$)	Calcium	Laboratory-grade	Scaffolds, coatings for implants	[63,64]
		Ammonium Phosphate ($(NH_4)_3PO_4$)	Phosphate	Laboratory-grade	Bone tissue regeneration, drug delivery	[67,68]
		Phosphoric Acid (H_3PO_4)	Phosphate	Laboratory-grade	Bio ceramics, porous bone graft materials	[65,66]
2.	Natural	Limestone ($CaCO_3$)	Calcium Carbonate	Sedimentary rock	Bone substitutes, dental fillers	[69,70]
		Eggshells	Calcium Carbonate	Poultry waste	Scaffolds, drug delivery, bone regeneration	[71,72]

		Seashells	Calcium Carbonate	Marine waste	Bio ceramic materials, bone tissue engineering	[73,74]
		Fish Scales and Bones	Calcium Phosphate	Fishery waste	Scaffolds, dental applications, tissue engineering	[75,76]
3.	Industrial	Gypsum ($CaSO_4 \cdot 2H_2O$)	Calcium Sulfate	Fertilizer and cement industries	Bone graft materials, porous scaffold production	[85,86]
		Phosphogypsum ($CaSO_4$)	Calcium Sulfate	Phosphate fertilizer production	Scaffolds, coatings, drug delivery systems	[79,80]
		Lime Sludge	Calcium Hydroxide/Carbonate	Paper and pulp industry	Bone regeneration, bio ceramic materials	[77,78]
		Blast Furnace Slag	Calcium Silicates/Aluminates	Steel industry	Composite materials for bone repair, tissue engineering	[81,82]

2.5 Types of biomaterials based on the generations

Biomaterials can be categorized based on their qualities. The synthesis of biomaterials has improved as a result of technological advancements. Scientists are currently placing a great deal of effort on developing fourth-generation biomaterials.

2.5.1 First Generation: Bio inert Biomaterials

First generation of biomaterials mainly focuses on creating materials that were both chemically stable and inert in biological environments. The main purpose of these materials was to offer mechanical support without causing the body to respond negatively. Their main objective was to provide biocompatibility by preventing rejection or immunological reactions. Metals like titanium, stainless steel, and

cobalt-chromium alloys are common examples, as are polymers like polyethylene and polymethyl methacrylate (PMMA), as well as ceramics like zirconia and alumina. These materials were widely used in heart valves, dental prosthesis, and orthopedic implants. The inability of first-generation biomaterials to integrate with the surrounding tissues, notwithstanding their success, frequently resulted in long-term difficulties like stress shielding or implants loosening [87].

2.5.2 Second Generation: Bioactive and Biodegradable materials

The second generation introduced bioactive and biodegradable materials, representing a significant leap in biomaterials science. Bioactive materials are designed to stimulate biological responses, promoting tissue bonding and regeneration. Examples include hydroxyapetite, bio glass, and calcium phosphate ceramics. On the other hand, biodegradable materials, such as polyglycolic acid (PGA), polylactic acid (PLA), and polycaprolactone (PCL), are engineered to degrade over time and be replaced by natural tissues. This generation of materials enabled advancements in bone grafts, tissue engineering scaffolds, sutures, and drug delivery systems. These innovations eliminated the need for secondary surgeries to remove implants and significantly improved healing processes. However, challenges remain in controlling their degradation rates and ensuring consistent bioactivity [88].

2.5.3 Third Generation: Smart and Functional materials

The third generation of biomaterials is marked by the emergence of intelligent and useful materials that can dynamically interact with their biological surroundings. These materials interact to stimuli like light, pH, and temperature and are designed to replicate biological processes. Hydrogels that react to stimuli, nanoparticles for precise medication administration, and bioengineered materials that include cell adhesion peptides are a few examples. Applications for third-generation biomaterials in wound healing, regenerative medicine, and advanced tissue engineering have grown. They provide up the possibilities to patient-specific treatments by facilitating precise medication delivery and adaptive therapeutic responses. Although their enormous potential, their widespread adoption has been constrained by the high

costs and complexity of manufacture, as well as regulatory barriers [89].

2.5.4 Fourth Generation: Regenerative and Personalized Biomaterials

The fourth generation is the most advanced biomaterials, which are made to actively support tissue regeneration and adjust to the specific requirements of each patient. These materials provide customized solutions by integrating technologies such as 3D bio printing, gene therapy, and stem cell engineering. Decellularized matrices, growth factor-containing hydrogels, gene-activated scaffolds, and nanostructured materials are a few examples. They are employed in targeted therapy, organ repair, and regenerative medicine. These materials have great potential to advance individualized and regenerative healthcare, despite constraints like production costs and scalability [90].

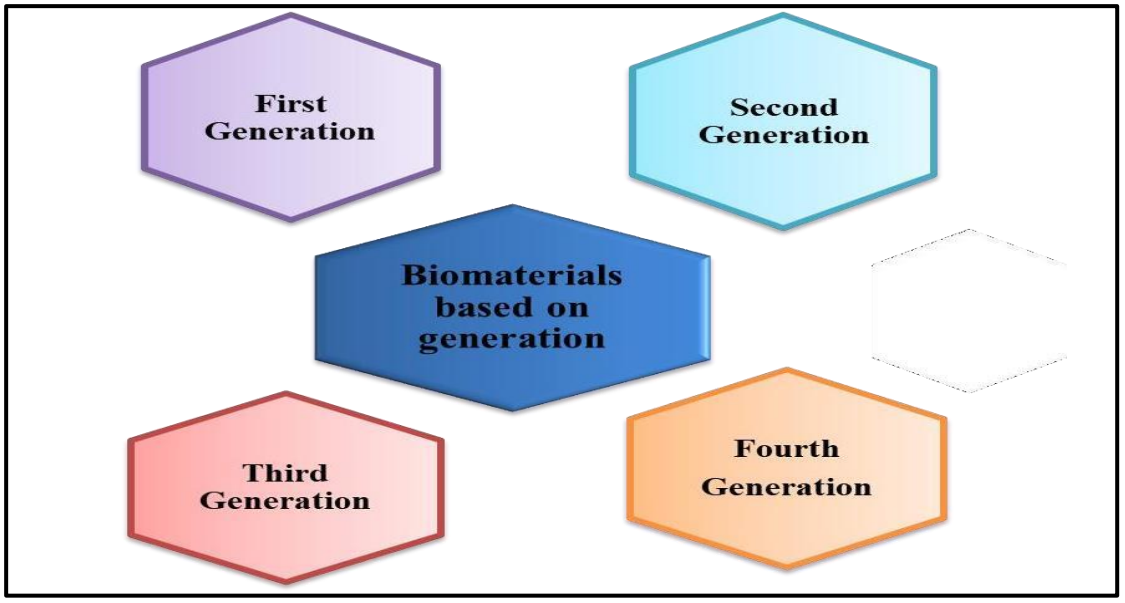

Figure 2.2: Classification of biomaterials based on its generation

2.6 Different fabrication methods

The incorporation of aluminum oxide (Al_2O_3) and titanium oxide (TiO_2) into hydroxyapetite (HAp) enhances its mechanical strength, bioactivity, thermal stability, and wear resistance, making it an excellent candidate for biomedical

applications like implants and coatings. Various fabrication methods are employed to achieve the desired properties and performance in these composites:

2.6.1 Sol Gel Method

The sol-gel process involves mixing calcium, phosphate, aluminum, and titanium precursors to form a colloidal solution (sol) that transitions into a gel. The gel is dried and heat-treated at controlled temperatures to achieve the composite structure. This method offers precise control over the particle size and distribution of Al_2O_3 and TiO_2 within the HAP matrix. This method produces nanostructured materials for bone tissue engineering and suitable for bioactive coatings on implants [91].

2.6.2 Mechanical Milling and Sintering

In this technique, HAp, Al_2O_3, and TiO_2 powders are mechanically mixed using ball milling to ensure uniform distribution. The blended powders are compacted into desired shapes and subjected to high-temperature sintering (1100–1500°C), which enhances the composite's density, mechanical strength, and phase stability, that are used for load-bearing implants and fabricates dense and durable bone graft substitutes [92].

2.6.3 Plasma Spraying

Plasma spraying is a thermal coating method where composite powders are melted and sprayed onto implant surfaces. The high temperature of the plasma ensures good adhesion and homogeneity of the HAp-Al_2O_3-TiO_2 coating, resulting in improved wear resistance and bioactivity. With plasma spraying Coating of metallic orthopedic and dental implants can be done which also improves Osseo integration and longevity of implants [93].

2.6.4 Spark Plasma Sintering (SPS)

SPS combines pulsed electric currents with pressure to sinter the composite powders at relatively low temperatures. This method minimizes grain growth and preserves the nanostructure of the HAp-Al_2O_3-TiO_2 composite, resulting in improved

mechanical properties and excellent biocompatibility. This method is used in high-performance implants for orthopedic and dental applications [94].

2.6.5 Hot Pressing

Hot pressing involves compacting the HAp, Al_2O_3, and TiO_2 powders under simultaneous heat and pressure. This technique reduces porosity and enhances the mechanical strength and toughness of the composite. With hot pressing, fabrication of dense ceramics for hip and knee replacements. This is also suitable for applications requiring high wear resistance [95].

2.6.6 3D Printing

3D printing techniques, such as selective laser sintering and direct ink writing, are increasingly used to fabricate HAP-Al_2O_3-TiO_2 composites. These methods allow for the creation of complex, patient-specific structures with controlled porosity and geometry, suitable for personalized implants and scaffolds. Custom implants for bone regeneration. Advanced scaffolds for tissue engineering [96].

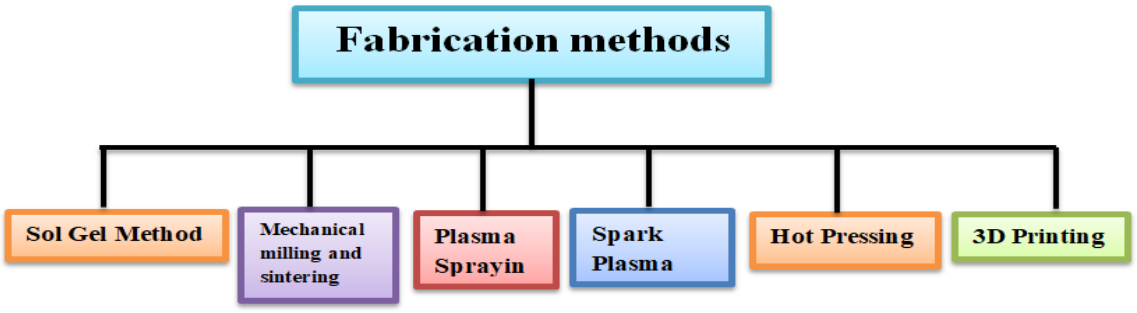

Figure 2.3: Different hydroxyapetite fabrication methods

2.7 Composite Biomaterials

Hydroxyapetite (HAp), a bioactive and biocompatible ceramic, is often combined with other materials to overcome its inherent brittleness and improve its mechanical properties, thermal stability, and functional versatility [97]. These composites are extensively used in biomedical applications such as bone grafts, dental implants, and coatings. Below are various types of composites formed with HAp and their fabrication method, processing techniques and their applications.

Table 2.3: Different types of composite used along with hydroxyapetite

S No	Composite Material	Fabrication Method	Processing Techniques	Applications	References
1.	HAP-Alumina (Al_2O_3)	Powder mixing and sintering	Sintering at high temperatures (1200–1500°C)	Orthopedic implants, dental crowns, and bone fillers	[98]
2.	HAP-Titanium Dioxide (TiO_2)	Sol-gel, powder mixing	Hot pressing, sintering	Load-bearing implants, dental prostheses	[99]
3.	HAP-Zirconia (ZrO_2)	Co-precipitation, powder blending	Spark plasma sintering, conventional sintering	Joint prostheses, dental implants	[100]
4.	HAP-Bioactive Glass	Sol-gel, melt quenching	Hot pressing, thermal annealing	Bone scaffolds, coatings for implants	[101]
5.	HAP-Polylactic Acid (PLA)	Solvent casting, melt blending	Electro spinning, extrusion	Bone tissue engineering scaffolds, drug delivery	[102]
6.	HAP-Polycaprolactone (PCL)	Solvent evaporation, 3D printing	3D printing, freeze drying	Soft tissue engineering, bone graft substitutes	[103]

7.	HAP-Chitosan	Freeze-drying, solution blending	Freeze drying, casting	Wound healing, drug delivery, scaffolds for tissue regeneration	[104]
8.	HAP-Stainless Steel	Coating via thermal spraying	Plasma spraying, electrophoretic deposition	Orthopedic implants, bone plates	[105]
9.	HAP-Magnesium	Powder metallurgy, biomimetic coating	Hot extrusion, surface modification	Temporary implants, biodegradable implants	[106]
10.	HAP-Graphene Oxide (GO)	Solution mixing, ultrasonic dispersion	Cold pressing, spark plasma sintering	Bone tissue engineering, enhanced wear resistance	[107]
11.	HAP-Silk Fibroin	Solution blending, freeze- drying	Freeze drying, hydrothermal processing	Bone scaffolds, tissue regeneration	[108]
12.	HAP-Carbon Nanotubes (CNTs)	Solution blending, ball milling	Sintering, spark plasma sintering	High-strength bone implants, dental applications	[109]
13.	HAP-Polyethylene Glycol (PEG)	Sol-gel, freeze- drying	Electro spinning, solvent casting	Tissue scaffolds, drug delivery	[110]
14.	HAP-Polyvinyl Alcohol (PVA)	Solution blending, freeze- drying	Gel casting, cross-linking	Cartilage repair, soft tissue engineering	

15.	HAP-Collagen	Co-precipitation, freeze- drying	Gel casting, hydrothermal processing	Bone tissue engineering, biocompatible scaffolds	[111]
16.	HAP-Alumina-Titanium Dioxide	Powder mixing and sintering	High-temperature sintering, hot pressing	Load-bearing implants, joint replacements	[112]

2.7.1 Aluminum Oxide (Al_2O_3) in HAp Composites

Aluminum oxide (alumina) is a crystalline ceramic material composed of aluminium (Al) and oxygen (O) atoms with the molecular formula Al_2O_3 [113].It is widely used in combination with hydroxyapetite (HAP) for biomedical applications due to its excellent mechanical and biocompatible properties.

2.7.1.1 An overview of Aluminum Oxide

Aluminum oxide nanoparticles is a class of porous nanomaterials that are a member of the metal oxide nanomaterials family, are assembled as a corundum-like structure with one aluminum atom surrounded by six oxygen atoms. Aluminium oxide nanoparticles are easily accessible and affordable, just like the other metal oxide nanoparticles (NPs). These affordable nanomaterials also have a large surface area, mechanical strength [114]. Moreover, their electrical conductivity is limited. The structure of alumina primarily exists in various phases, with α-Al_2O_3 (corundum) being the most thermodynamically stable and commonly used. This phase features a hexagonal close-packed (hcp) crystal structure, where aluminum cations (Al^{3+}) occupy octahedral sites within a dense oxygen anion (O^{2-}) lattice. The strong ionic bonds in this arrangement provide exceptional hardness, strength, and stability. Transition phases such as γ-Al_2O_3 (gamma) and θ-Al_2O_3 (theta) exist but convert to the stable α-phase at elevated temperatures [115].

The chemical composition of alumina is represented by its molecular formula Al_2O_3, consisting of two aluminum atoms bonded with three oxygen atoms.

Biomedical-grade alumina is characterized by its high purity (≥99.9%) to ensure biocompatibility and reliable mechanical properties. Impurities like silica or alkali oxides are minimized to enhance performance in medical applications. With a theoretical density of ~3.98 g/cm³, alumina exhibits high compressive strength, making it an ideal metal oxide for reinforcing brittle materials like hydroxyapetite. According to recent economic research, the market for AlNPs is expanding quickly across a range from industries and the biomedical applications. Consequently, they have been regarded as a strategic nanomaterial in many areas of life. Concerning the extremely beneficial qualities, the availability of several pathways for AlNP synthesis, and the strategic significance of AlNPs, they have been discovered various uses in human life, especially in biotechnology and biomedicine. They are utilized in biomolecular stabilization, drug delivery, and biosensing for disease treatment. [114].

Alumina is combined with hydroxyapetite to overcome the intrinsic brittleness of HAP, thereby improving its mechanical properties. The high hardness (~15–20 GPa) and compressive strength (~300–400 MPa) of alumina significantly enhance the wear resistance and durability of the composite. This makes the material suitable for load- bearing applications such as orthopedic implants and dental prostheses. Furthermore, alumina's excellent thermal stability allows it to endure high-temperature sintering processes (≥1200°C) without undergoing degradation or phase transformations [116]. The biocompatibility of alumina is another crucial factor in its application. High- purity alumina is chemically inert and does not provoke adverse reactions in physiological environments, making it safe for long-term implantation. Additionally, while hydroxyapetite is inherently osteoconductive, the inclusion of alumina provides enhanced mechanical support for new bone growth without compromising bioactivity [117].

Overall, aluminum oxide serves as an indispensable reinforcement in hydroxyapetite composites, contributing to improved mechanical properties, thermal stability, and wear resistance while maintaining excellent biocompatibility. These enhanced composites find extensive use in biomedical applications such as bone

substitutes joint prostheses, and dental implants, meeting the demands of both performance and biocompatibility in clinical settings [117].

Figure 2.4: Applications of aluminium oxide in biomedical field.

2.7.2 Titanium dioxide in HAp composite

Titanium dioxide (TiO_2) is a widely utilized ceramic material, known for its unique structural and functional properties. It is commonly combined with hydroxyapetite (HAP) in composite materials to enhance mechanical strength, biocompatibility, and functional performance for biomedical applications.

2.7.2.1 Structure and properties of Titanium dioxide

The structure of titanium dioxide plays a significant role in its utility. TiO_2 exists in three primary polymorphs: anatase**,** rutile**,** and brookite, with anatase and rutile being the most widely used. Anatase has a tetragonal crystal structure with a slightly open arrangement that provides high surface area. Rutile, on the other hand, also has

a tetragonal crystal structure but with a more compact and stable lattice, contributing to its excellent thermal and mechanical stability. Brookite, while less common, has an orthorhombic crystal structure and is rarely used in industrial or biomedical applications due to its instability [118].

The chemical composition of titanium dioxide is simple, represented by the molecular formula TiO_2, which consists of one titanium atom bonded to two oxygen atoms. Titanium atoms are surrounded by oxygen atoms in a distorted octahedral configuration, creating a robust and stable ionic lattice. Biomedical-grade TiO_2 is produced with high purity to ensure biocompatibility and to prevent adverse reactions. Impurities are minimized to maintain its performance in biological environments.

One of the primary reasons for combining TiO_2 with hydroxyapetite is to enhance the mechanical properties of HAP, which is inherently brittle and unsuitable for load- bearing applications. TiO_2 improves the fracture toughness and compressive strength of the composite. It acts as a reinforcement phase, enabling the material to withstand greater mechanical loads without failure. This makes HAP-TiO_2 composites highly suitable for orthopedic implants, dental restorations, and bone scaffolds. An additional advantage of TiO_2 in HAP composites is its thermal stability. Rutile TiO_2, in particular, has a high melting point of ~1843°C and retains its structural integrity during high-temperature sintering processes used in composite fabrication. This ensures the uniform distribution of TiO_2 within the hydroxyapetite matrix, resulting in a composite material with enhanced mechanical properties and stability [119].

In terms of biocompatibility, TiO_2 is widely recognized as a safe and inert material for biomedical use. It does not provoke inflammatory or toxic responses in the body and has been shown to support the attachment and proliferation of bone cells (osteoblasts). This enhances the osteoconductive properties of hydroxyapetite, facilitating better integration with the surrounding bone tissue when used in implants [120].

In summary, the structure and composition of titanium dioxide make it a versatile and valuable component in hydroxyapetite composites. Its polymorphic flexibility, mechanical reinforcement, thermal stability, photo catalytic activity, and excellent biocompatibility contribute to the overall performance of the composite in biomedical applications. The combination of TiO_2 and HAP results in a material that is stronger, more durable, and better suited for orthopedic, dental, and bone regeneration purposes.

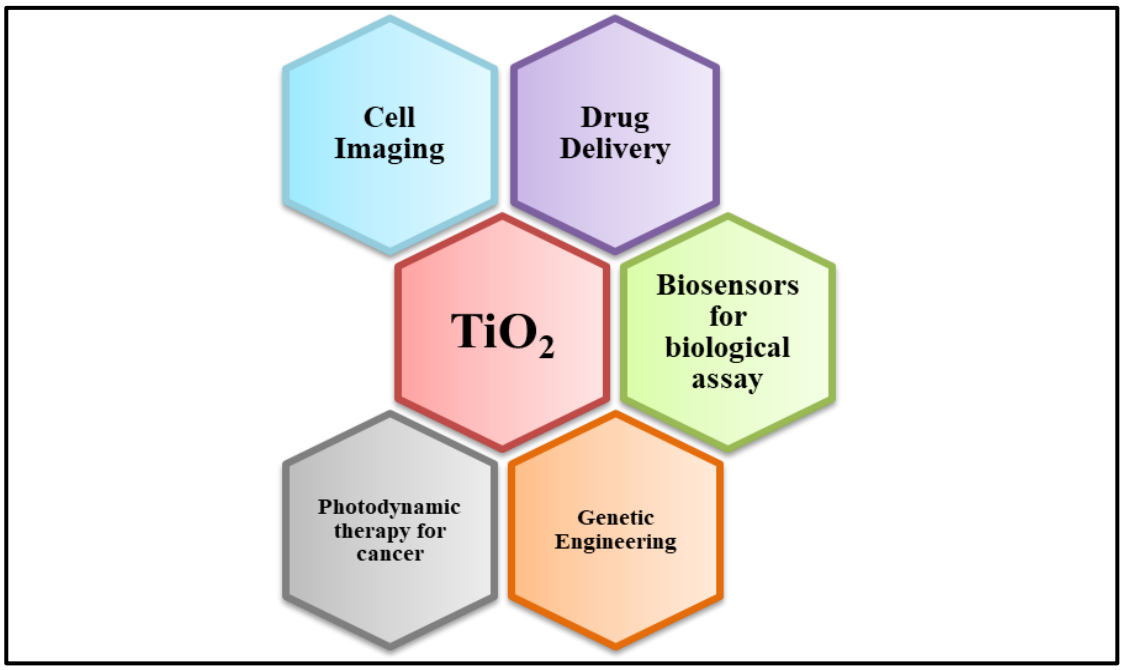

Figure 2.5: Applications of Titanium dioxide in biomedical field.

2.8 Biocompatibility

Hydroxyapetite (HAP) is widely recognized for its exceptional biocompatibility, making it one of the most valuable materials in biomedical applications. As a naturally occurring mineral form of calcium phosphate, HAP is the major inorganic component of human bone and teeth, which explains its inherent compatibility with biological systems. Its chemical composition and structure closely resemble that of natural bone, allowing it to interact harmoniously with surrounding tissues and cells. This structural similarity contributes significantly to its role in promoting Osseo integration the process through which bone grows onto and integrates with an

implant making it highly suitable for use in bone substitutes**,** orthopedic implants**,** dental applications**,** and bone tissue engineering [121].

2.9 Applications of hydroxyapetite

2.9.1 Cellular Response and Tissue Integration

One of the most crucial aspects of Hap's biocompatibility is its ability to promote cellular response. The surface of hydroxyapetite provides favorable sites for the attachment, proliferation, and differentiation of osteoblasts (bone-forming cells), leading to the formation of new bone tissue around the implant. The osteoconductivity of HAp, meaning its ability to support the growth of new bone along its surface, further enhances its effectiveness in promoting Osseo integration. This makes HAp an ideal material for bone grafts and bone scaffolds that support the regeneration of lost or damaged bone tissue. Additionally, osteocytes(mature bone cells) and osteoclasts (cells responsible for bone resorption) interact with the material to maintain healthy bone turnover and remodeling, which is crucial for maintaining long-term implant stability [122].

2.9.2 Non-toxic and Safe for Long-Term Use

HAP is considered non-toxic, chemically stable, and biologically inert within the body. Its degradation rate is slow, which means that it does not release harmful by-products that could cause adverse reactions or inflammation. Furthermore, as it closely resembles the inorganic matrix of natural bone, HAP can safely coexist with living tissue over extended periods, without inducing a foreign body response or immune rejection. These attributes make hydroxyapetite a favored material for biomaterials intended for long-term implantation, such as joint replacements**,** spinal implants, and dental restorations [123].

2.10 Applications of Al_2O_3-HAp-TiO_2 composite

The synergistic effect of combining aluminum oxide (Al_2O_3), titanium dioxide (TiO_2), and hydroxyapetite (HAP) in biomedical applications results in composite materials that exhibit enhanced mechanical, biological, and functional properties, making them suitable for a wide range of clinical applications. These materials combine the strength, durability and bioactivity needed for advanced medical implants, prosthetics, and tissue engineering.

2.10.1 Orthopedic Implants

The combinations of Al_2O_3, TiO_2, and HAP in orthopedic implants significantly enhance their mechanical strength and wear resistance, which is critical for load-bearing joints like hip and knee replacements. Aluminum oxide contributes superior hardness and fracture toughness, allowing the composite to endure high compressive forces without failure. Titanium dioxide improves the Osseo integration of the implant, ensuring a strong bond between the implant and surrounding bone. Additionally, the bioactivity of hydroxyapetite ensures that the implant supports bone growth, facilitating effective healing [124].

2.10.2 Dental Implants

In dental implants, the combination of these materials improves both the mechanical stability and biocompatibility of the implant, making it more effective in long-term oral applications. Aluminum oxide provides hardness and wear resistance, making dental implants more durable against biting forces and wear over time. Titanium dioxide enhances the implant's ability to integrate with the bone (Osseo integration), reducing the risk of implant rejection and ensuring long-term stability. The hydroxyapetite coating provides a bone-like surface that encourages bone formation and better bonding with the natural bone tissue [125].

2.10.3 Bone Regeneration and Tissue Engineering

The synergistic composite of Al_2O_3, TiO_2, and HAP is highly effective in bone regeneration and tissue engineering**.** Hydroxyapetite promotes bone growth and provides a structure similar to natural bone, acting as a scaffold for new tissue to grow. The addition of aluminum oxide and titanium dioxide enhances the mechanical properties of the composite, making it suitable for load-bearing bone scaffolds that can support weight during healing and regeneration. This composite is used in bone grafting applications, where it helps repair damaged or lost bone tissue. Additionally, the bioactive properties of TiO_2 and HAP encourage the differentiation of bone- forming cells (osteoblasts), improving the speed and quality of bone regeneration [126].

2.10.4 Drug Delivery Systems

The composite of Al_2O_3**,** TiO_2**,** and HAp can also be used in drug delivery systems**.** The biocompatibility of these materials allows them to be safely used for controlled and sustained drug release. Hydroxyapetite**'s** porous structure allows for the entrapment of drugs, while titanium dioxid**e's** surface modification potential can be utilized to target specific tissues. Aluminum oxide**,** with its excellent mechanical properties, ensures that the composite can withstand the forces of the body without degrading prematurely. These composites can be used for local drug delivery at the site of injury or disease, offering a more controlled and targeted therapeutic approach [127].

Table 2.4: Year wise literature for the raw material used for the synthesis of hydroxyapetite.

S. No.	Raw Material	Composition	Summary	Year-wise Literature	References
1	Eggshells	Calcium Carbonate	A sustainable waste-derived calcium source promoting eco-friendly hydroxyapetite production.	2007, 2024	[71,72]
2	Blast Furnace Slag	Calcium Silicates/Aluminate	Steel industry waste converted into composite materials for bone repair and tissue engineering.	2022, 2024	[82,81]
3	Lime Sludge	Calcium Hydroxide/Carbonate	Paper and pulp industry waste suitable for bone regeneration and bioceramic production.	2021, 2022	[78,77]
4	Limestone ($CaCO_3$)	Calcium Carbonate	A naturally abundant calcium source suitable for large-scale hydroxyapetite synthesis with good biocompatibility.	2017, 2020	[70,69]
5	Fish Scales and Bones	Calcium Phosphate	Fishery waste used for scaffolds, dental applications, and tissue engineering.	2016, 2019	[75,76]
6	Calcium Hydroxide ($Ca(OH)_2$)	Calcium	A pure and reactive calcium source enabling uniform precipitation and	2010, 2019	[61,62]

			phase purity in hydroxyapetite synthesis.		
7	Phosphoric Acid (H_3PO_4)	Phosphate	Acts as a controllable phosphate donor, influencing the crystallinity and morphology of HAP.	2014, 2018	[66,65]
8	Phosphogypsum ($CaSO_4$)	Calcium Sulfate	Byproduct from phosphate fertilizer production used for scaffolds, coatings, and drug delivery systems.	2017, 2018	[80,79]
9	Seashells	Calcium Carbonate	Marine waste-derived material suitable for bioceramics and bone tissue engineering.	2012, 2017	[73,74]
10	Calcium Nitrate ($Ca(NO_3)_2$)	Calcium	Provides a soluble calcium source that ensures strong bonding and homogeneous coating in HAP composites.	2007, 2010	[64,63]
11	Ammonium Phosphate ($(NH_4)_3PO_4$)	Phosphate	Maintains the desired Ca/P ratio, promoting stoichiometric and crystalline hydroxyapetite formation.	2004, 2019	[68,67]
12	Gypsum ($CaSO_4 \cdot 2H_2O$)	Calcium Sulfate	Fertilizer and cement industry byproduct used for bone graft materials and porous scaffolds.	1985, 1986	[85,86]

2.11 Research Gap

The potential of carbide lime, a by-product of the acetylene industry, as a biomaterial remains largely underexplored despite its promising characteristics. This material is abundant and calcium-rich, making it chemically aligned with substances like hydroxyapetite, which are widely used in biomedical applications such as bone repair and regeneration. However, research into its utilization has been minimal, leaving significant gaps in understanding its suitability and performance. Key areas of concern include the lack of established methods for processing and purifying carbide lime to meet the stringent biocompatibility and safety standards required for medical use. Furthermore, in this thesis the research has been done to optimize its structural and mechanical properties of hydroxyapetite for enhanced bioactivity and compatibility with by incorporating sintering additives. Additionally, studies investigating its biological performance, including cytotoxicity, bioactivity, and Biodegradation in vitro are scarce. There is also a noticeable gap in exploring its potential applications, such as its use in bone scaffolds, dental materials, or drug delivery systems. Beyond its biomedical potential, the dual advantage of reducing industrial waste while creating sustainable biomaterials has not been fully assessed, leaving a valuable opportunity untapped. These research gaps underscore the need for comprehensive and interdisciplinary studies to unlock the full potential of carbide lime in the biomedical field.

2.12 Hypothesis

After identifying the research gaps and thoroughly reviewing related literature, researchers may hypothesize that carbide lime, a byproduct of the acetylene industry, can be utilized for the synthesis of hydroxyapetite. When carbide lime is used in this way, it ensures the proper utilization of industrial waste, thereby reducing environmental pollution and promoting sustainable waste management. This strategy simultaneously addresses two major issues: effective waste management and the sustainable production of materials for hydroxyapetite (HAP) synthesis. Furthermore, incorporating aluminum oxide (Al_2O_3) and titanium dioxide (TiO_2) into

HAP composites produces a synergistic effect that markedly improves the material's mechanical strength, thermal stability, and biological performance. Each component contributes unique properties that enhance hydroxyapetite's overall functionality, making the composite highly suitable for advanced biomedical applications.

Carbide lime, generated as a byproduct during acetylene production, represents a promising alternative source of calcium for synthesizing hydroxyapetite (HAP). Its high calcium hydroxide content allows the transformation of industrial waste into a functional bioceramic, thereby minimizing environmental impact and encouraging sustainable material utilization. Hydroxyapetite produced from carbide lime demonstrates excellent purity, crystallinity, and bioactivity comparable to that obtained from conventional chemical sources, highlighting its potential as an environmentally friendly material for biomedical and environmental uses.

Aluminum oxide primarily acts as a mechanical reinforcement in HAP composites. It provides exceptional hardness (~15–20 GPa), compressive strength (~300–400 MPa), and wear resistance, which are crucial for improving the durability and toughness of HAP. Hydroxyapetite, while biocompatible and osteoconductive, is inherently brittle and unsuitable for load-bearing applications on its own. The inclusion of alumina addresses this limitation, making the composite strong enough to withstand mechanical stresses encountered in orthopedic implants and dental prostheses. Furthermore, the high thermal stability of Al_2O_3 ensures that the composite maintains its structural integrity during high-temperature sintering processes, which are often required for fabrication.

Titanium dioxide, on the other hand, brings unique advantages to the composite. TiO_2 enhances the fracture toughness of HAP composites while contributing to their thermal and mechanical stability. The polymorphic forms of TiO_2, particularly anatase and rutile, play distinct roles. Rutile TiO_2, with its compact and stable crystal structure, improves the overall stability of the material under physiological and mechanical conditions. TiO_2 also promotes better cell attachment and proliferation, contributing to the composite's biocompatibility and osteoconductivity.

When Al_2O_3 and TiO_2 are combined within a hydroxyapetite matrix, their complementary properties create a highly functional composite. The dual reinforcement enhances the material's toughness and wear resistance, ensuring longevity and performance in load-bearing applications. Al_2O_3 provides the strength required for mechanical stability, while TiO_2 contributes to improved fracture toughness and antibacterial properties, making the composite versatile and reliable in various biomedical contexts.

The synergistic role of these reinforcements also extends to the processing and fabrication of the composite. Both Al_2O_3 and TiO_2 exhibit high thermal stability, enabling the composite to undergo sintering at elevated temperatures without significant degradation. This leads to better particle bonding and a uniform microstructure, which are essential for achieving optimal mechanical properties. Additionally, the combined effect of Al_2O_3 and TiO_2 reduces the porosity of the composite, further improving its mechanical performance and durability.

From a biological perspective, the composite benefits from the combined contributions of Al_2O_3 and TiO_2. While hydroxyapetite ensures osteoconductivity and bone integration, Al_2O_3 enhances biocompatibility, and TiO_2 adds bioactive properties that promote healing and minimize the risk of infection. These characteristics make the composite particularly suitable for biomedical applications such as orthopedic implants, bone grafts, and dental restorations, where both mechanical strength and biological performance are essential. As a result, this advanced composite material is projected to emerge as a next-generation biomaterial for biomedical applications, offering a sustainable, high-performance solution for various medical and dental fields.

Chapter III

RESEARCH OBJECTIVES

AND MATERIAL METHODS

RESEARCH OBJECTIVES

1. Isolation and characterization of the carbide lime from the acetylene industry.

2. Chemical synthesis and control of process parameters for the synthesis of hydroxyapetite.

3. Characterization of the hydroxyapetite synthesis from carbide lime.

4. Development of mechanical strength in synthesized hydroxyapetite.

5. In vitro study of the hydroxyapetite and study of its biocompatibility.

3. Materials and methods

This chapter begins with the collection and purification of carbide lime, a waste material from the acetylene industry, using a dilution method. Before purification carbide lime undergoes characterization. The purification process yields calcium hydroxide, which is then characterized using various techniques, including X-ray Diffraction (XRD), Fourier Transform Infrared Spectroscopy (FTIR), and Field Emission Scanning Electron Microscopy (FESEM).The synthesis of hydroxyapetite from the carbide lime waste is then successfully carried out, with its characterization detailed through XRD, FTIR, FESEM, Thermo gravimetric Analysis (TGA), and particle size analysis. To enhance the mechanical properties of the hydroxyapetite, sintering is performed by incorporating sintering additives such as aluminum oxide and titanium dioxide and their impact on sintered density, relative density, bulk density, porosity, and linear shrinkage is briefly discussed using the Taguchi L25 orthogonal array. Finally, in vitro studies including biocompatibility, cell viability, and biodegradation are also discussed.

PART 1: Isolation and characterization of carbide lime from acetylene industry.

3.1 Collection of sample

Carbide lime, a byproduct of the acetylene industry, was collected from J.K. Enterprises located on Jalandhar Road, Nasrala, Hoshiarpur, Punjab, India, 146001.

3.1.1 Geographical location of the industry

J.K. Enterprises is situated in Punjab, on Jalandhar Road, Nasrala, and Distt. Hoshiarpur, 146001. The geographical coordinates of the industry are 31°29'49.9"N latitude and 75°50'03.4"E longitude.

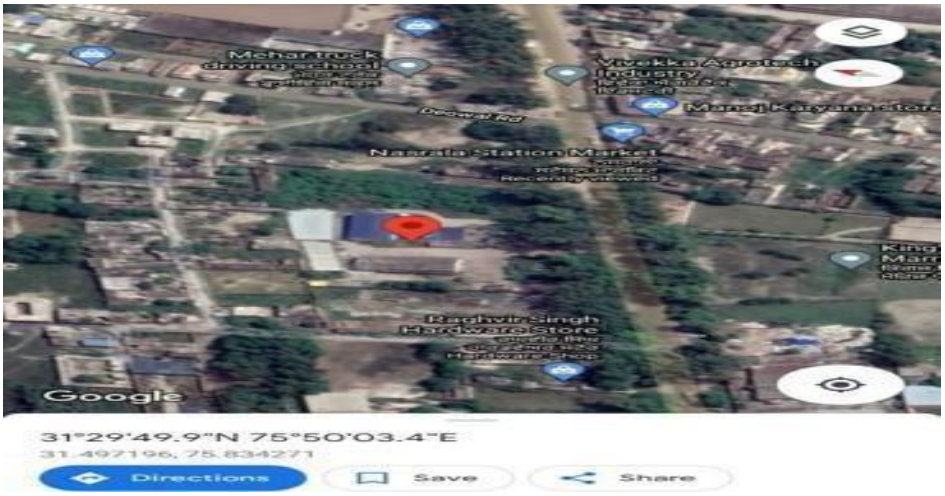

Figure 3.1: Geographical location of J.K. Enterprises an acetylene industry

3.1.2 Procedure for sample collection

Carbide lime was collected following a visit to an acetylene production industry. Calcium carbide reacts with water to produce acetylene gas and calcium hydroxide slurry, commonly referred to as carbide lime. In acetylene production facilities, carbide lime slurry is managed through a series of ponds designed to facilitate moisture reduction and material solidification. Initially, the high-moisture-content slurry is deposited into the first pond. As water evaporates, the slurry's moisture content decreases, allowing it to be transferred to the second pond for continued drying. Subsequently, the partially dried slurry is moved to the third pond, where it undergoes further evaporation and solidifies into a more stable form. This solidified carbide lime can be repurposed for various applications, including use in construction materials like concrete and bricks, pH adjustment of industrial acids, or disposal. Figure 3.2 illustrates the collection process of carbide lime in the acetylene industry.

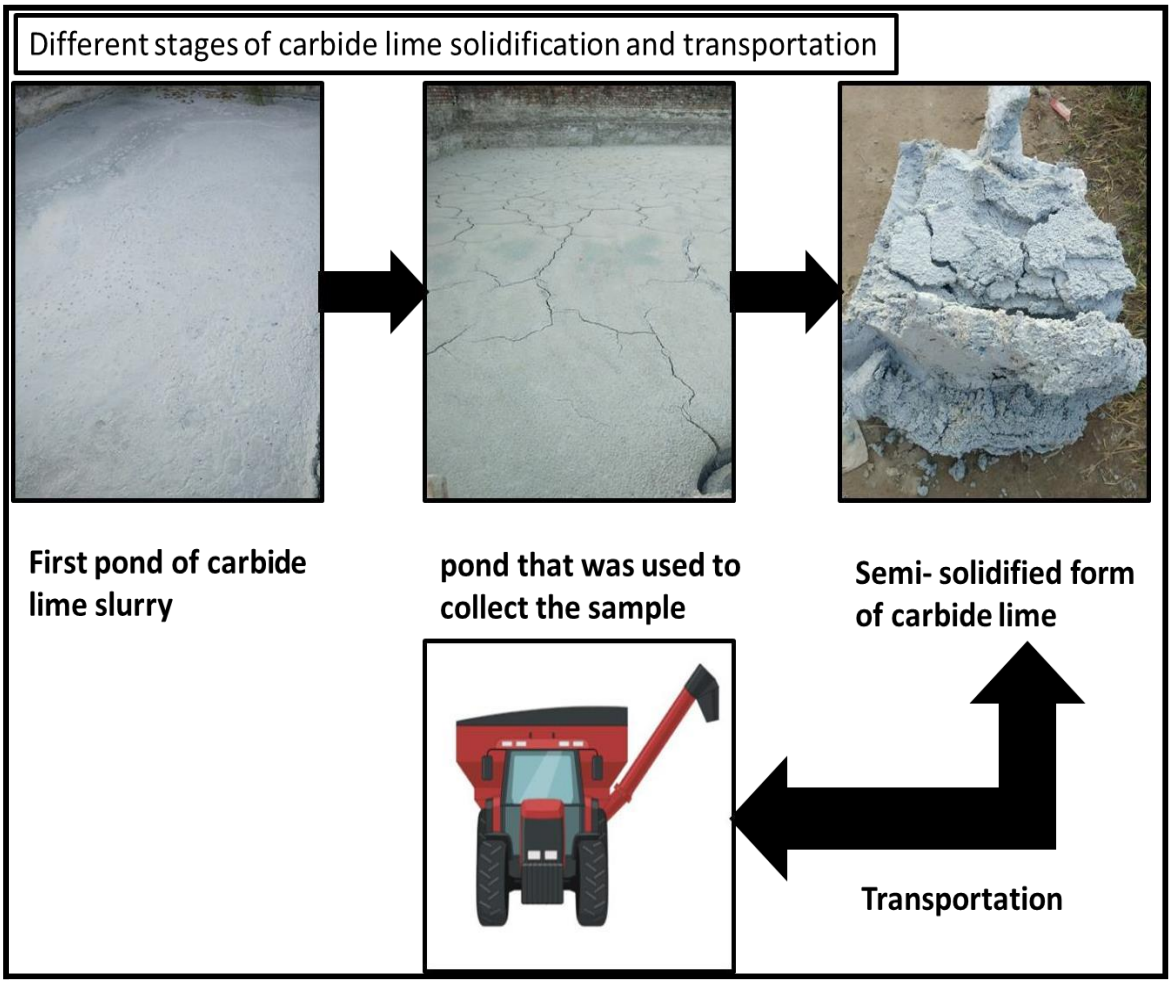

Figure 3.2: Procedure for the collection of carbide lime from an acetylene industry.

For our research, samples were collected from the third pond, where semi-solidified carbide lime was stored. Samples were gathered from five different points within the pond, combined, and sun-dried for two to three days. Subsequently, the samples were dried overnight at 60°C in an oven. Once fully dried, the material was ground using a mortar and pestle, sieved through an 80 μm sieve, and prepared for characterization via X-ray diffraction (XRD), Fourier-transform infrared spectroscopy (FTIR), and field emission scanning electron microscopy (FESEM). Figure 3.3 depicts the collection, drying, and characterization processes of carbide lime.

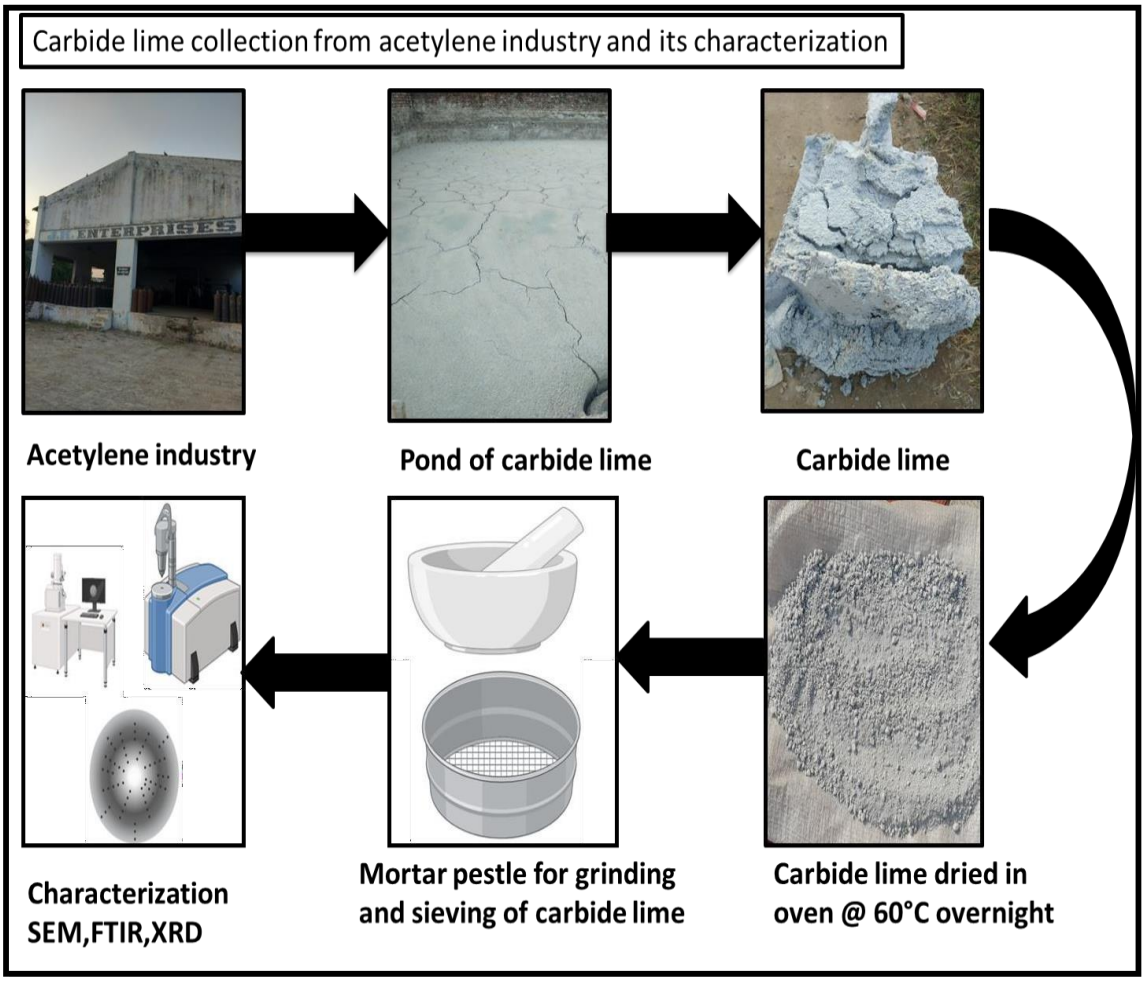

Figure 3.3: Carbide lime collection from an acetylene industry and its characterization.

PART 2: Chemical synthesis and control of process parameters for the synthesis of hydroxyapetite.

3.2 Extraction of calcium hydroxide from carbide lime by dilution method

Calcium hydroxide ($Ca(OH)_2$) was extracted from carbide lime by dissolving it in distilled water at varying dilution ratios and time intervals. The carbide lime, a byproduct of acetylene production, contains primarily calcium hydroxide along with some impurities like calcium carbonate ($CaCO_3$), unreacted calcium carbide (CaC_2), and silica. First of all, 1 g of carbide lime was accurately weighed using an analytical balance and transferred to a 250 mL beaker. Distilled water was then added in different ratios to the carbide lime, specifically 1:100, 1:200, 1:300, 1:400,

1:500, 1:600, 1:700, 1:800, 1:900, and 1:1000 (g/mL). These dilution ratios were prepared by adjusting the volume of water, ranging from 100 mL to 1000 mL, to create suspensions of varying concentrations of carbide lime in the water [129].

Each mixture was stirred vigorously using a magnetic stirrer for 5 minutes to ensure thorough dispersion of the carbide lime in the water. The beakers were then left at room temperature to react for different time periods: 6, 12, or 24 hours. Over time, the carbide lime dissolved to form a milky white suspension known as limewater, which contained both dissolved calcium hydroxide and undissolved particles of calcium hydroxide. Figure 3.4 explains the protocol for the extraction of calcium hydroxide from carbide lime by dilution method.

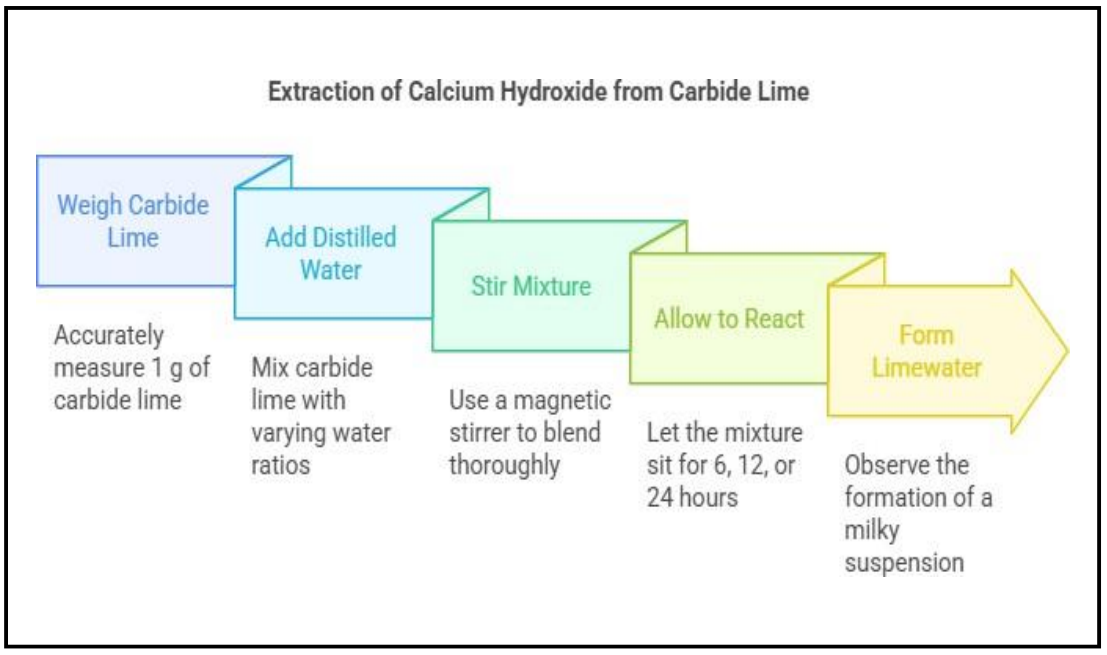

Figure 3.4: Extraction of calcium hydroxide by dilution method.

3.2.1 Reaction of carbide lime with water

The reaction of carbide lime (also known as calcium hydroxide, $Ca(OH)_2$) with water is relatively straightforward. Carbide lime itself is a byproduct from the reaction of calcium carbide (CaC_2) with water, and it typically contains a high percentage of calcium hydroxide [130].

When calcium hydroxide ($Ca(OH)_2$) interacts with water, it dissolves slightly to form

a limewater solution. The process can be represented by the following reaction:

$$Ca(OH)_2(s) + H_2O\ (l) \rightleftharpoons Ca^{2+}\ (aq) + 2OH^-(aq) \quad (1)$$

After the reaction time had ended, the mixtures were allowed to settle for approximately 30 minutes to allow any solid impurities, such as calcium carbonate or unreacted materials, to settle at the bottom of the beaker. The clear upper liquid known as the supernatant was carefully decanted into a separate clean container, leaving the solid residue behind. The decanted supernatant, which contained dissolved calcium hydroxide, was then filtered through Watman filter paper no. 42 to remove any remaining fine suspended particles using a vacuum filter.

3.3 Synthesis of hydroxyapetite by Wet precipitation method

Step 1: Preparation of Calcium Hydroxide Solution

Calcium hydroxide ($Ca(OH)_2$) was extracted from carbide lime using the dilution method, resulting in a fine powder. This powder was then subjected to calcination in a muffle furnace (Steel Fab engineers, model no. S-9335) at 800°C for 2 hours, a process intended to remove residual impurities and convert calcium hydroxide to calcium oxide (CaO) by releasing water molecules. Subsequently, the purified (CaO) was rehydrated by carefully adding it to water during the synthesis process, converting it back to ($Ca(OH)_2$). This two-step process ensures that the calcium hydroxide used in hydroxyapetite synthesis is of high purity, free from impurities present that are in the original carbide lime. The chemical transformations involved in this process are as follows:

Calcination:

$$Ca(OH)_2(s) \rightarrow CaO\ (s) + H_2O\ (g) \quad \text{----------(2)}$$

Rehydration:

$$CaO\ (s) + H_2O\ (l) \rightarrow Ca(OH)_2(l) \quad \text{----------(3)}$$

Step 2: Preparation of Phosphate Solution

The phosphate was obtained from 85% orthophosphoric acid provided by Loba Chemie Pvt. Ltd, India.

Step 3: Mixing of Calcium and Phosphate Solutions

Hydroxyapetite (Ca_{10} $(PO_4)_6(OH)_2$ is synthesized by gradually adding calcium hydroxide ($Ca(OH)_2$ to 85% orthophosphoric acid (H_3PO_4) under continuous stirring using magnetic stirrer with hot plate (Manti lab solutions/model no.MT-142) maintaining a Ca/P molar ratio of 1.67.

Step 4: Precipitation and Aging

During the titration process, the resulting $Ca(OH)_2$ was titrated with 85% orthophosphoric acid at temperatures between 40–60°C using a magnetic stirrer, ammonium hydroxide (NH_4OH) was added to maintain a pH above 10 throughout the titration. After the titration was complete, the mixture was left to age at room temperature overnight. Once the reaction was complete and all the orthophosphoric acid was added to the calcium hydroxide solution, precipitation occurred, confirming the formation of calcium phosphate.

Step 5: Filtration and Washing

The calcium phosphate precipitates are then filtered using a filter paper no. 42 to separate the white precipitates from the liquid phase. The precipitate is then thoroughly washed thrice with distilled water to remove excess ammonium hydroxide and other unwanted impurities. This washing process ensures that the final product is free from any undesired impurities that could interfere with the quality of the hydroxyapetite.

Step 6: Drying the Precipitate

After washing, the calcium phosphate precipitate is dried in hot air oven (Bharat instruments and chemicals/ model no. HAO-45) at a temperature of around 60–80°C for 5 to 6 hours to remove remaining moisture. This results in a fine, dry powder of calcium phosphate.

Step 7: Calcination

The dried calcium phosphate is then subjected to calcination at a temperature of 800°C in muffle furnace (Steel Fab engineers, model no. S-9335) for 2 hours. This step is crucial for converting the calcium phosphate into hydroxyapetite ($Ca_{10}(PO_4)_6(OH)_2$). During calcination, the calcium phosphate undergoes a solid-state reaction, where the phosphate ions react with the calcium ions to form the hydroxyapetite structure. The heat treatment also helps to promote the crystallization of hydroxyapetite, ensuring that the material has the desired properties for biomedical applications [131]. The reaction between calcium hydroxide and orthophosphoric acid can be represented as follows:

$10Ca(OH)_2+6H_3PO_4 \rightarrow Ca_{10}(PO_4)6(OH)_2+8H_2O$----------(4)

Step 8: Characterization

After calcination, the resulting hydroxyapetite is allowed to cool to room temperature. The final product is then characterized using various techniques, such **as** X-ray diffraction (XRD)**,** scanning electron microscopy (SEM) and Fourier transform infrared spectroscopy (FTIR)**.**Field Emission Scanning Electron Microscope (FESEM), Thermo gravimetric analysis (TGA) [132].

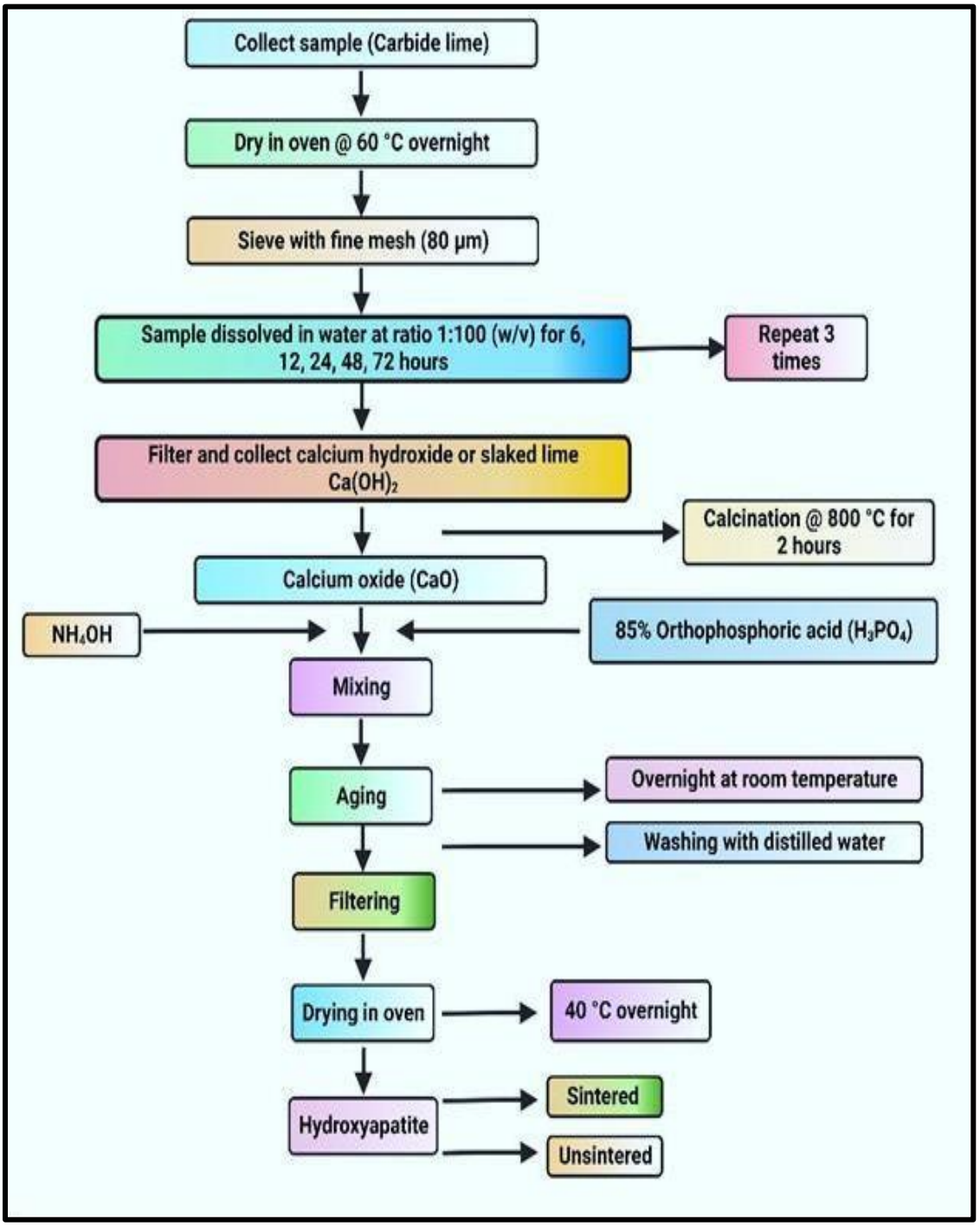

Figure 3.5: The flow chart shows the detailed procedure for synthesizing HAp using the chemical precipitation method [129,131].

3.3.1 Production of hydroxyapetite at industrial scale

To scale up the production of hydroxyapetite (HAP) from carbide lime while maintaining a Ca:P molar ratio of 1.67, the laboratory wet-precipitation method can be adapted for industrial-scale operations. Initially, carbide lime a byproduct of the acetylene industry is pretreated by washing, drying, and sieving using industrial washing tanks, rotary dryers, and vibrating sieves to remove impurities and standardize particle size. The material is then hydrated and dissolved in water to form a uniform calcium hydroxide [$Ca(OH)_2$] slurry in large-capacity mixing tanks equipped with agitators**,** which acts as the calcium source, phosphate solution, such as ammonium phosphate ($(NH_4)_2HPO_4$) or orthophosphoric acid (H_3PO_4), is prepared in stirred solution tanks**.**

The calcium and phosphate solutions are combined in a continuous stirred-tank reactor (CSTR)**,** maintaining a Ca:P molar ratio of 1.67, pH between 9 and 11, and a temperature of 25–60 °C. Controlled mixing and gradual addition of reagents are essential to prevent local supersaturation and ensure uniform nucleation of HAP particles.

Following precipitation, the slurry is aged for 1–12 hours to promote crystal growth and structural stability. Solid-liquid separation is achieved using industrial filter presses or decanter centrifuges, and the collected HAP precipitate is washed multiple times with distilled water in washing tanks to remove residual ions. The washed material is dried using tray dryers or spray dryers**.** To enhance crystallinity and purity, the dried powder is calcined in industrial muffle furnaces at around 800 °C for approximately two hours, as optimized in laboratory studies, and subsequently milled using ball mills or jet mills and sieved to achieve the desired particle size distribution.

PART 3: Characterization of the hydroxyapetite synthesized from carbide lime

3.4 Characterization

3.4.1 X-Ray diffraction Analysis (XRD)

All the samples, including carbide lime, extracted calcium hydroxide, calcium oxide, synthesized hydroxyapetite, and calcined hydroxyapetite, were submitted as powder to the Central Instrumental Facility at Lovely Professional University, India, for XRD characterization. This was done to analyze the crystal structure, composition, and material properties using Bruker D8 Advance Diffractometer instrument (Bruker, USA) with CuKα radiation. With the copper target, the voltage and current were set at 35 kV and 30 mA, respectively. The step size was 0.020 (2θ), and each step had a count time of one second. The X-ray intensity (counts/sec) was plotted against the angle theta (θ) [133].

3.4.1.1 Working of X-ray Diffraction

The basis of X-ray diffraction techniques is the observation of the scattered intensity of an X-ray beam contacting a sample as a function of wavelength or energy, incident and scattered angle, and polarization. To prepare for the X-ray tube to irradiate a powdered mineral sample, it is packed on a sample stage. An electronic detector is positioned on the other side of the sample from the X-ray tube, and the sample is rotated to create angles ranging from 0 to 90° in order to detect the diffracted X-rays. A goniometer is the device that rotates the detector as well as the X-ray tube. The detector captures the rate of X-rays exiting the opposite side of the sample (in counts/sec) and transmits this data to the computer, while the goniometer measures the angle θ. A powder X-ray diffraction research is used to identify the various phases. With the copper target, the voltage and current were set at 35 kV and 30 mA, respectively. The step size was 0.020 (2θ), and each step had a count time of one second. The X-ray intensity (counts/sec) was plotted against the angle theta (θ) following the sample scan.

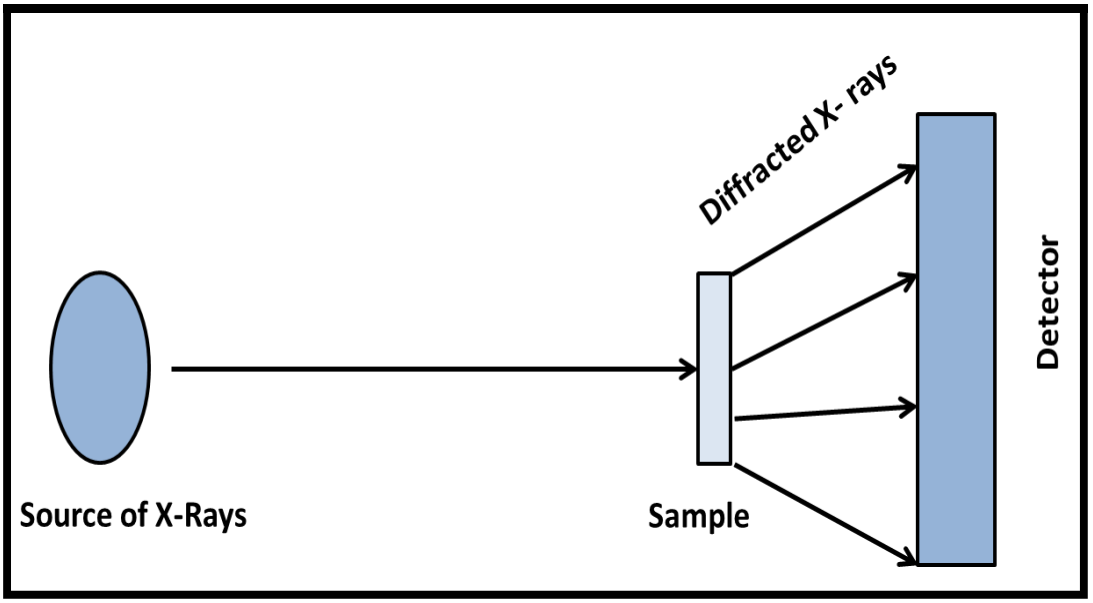

Figure 3.6: Working of X- Ray Diffraction

3.4.2 Fourier Transformed Infrared Radiation (FTIR) Analysis

The samples comprising carbide lime, extracted calcium hydroxide, calcium oxide, and calcined hydroxyapetite, were provided in powder form for FTIR analysis to the Central Instrumental Facility at Lovely Professional University, India by using Bruker Tensor 27 I.R. series. FTIR is used to identify the chemical composition and how they absorb infrared light, helping to detect specific functional groups, impurities, and changes in molecular structure.

3.4.2.1 Working of Fourier Transformed Infrared Radiation (FTIR)

FTIR (Fourier Transform Infrared Spectroscopy) operates by directing infrared light through a sample and analyzing the absorption at various wavelengths. The process begins with an infrared light source that emits a range of wavelengths. When the light interacts with the sample, the molecules absorb specific wavelengths based on the types of chemical bonds and functional groups present in the material. Each bond type absorbs light at characteristic frequencies. The light that passes through the sample is then detected by a sensor, which measures the absorption at each wavelength. The raw data collected is processed using a mathematical technique called Fourier Transform, which converts it into a spectrum. The

resulting spectrum displays absorption peaks that correspond to specific functional groups and bonds in the sample, providing valuable information about the chemical composition and molecular structure of the material [134].

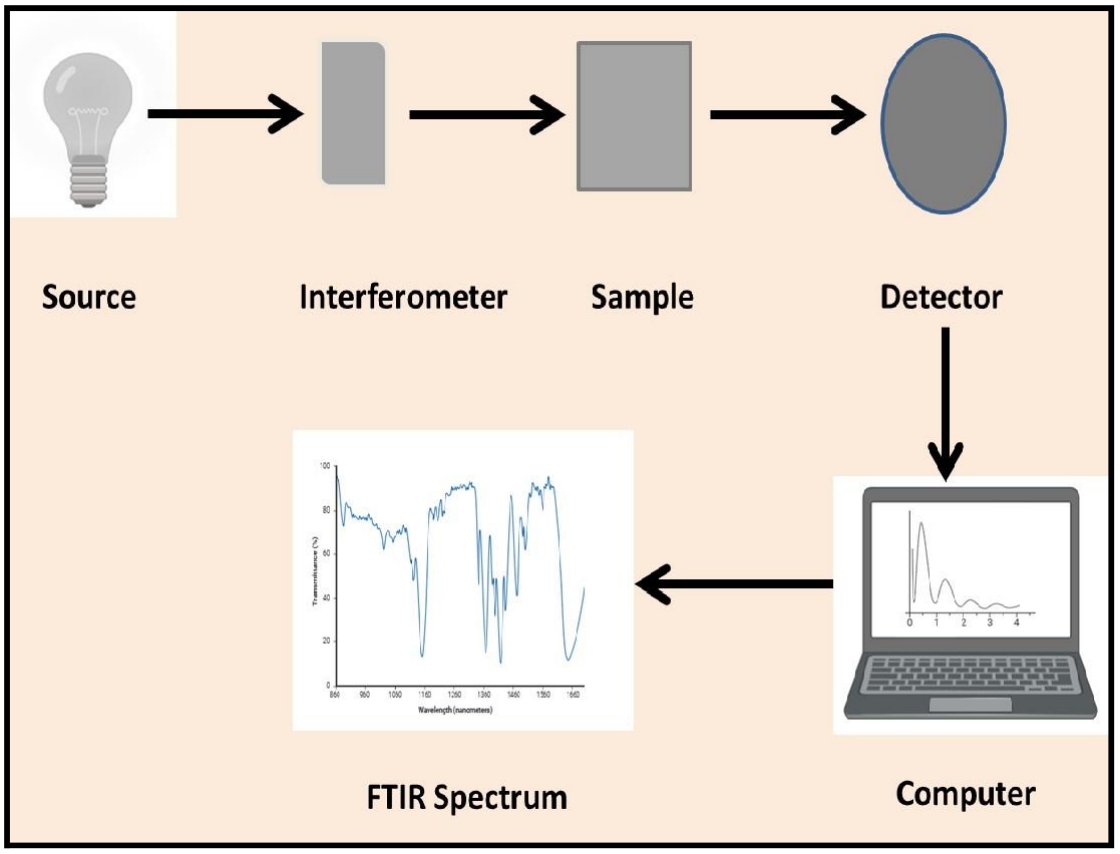

Figure 3.7: Overview of Fourier Transformed Infrared Spectroscopy.

3.4.3 Field Emission Scanning Electron Microscopy (FESEM) with Energy Dispersive X-ray analysis (EDX)

The samples of carbide lime and synthesized hydroxyapetite were provided in powder form to the Central Instrumental Facility at Lovely Professional University, India, for Field Emission Scanning Electron Microscope (FESEM) analysis. To examine the morphology of carbide lime and synthesized hydroxyapetite, as well as their elemental composition, EDX analysis was performed by FESEM JOEL.

3.4.3.1 Working of Field Emission Scanning Electron Microscope

Field Emission Scanning Electron Microscopy (FESEM) combined with Energy-Dispersive X-ray Spectroscopy (EDX) is a powerful analytical technique that allows for the detailed study of a sample's surface morphology and elemental composition at high magnifications. FESEM utilizes a focused electron beam generated by a field emission gun (FEG) to scan the sample. The electron beam is accelerated and directed towards the sample, where it interacts with the surface, generating various signals such as secondary electrons, backscattered electrons, and X-rays. The secondary electrons, in particular, are used to create high-resolution images of the sample's surface morphology, revealing fine details about the texture, structure, and surface features at the Nano scale [135].

In addition to providing detailed surface images, FESEM can be paired with EDX for elemental analysis. When the electron beam interacts with the atoms in the sample, it excites the atoms, causing them to emit X-rays. These X-rays have characteristic energies that correspond to the elements' unique atomic structure. The emitted X-rays are detected by the EDX detector, which measures the energy of each X-ray and identifies the specific elements present in the sample. The resulting X-ray spectrum provides peaks that represent the elemental composition of the sample, allowing for both qualitative and quantitative analysis of the material.

The combination of FESEM and EDX provides a comprehensive analysis of a material's surface. FESEM offers detailed imaging of the sample's morphology, while EDX complements this by identifying the elemental composition at specific locations on the surface [136].

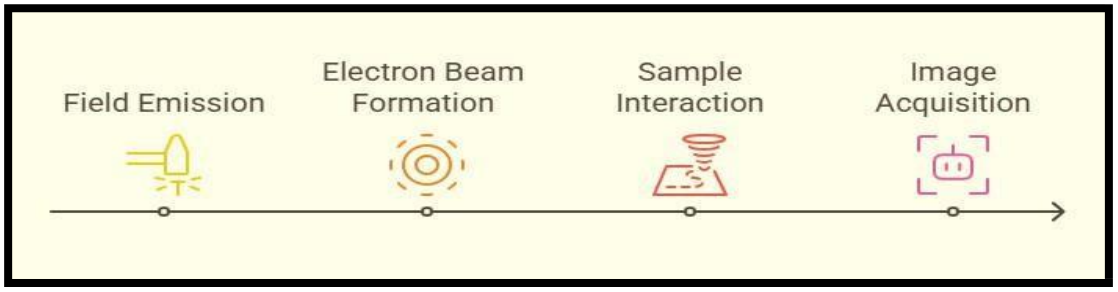

Figure 3.8: Working of Field Emission Scanning Electron Microscope

3.5 Thermo gravimetric analysis (TGA)

Thermo gravimetric analysis of carbide lime and synthesized hydroxyapetite was carried out by thermo gravimeter by Perkin Elmer. The powder samples of carbide lime and synthesized hydroxyapetite was submitted in central instrumental facility of Lovely Professional University. The thermal stability and phase transitions of hydroxyapetite (HAp) have been evaluated using thermo gravimetric analysis (TGA). By measuring weight changes as a function of temperature, TGA was able to obtain information about Hydroxyapetite stability, moisture loss, and breakdown. A thermal analyzer with a heating rate of 10°C/min up to 1000°C was used for the analyses, which were carried out in a controlled environment (air). These studies yielded important details regarding the thermal behavior of HAp, such as its breakdown temperature and the impact of impurities or carbonate groups on its thermal properties.

3.5.1 Working of Thermo gravimetric analysis

Thermo gravimetric Analysis (TGA) is a powerful analytical technique used to measure the change in weight of a sample as it is heated or cooled, providing valuable insights into the material's thermal stability and composition. The process begins with the preparation of a small sample, typically weighing just a few milligrams, which is placed in a sample pan. This pan is then positioned inside a controlled furnace or heating chamber. The sample is subjected to a specific temperature program, where it is heated or cooled at a controlled rate, such as 5°C to 50°C per minute. The temperature range can extend from room temperature up to 1000°C or higher, depending on the material being analyzed.

As the sample is heated, the TGA instrument continuously measures any changes in the sample's weight. A highly sensitive balance is used to detect mass loss or gain during the thermal process. Various thermal events may occur as the sample undergoes heating, such as dehydration (loss of water), decomposition (breaking down of chemical bonds with mass loss), oxidation/reduction reactions

(causing changes in weight), or sublimation (transition from solid to gas without passing through a liquid phase). These events cause specific weight changes that are closely monitored [137].

The data obtained from the analysis is presented as a graph, where weight loss (%) is plotted against temperature (°C)**.** Peaks or steps in the curve indicate significant thermal events, such as dehydration or the onset of decomposition. By interpreting these changes, researchers can gain valuable information about the sample's thermal behavior, composition, and stability. TGA is particularly useful for determining the decomposition temperature of materials, assessing the presence of volatile compounds, and understanding the overall thermal properties of a substance.

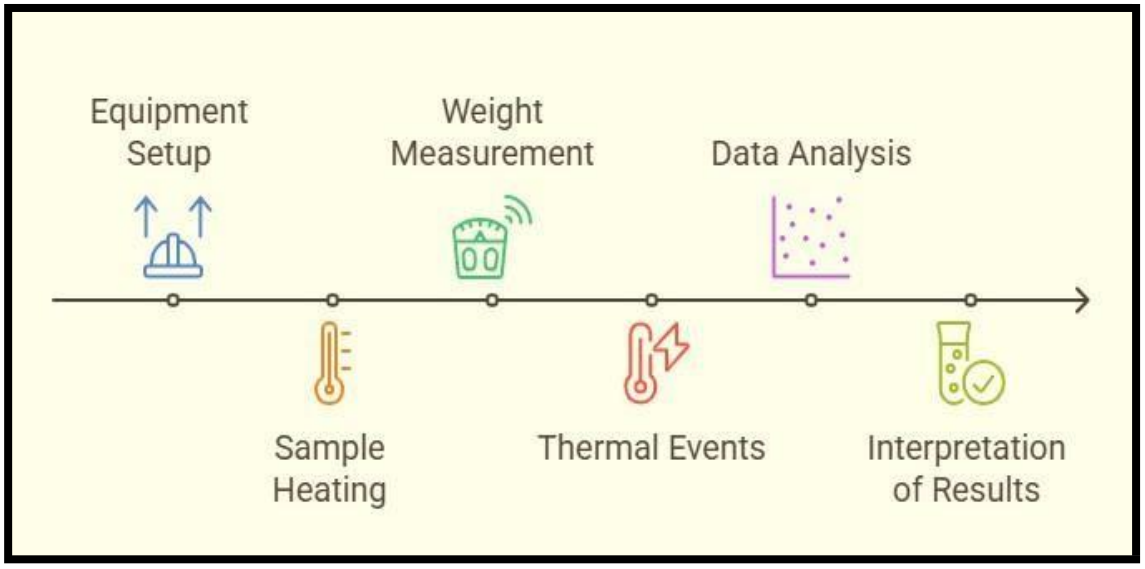

Figure 3.9: working of Thermo gravimetric analysis (TGA)

3.6 Dynamic Light Scattering (DLS)

The sample calcined hydroxyapetite, was submitted for particle size analysis to the Central Instrumental Facility at Lovely Professional University, India by Malvern.

Dynamic Light Scattering (DLS) is a technique used to measure the size distribution of particles in suspension, particularly in the nanometer range. The method operates based on the principle of light scattering, where a laser light is directed at a sample containing nanoparticles or colloidal particles. The particles in the sample scatter

the light, and the intensity of this scattered light fluctuates over time due to the random Brownian motion of the particles. Detectors measure the intensity of the scattered light at various angles, capturing the fluctuations caused by particle movement. The rate of these fluctuations is then analyzed to determine the diffusion rate of the particles, which is related to their size. Using the Stokes-Einstein equation, the diffusion coefficient is converted into particle size, and a particle size distribution is generated, typically displayed as a graph of particle size versus intensity or number. This allows for a comprehensive analysis of the sample's size characteristics. DLS is a non-invasive and effective method widely used in applications such as drug delivery, colloidal chemistry, and materials science to determine the size distribution of nanoparticles [138].

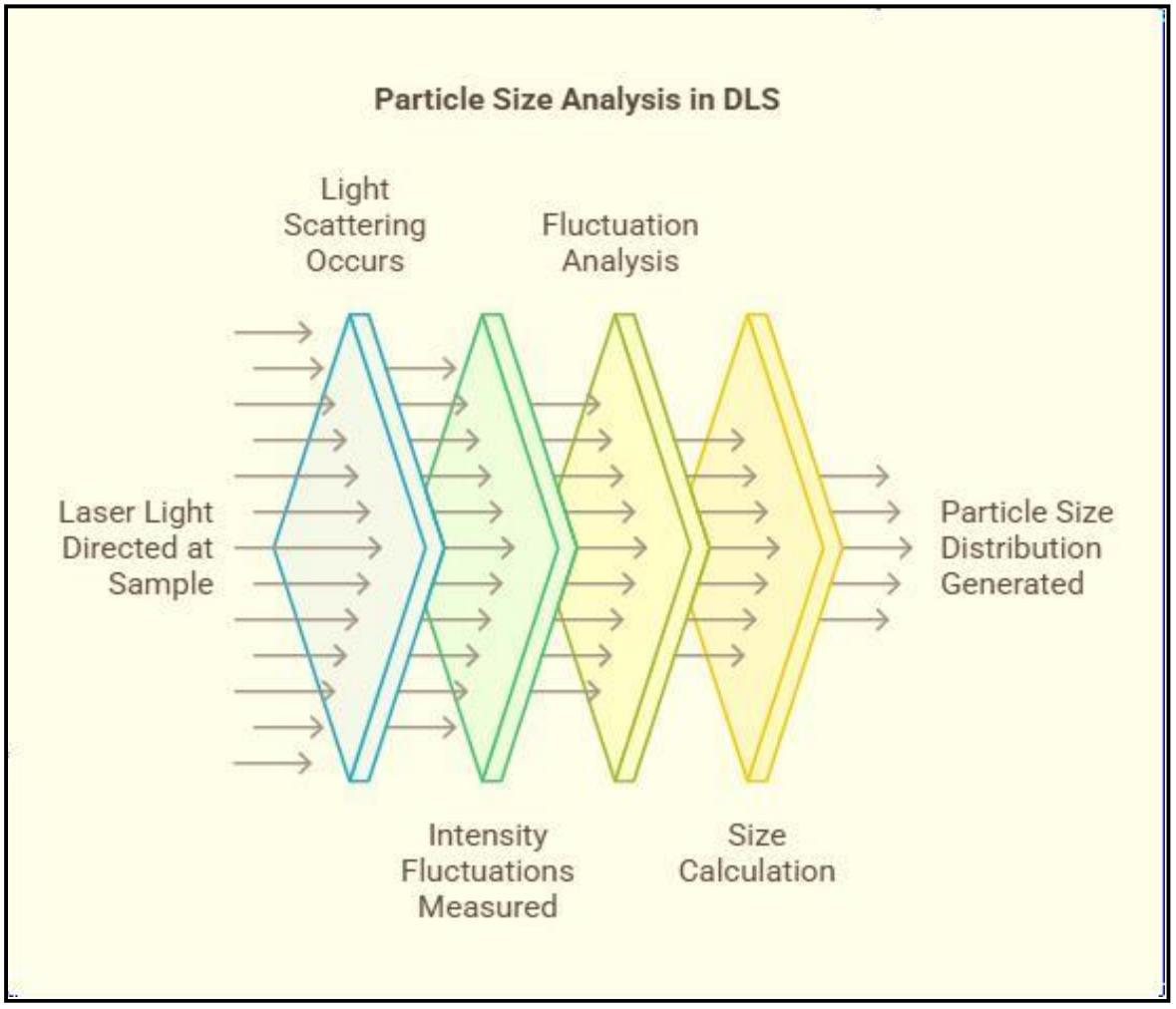

Figure 3.10: working of dynamic light scattering

PART 4: Development of mechanical strength in synthesized hydroxyapetite

3.7 Sintering

Sintering is a crucial process in the fabrication of hydroxyapetite (HAp) ceramics, where the material is heated to a temperature below its melting point to promote bonding between particles, reduce porosity, and increase density and strength**.** During sintering, the individual hydroxyapetite particles coalesce, and as the temperature rises, diffusion and grain growth occur, resulting in a more solid and mechanically robust structure. The porosity decreases, which improves the overall density and crystallinity of the material, leading to stronger, more durable hydroxyapetite [139].

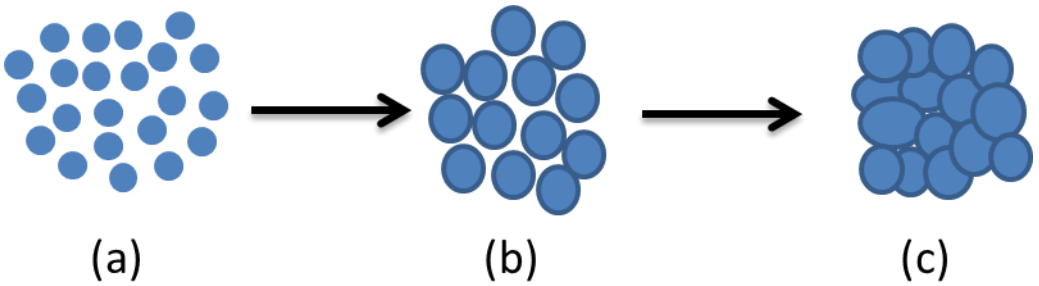

Figure 3.11: Different stages of sintering as the temperature increases (a) Loose Hydroxyapetite particles (b) Pores decreases (c) Densification of particles.

3.7.1 Need to add sintering additives

However, despite its biocompatibility and bioactivity, pure hydroxyapetite has limited mechanical strength and is relatively brittle, making it unsuitable for high-stress applications. To overcome these limitations, sintering additives are often required. Some of the sintering additives used to enhance the mechanical strength of hydroxyapetite include aluminum oxide (Al_2O_3), titanium dioxide (TiO_2), zirconium oxide (ZrO_2), Magnesium oxide and silica. These additives help to enhance the hydroxyapetite's mechanical properties by reinforcing the material's structure and improving its densification during the sintering process [140]. In this research, a ternary blend was made by incorporating two additives, aluminum oxide (Al_2O_3) and titanium dioxide (TiO_2) purchased from Loba Chemie Pvt. Ltd. India, with

hydroxyapetite synthesized from carbide lime. The weight percentage ratios of Al_2O_3, TiO_2, and by keeping HAp constant, as outlined in the table below, were systematically varied. Experiments were conducted at five different temperatures 900, 950, 1000, 1050, and 1100°C along with soaking durations of 1, 2, 3, 4, and 5 hours. These parameters were optimized using the Taguchi L25 orthogonal array. The inclusion of these additives helps improve the sintering behavior, allowing the hydroxyapetite to achieve higher sintered density and strength without compromising its bioactivity.

Table 3.1: Different weight percentage of sintering additives used

S No	Aluminium oxide (Al_2O_3) (wt %)	Titanium dioxide (TiO_2) (wt %)	HAp (wt %)
1	20	10	70
2	22	8	70
3	24	6	70
4	26	4	70
5	28	2	70

3.8 Taguchi orthogonal array

Taguchi orthogonal arrays are a systematic method used in experimental design to optimize processes, products, or systems by studying the effects of multiple factors simultaneously. Developed by Japanese engineer Genichi Taguchi, these arrays help identify the most influential factors affecting a system's performance while minimizing the number of experiments required [141]. In this research the Taguchi L25 orthogonal array were opted because number of factors was five. The optimized table, derived from applying the Taguchi L25 orthogonal array, is given below.

Table3.2: Ratios optimized using Taguchi L25 orthogonal array.

S No	Aluminium oxide+ Titanium dioxide (wt %)	Temperature (°C)	Time (Hours)
1	20+10	900	1
2	20+10	950	2
3	20+10	1000	3
4	20+10	1050	4
5	20+10	1100	5
6	22+8	900	2
7	22+8	950	3
8	22+8	1000	4
9	22+8	1050	5
10	22+8	1100	1
11	24+6	900	3
12	24+6	950	4
13	24+6	1000	5
14	24+6	1050	1
15	24+6	1100	2
16	26+4	900	4
17	26+4	950	5
18	26+4	1000	1
19	26+4	1050	2
20	26+4	1100	3
21	28+2	900	5
22	28+2	950	1
23	28+2	1000	2
24	28+2	1050	3
25	28+2	1100	4

3.9 Preparation of the Ternary blend

To prepare the ternary blend, the synthesized HAP powder was calcined at 800°C for 2 hours in a muffle furnace. The calcined hydroxyapetite, aluminum oxide, and titanium dioxide were selected based on the Taguchi L25 orthogonal array [142]. All the powders were sieved using a sieve having (mesh size 80 µ) and then mechanically milled in a Falcon tube with stainless steel balls, maintaining a ball-to-powder ratio of 20:1. The mixture was vortexes for 25-30 minutes using a vortex shaker. For the formation of green pellet, the ternary mixture, prepared according to the weight percentages specified in the Taguchi L25 orthogonal array, was then compacted using a 13 mm cylindrical die in a 5-ton high-carbon steel mold for one minute with a KBR hydraulic Press machine. The die was cleaned with acetone and stearic acid before placing the samples inside. The uniaxially pressed samples were transferred to a vacuum desiccator, where air was evacuated using a vacuum pump. Each sample was then isostatically compressed at 5 ton pressure for two minutes. The pellets were formed in triplicates for each ratio [143].

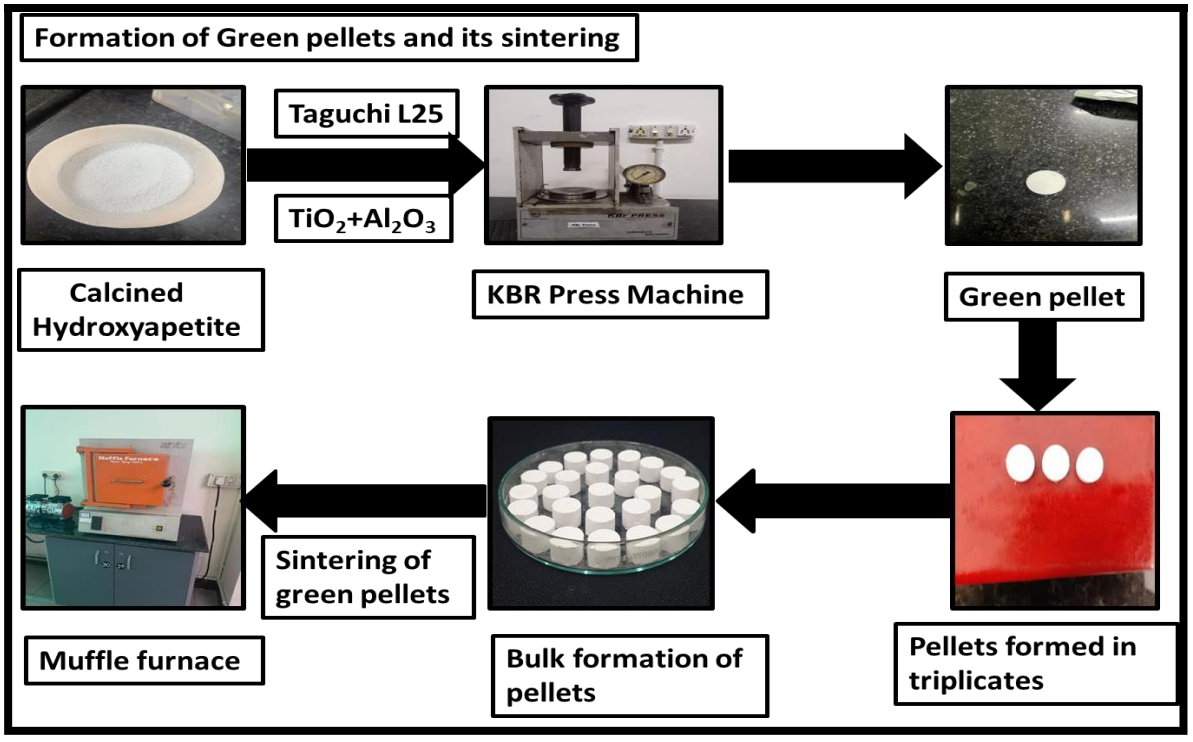

Figure 3.12: Formation of green ternary blend pellets and its sintering.

3.9.1 Sintering of the Ternary Blend pellets

The green pellets were sintered at different temperatures and time according to Taguchi L25 orthogonal array in a muffle furnace, heated at a rate of 10°C per minute, using the Ants Prosys High-Performance Muffle Furnace by Ants Innovations Pvt Ltd, India [144].

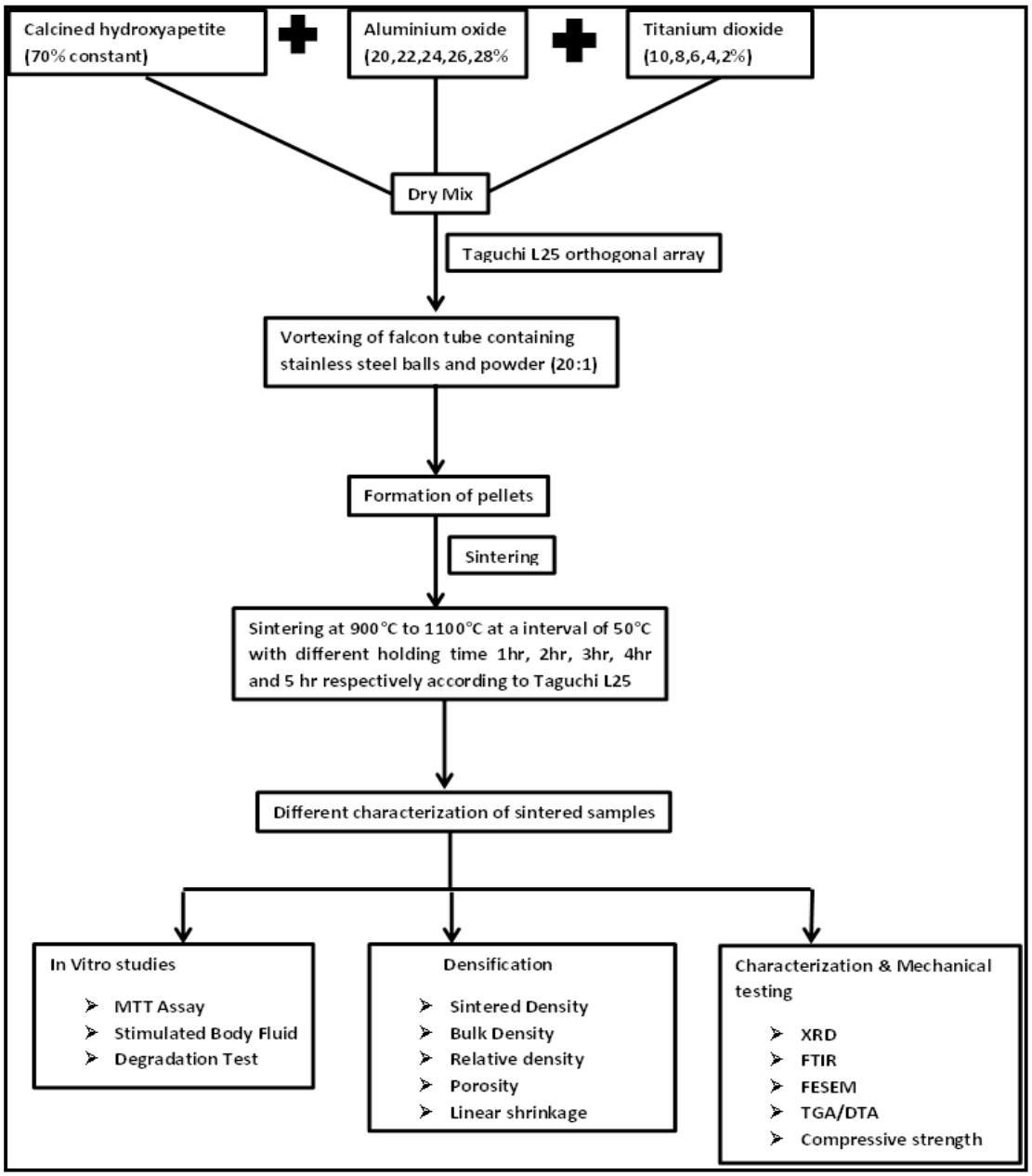

Figure 3.13: Flow diagram of the fabrication of pellets and its different characterization and invitro studies.

3.9.1.1 Calculation of Sintered Density, Relative Density, Bulk Density, Porosity and Linear Shrinkage

The diameter and height of the sintered pellets were measured using a vernier caliper to calculate their sintered density. The mass of the pellet after sintering was recorded with an electronic balance, and the sintered density was then determined using the appropriate formula. The relative density of the sintered pellet was calculated by dividing the sintered density by the theoretical density and multiplying the result by 100. The relative density of the sintered samples was obtained by dividing the bulk density by the theoretical density. Finally, the length of the pellets before and after sintering was measured, and linear shrinkage was calculated using the provided formula [145].

Formulas for calculations

$$\text{Sintered Density} = \frac{\text{Mass (grams)}}{\text{Volume}(cm^3)}$$

Volume of cylinder = $\pi r^2 h$
Where, r = radius of sintered pellet
h = height of the sintered pellet

$$\text{Bulk density} = \frac{\text{Dry weight}}{\text{Soaked weight- Suspended weight}}$$ (Without the effect of open pores)

$$\text{\% Apparent Porosity} = \frac{\text{Soaked weight- Dry weight}}{\text{Soaked weight- suspended weight}}$$

$$\text{\% Relative Density} = \frac{\text{Bulk Density}}{\text{Theoretical Density}} \times 100$$

$$\text{\%Linear Shrinkage} = \frac{\text{Diameter before sintering} - \text{Diameter after sintering}}{\text{Diameter before sintering}} \times 100$$

Figure 3.14: Formulas for calculating sintered density, bulk density, apparent porosity, relative density, linear shrinkage.

3.9.1.2 Protocol for Bulk density and apparent porosity

Archimedes' principle was used to determine the apparent porosity and bulk density of the sintered samples. Initially, the dry weight of the sintered sample was recorded using an electronic scale. To ensure that the open pores were completely filled

with distilled water and all air was evacuated, the samples were submerged in distilled water and subjected to a vacuum for two hours. The weights of the soaked and suspended samples were then measured. The bulk density and apparent porosity were calculated using the appropriate formula [146].

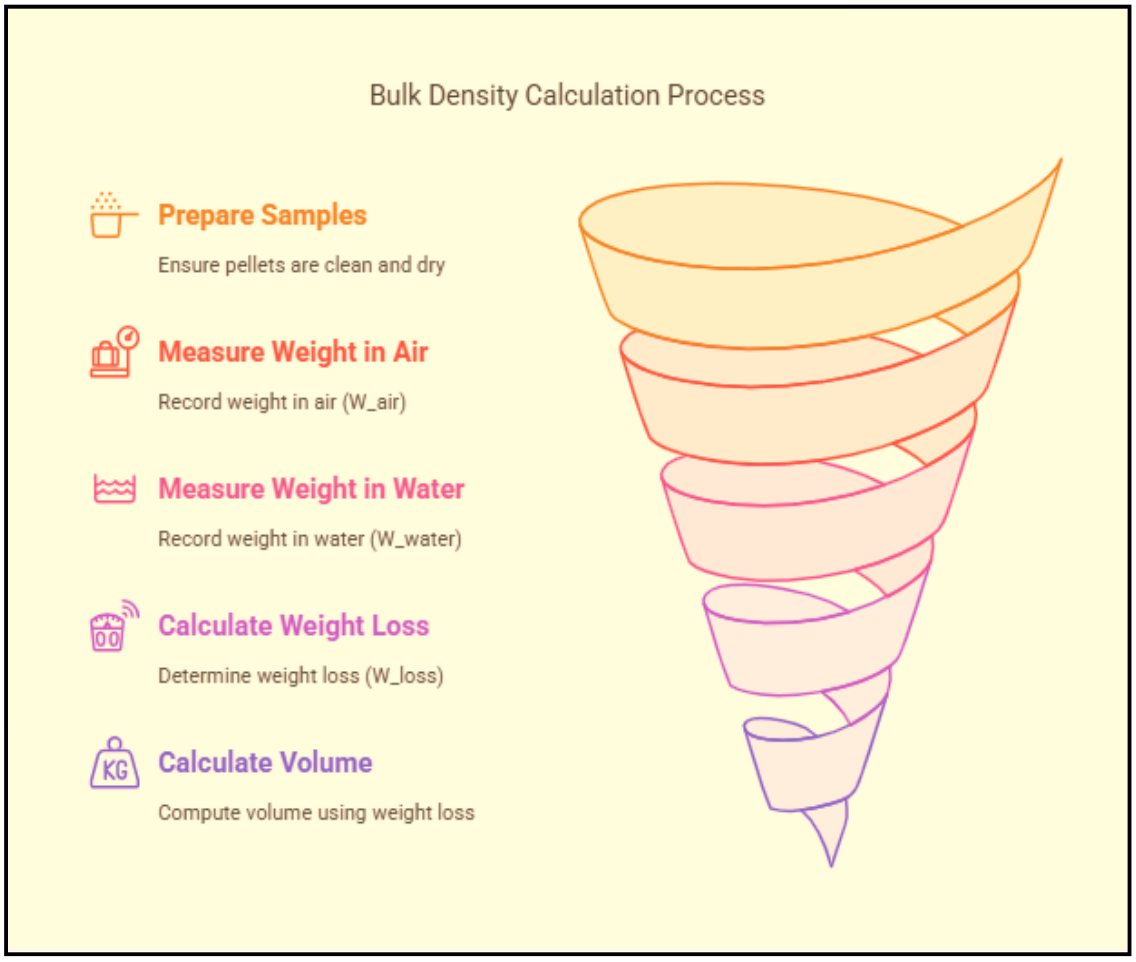

Figure 3.15: Measurement of Bulk density using Archimedes principle

3.9.1.3 Measurement of porosity

To calculate porosity using Archimedes' principle, first weigh the dry sample. Submerge the sample in distilled water and evacuate any trapped air by applying a vacuum for 2 hours. After this, weigh the sample while it is submerged in water and then weigh it while suspended in the water.

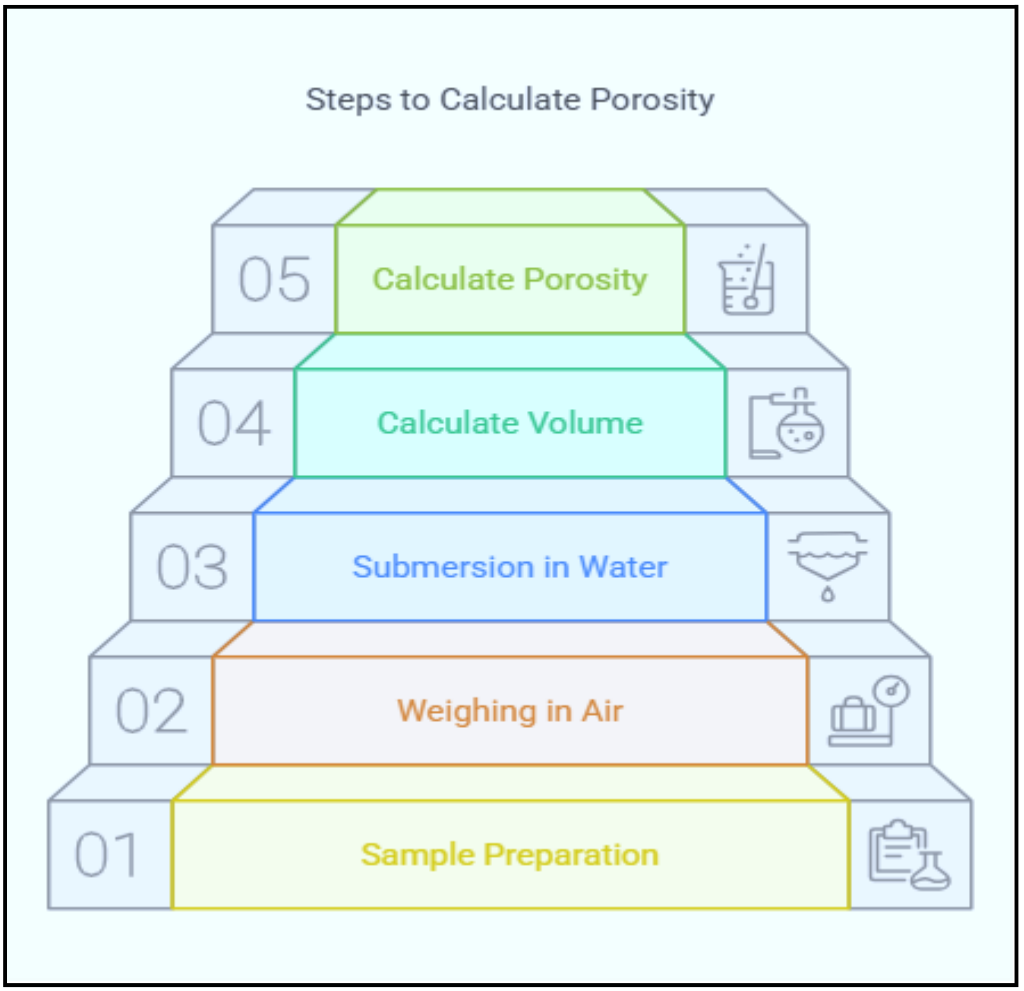

Figure 3.16: Steps to calculate porosity.

3.10 Taguchi method

The Taguchi method has been used to determine the optimal levels of factors for efficient results by systematically altering various components through an orthogonal array. To minimize the number of practical experiments; the experimental process was optimized using the Taguchi approach. The L25 orthogonal array, which consists of three columns and twenty-five rows, was employed. This array allows for the efficient study of factors with multiple levels by systematically varying the experimental conditions. Each column represents a factor, and the rows correspond to different combinations of factor levels. Using this array, the interactions between the factors can be studied while keeping the number of experiments manageable. This technique ensures that the results are statistically

robust and can identify the most significant factors influencing the outcome, while reducing the time and resources required for experimentation [147].

3.10.1 ANOVA analysis

ANOVA (Analysis of Variance) using the Taguchi method is a statistical technique used to analyze the impact of different factors and their interactions on a process's performance. In this method, factors and their levels are selected, and an orthogonal array, such as L25, is used to design the experiments efficiently. After conducting the experiments, the results are often converted into a signal-to-noise (S/N) ratio, which quantifies the process quality. ANOVA is then performed to calculate the sum of squares (SS) for each factor and interaction, partitioning the total variation into contributions from individual factors and experimental errors. The ANOVA table includes degrees of freedom, sum of squares, mean squares, F-values, and p-values, which help assess the significance of each factor. Factors with higher F-values and lower p-values are deemed more significant. The ANOVA results provide insights into which factors most influence the output, allowing for the selection of optimal factor levels to minimize variation and optimize performance [148].

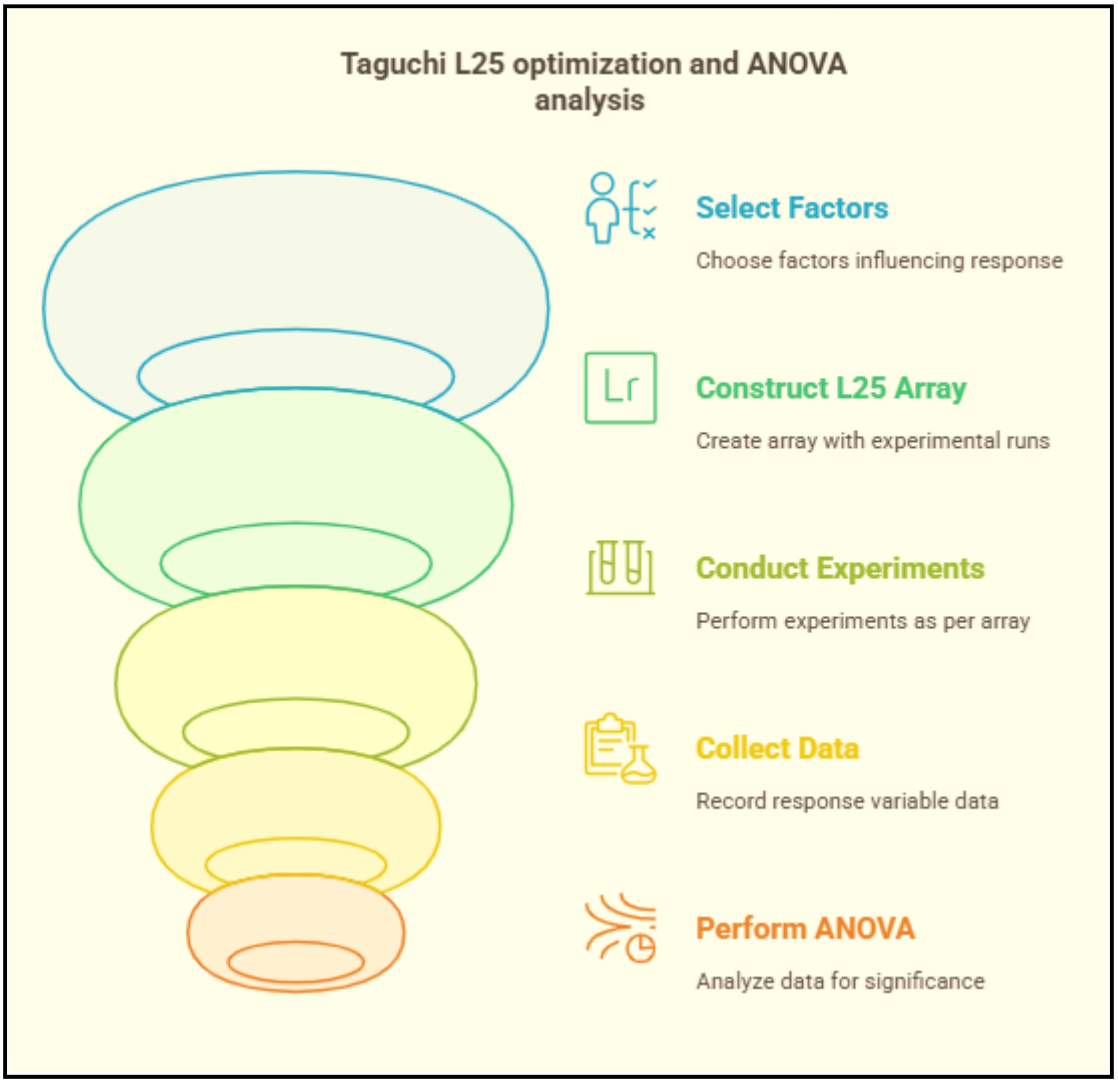

Figure 3.17: Optimization using Taguchi L25 orthogonal array and ANOVA analysis.

3.11 Characterization of Ternary Blends

The ternary blend was prepared using the weight ratios determined by the Taguchi L25 orthogonal array. The optimal ratio was selected based on the results obtained from various density measurements, including sintered density, bulk density, relative density, porosity, and linear shrinkage. This selected ratio was then used for characterization through techniques such as XRD, FTIR, and FESEM, as well as for mechanical testing, including compressive strength analysis [149].

3.11.1 Physiochemical characterization

3.11.1.1 X-ray diffraction (XRD)

For XRD analysis, five different ratios from the Taguchi L25 orthogonal array were selected for comparison with the optimal ratio. The optimal ratio was determined based on sintered density, relative density, bulk density, porosity, and linear shrinkage. To facilitate comparison, the same temperature ratios were used with varying sintering times for XRD studies. For XRD analysis, the samples were submitted in powder form to the Central Instrumentation Facility at Lovely Professional University, Punjab, and India.XRD analysis was conducted using a using Bruker D8 Advance Diffract meter instrument (Bruker, USA) with CuKα radiation. X-ray diffraction (XRD) is a technique used to analyze the crystalline structure of materials by measuring the diffraction pattern of X-rays interacting with the sample. When X-rays strike a crystal, they are scattered in specific directions based on the atomic arrangement, producing a unique diffraction pattern that helps identify phases, crystallinity, and structural properties [150].

3.11.1.2 Fourier Transformed Infrared Spectroscopy (FTIR)

For FTIR analysis, only the best ratio was selected, as FTIR identifies the functional groups in the composites without being influenced by temperature variations. The chosen sample was the one with the optimal ratio, determined based on sintered density, relative density, bulk density, porosity, and linear shrinkage. For FTIR analysis, the sample was submitted in powder form to the Central Instrumentation Facility at Lovely Professional University, Punjab, India. FTIR analysis was conducted using a PERKIN ELMER FTIR instrument. Fourier Transform Infrared (FTIR) spectroscopy is a technique used to identify functional groups in a material by measuring its infrared absorption. When infrared light passes through a sample, specific molecular bonds absorb characteristic wavelengths, producing a unique spectrum that reveals the chemical composition and structure of the material [151].

3.11.1.3 Field Emission Scanning Electron Microscopy (FESEM)

For FESEM analysis, five different samples were selected based on the best ratio, which was determined by sintered density, relative density, bulk density, porosity, and linear shrinkage. This selection aimed to visualize the effect of temperature on the composite's morphology, including the reduction in pore size and increased densification with rising temperature. Different temperatures and sintering times were chosen for each ratio to study these effects. All five samples were submitted as pellets to the Central Instrumentation Facility at Lovely Professional University, Punjab, India. FESEM analysis was conducted using a JOEL FESEM.Field Emission Scanning Electron Microscopy (FESEM) is an advanced imaging technique that uses a focused electron beam to produce high-resolution surface images of materials. The field emission source provides enhanced resolution and depth of field, allowing for detailed visualization of surface morphology, microstructure, and porosity at the Nano scale [152].

3.12 Mechanical testing (Compressive strength)

The samples for the compressive strength test were selected based on the maximum sintered density achieved among all the samples according to the Taguchi L25 used to optimize the ratios. The highest density was observed in the sample with a composition ratio of 20:10:70 (Al_2O_3:TiO_2:HAp)**,** sintered at1100℃ for 5 hours**,** making it the optimal choice for compressive strength testing. Additionally, samples sintered at 1100℃ for 1, 2, 3, and 4 hours having different ratios exhibited relatively higher sintered densities, so they were also chosen for compressive strength testing for comparison purposes. All selected samples were cylindrical pellets with a uniform diameter of 13mm and height of 7mm**.** These specimens were then sent to Advanced Scientific and Engineering Services (AdvanSES) in Gujarat, India**,** for compressive strength evaluation [153].

3.12.1 Working of Universal Testing Machine

A universal testing machine (UTM) was used to analyze the compressive strength of hydroxyapetite samples in order to assess how well they performed mechanically under axial loading. Uniformly sized (13mm diameter and 7mm

height) cylindrical samples were then placed between the UTM's flat, parallel platens, and an axial load that increased progressively was applied until the samples broke. The formula $\sigma = F$ / A, where is the applied force and is the sample's cross-sectional area, was used to determine the compressive stress (σ). The ultimate compressive strength was determined by taking the maximum stress before failure and recording the load and related deformation during the test to create a stress-strain curve. While the sintering conditions were optimized to produce dense, homogeneous microstructures, care was made to assure uniformity in sample preparation to minimize variability. This technique made it feasible to characterize the mechanical characteristics of hydroxyapetite, taking into account the impact of porosity and the different additives added during the sintering process [154].

A Universal Testing Machine (UTM) is a mechanical testing device used to determine a material's mechanical properties, such as compressive strength**.** The UTM operates on the Load vs. Deformation principle, where a controlled force is applied to a specimen until failure occurs. This force is exerted through a movable crosshead, which moves downward during compression tests or upward in tensile tests. A load cell accurately measures the applied force, while an extensometer or displacement sensor records deformation. The collected data generates a stress-strain curve, which is crucial for analyzing material behavior. In compression mode, a cylindrical specimen is placed between compression plates, and force is applied uniformly until failure. The compressive strength (σ_c) is then calculated using the formula:

$\sigma_c = F_{max} / A$

Where $\mathbf{F_{max}}$is the maximum force applied, and **A** is the cross-sectional area of the specimen.

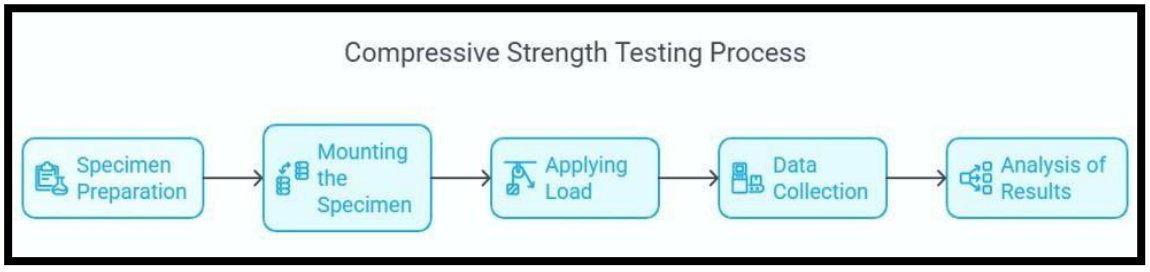

Figure 3.18: working of Universal Testing Machine.

PART 5: In vitro study of the hydroxyapetite and study of its biocompatibility.

3.13 In vitro Studies

In vitro studies are conducted for biomaterials to check their biocompatibility, Biodegradation, and cytotoxicity before they are used in vivo (within living organisms). These studies help to evaluate how the biomaterial interacts with cells or tissues, including factors like cell adhesion, proliferation, differentiation, and potential toxicity. In vitro testing is essential to ensure that the biomaterial will not cause adverse reactions, such as inflammation or immune responses, when implanted or used in medical applications. It provides valuable insights into the material's performance and its suitability for clinical use, reducing the risk of harm to patients. So, these in vitro studies were conducted to evaluate the biocompatibility, biodegradation, and cytotoxicity of the ternary composite [155].

3.13.1 Biocompatibility of the ternary blend (Synthetic Body Fluid (SBF))

In the ternary composite with the markedly enhanced mechanical strength, the deposition of calcium and phosphorus ions was further examined. The samples were immersed in synthetic body fluid (SBF) for three weeks. The SBF solution was made using the procedure described by Fathi et al in 2008 order to obtain an ion concentration comparable to that of human blood plasma. The ion formulation for the blood plasma and SBF solution is shown in table 3.3 below. Each sample was in the form of pellets of 13mm diameter and 2mm height, and it was soaked in 100 ml of SBF solution at a temperature of 37°C and a pH of 7.4. Following the immersion procedure, the samples were removed from the SBF, washed with deionized water, and allowed to dry. Additionally, a scanning electron microscope (SEM) was used to analyze the sample's microstructure, and energy dispersive spectroscopy (EDS) was used to assess the calcium and phosphorus ion levels [156].

Table 3.3: Reagent composition of synthetic body fluid solution.

S.No.	Reagents	Composition(g/l)
1.	Potassium chloride (KCl)	0.373
2.	Sodium Chloride (NaCl)	6.547

3.	Sodium Bicarbonate ($NaHCO_3$)	2.268
4.	Magnesium Chloride hexahydrate ($MgCl_2.6H_2O$)	0.305
5.	Calcium Chloride dihydrate ($CaCl.2H_2O$)	0.368
6.	Sodium Sulfate (Na_2SO_4)	0.071
7.	Sodium Phosphate dibasic dehydrate ($Na_2HPO_4).2H_2O$	0.178
8.	Tris(hydroxymethyl)amino methane $(CH_2OH)_3CNH_2$	6.057

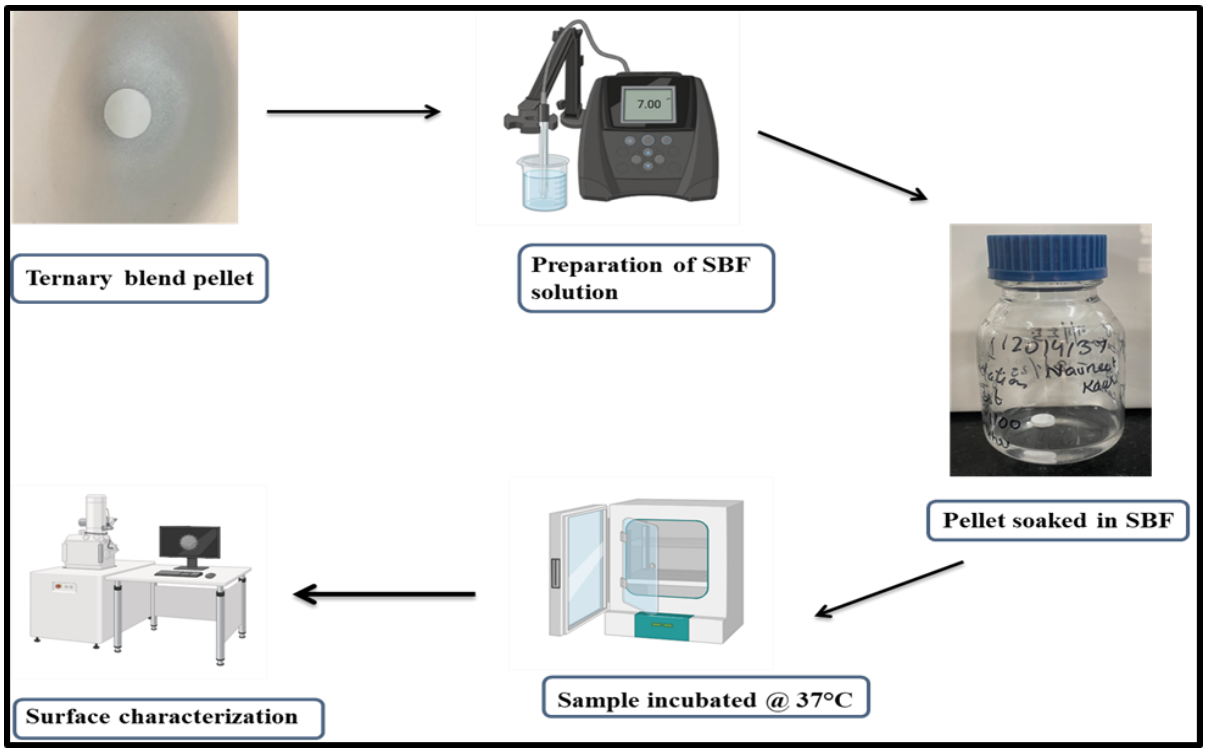

Figure 3.19: Flow chart for performing biodegradation test.

3.13.2 MTT assay (Cell viability assay)

3.12.2.1 Cell culture

MG-63 cells (human bone cancer cells) were obtained from the National Centre for Cell Science (NCCS) in Pune. The cells were cultured in DMEM medium enriched with 10% Fetal Bovine Serum (FBS), 100 µg/mL of penicillin and streptomycin, and kept at 37°C in a 5% CO_2 atmosphere.

3.13.2.2 Procedure for MTT assay

MTT assay was performed to assess the in vitro cytotoxicity of the synthesized hydroxyapetite, used as a control, in comparison to the ternary blend with the optimal ratio determined from the Taguchi L25 orthogonal array, on MG63 cancerous cells. In brief, MG63 cancerous cells were collected from a T flask after trypsinization and transferred to a 15 mL Falcon tube. A total of 10,000 cells in 200 µL were seeded into each well of a 96-well plate and allowed to adhere overnight. The following day, the cells were treated with varying concentrations of both synthesized HAp and ternary blend composite, and then incubated at 37°C in a humidified 5% CO_2 environment for an additional 24 hours. After incubation, 10 µL of 5 mg/mL MTT solution was added to each control and treated well, and the plate was left for 2-4 hours until purple precipitates appeared under an inverted microscope. Lastly, the medium and MTT dye were removed from the wells, and the wells were rinsed with 200 µL of 1x PBS solution. Next, 100 µL of DMSO was added to dissolve the formazan crystals. The absorbance of each well was then measured at 570 nm using a micro plate reader (Thermo Fisher Scientific, USA), and the cell viability percentages were calculated. This experiment was repeated three times independently, with each set performed in triplicates (n = 3) [157].

Cell viability (%) = (OD of Test/OD of Control) x 100

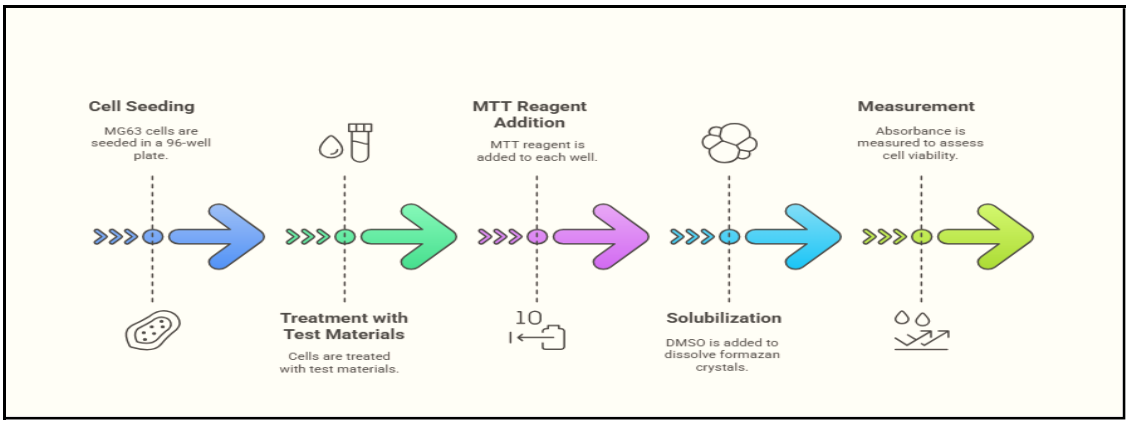

Figure 3.20: Procedure for MTT assay using MG63 cell lines.

3.13.3 Biodegradation Test

The degradability of the calcined HAp and ternary blend pellet was determined by measuring its weight loss percentage in a Tris-HCl buffer solution. A 0.05M Tris-HCl buffer solution was prepared, calcined hydroxyapetite and the ternary blend pellet was immersed in it. The pH of the solution was maintained at 7.4 at 37°C by adding 1M HCL. The calcined HAp and the optimal ratio of the ternary blend composite based on mechanical strength, sintered density, relative density, bulk density, porosity, and linear shrinkage, were soaked for 7 days in glass bottle containing 100 mL of 0.05M Tris-HCl buffer solution in a water bath shaker. After 7 days, the samples were removed, washed with distilled water, and dried in an oven at 150°C. Finally, the following formulas were used to calculate the weight loss of the samples [158].

$$\% \text{ Weight Loss} = \frac{W1 - W2}{W2} X100$$

Where, W1 = initial weight of sample before soaking in Tris- HCl solution.

W2 = final weight of sample after soaking in Tris-HCl solution

Figure 3.21: Formula for calculating the weight loss % in biodegradation test

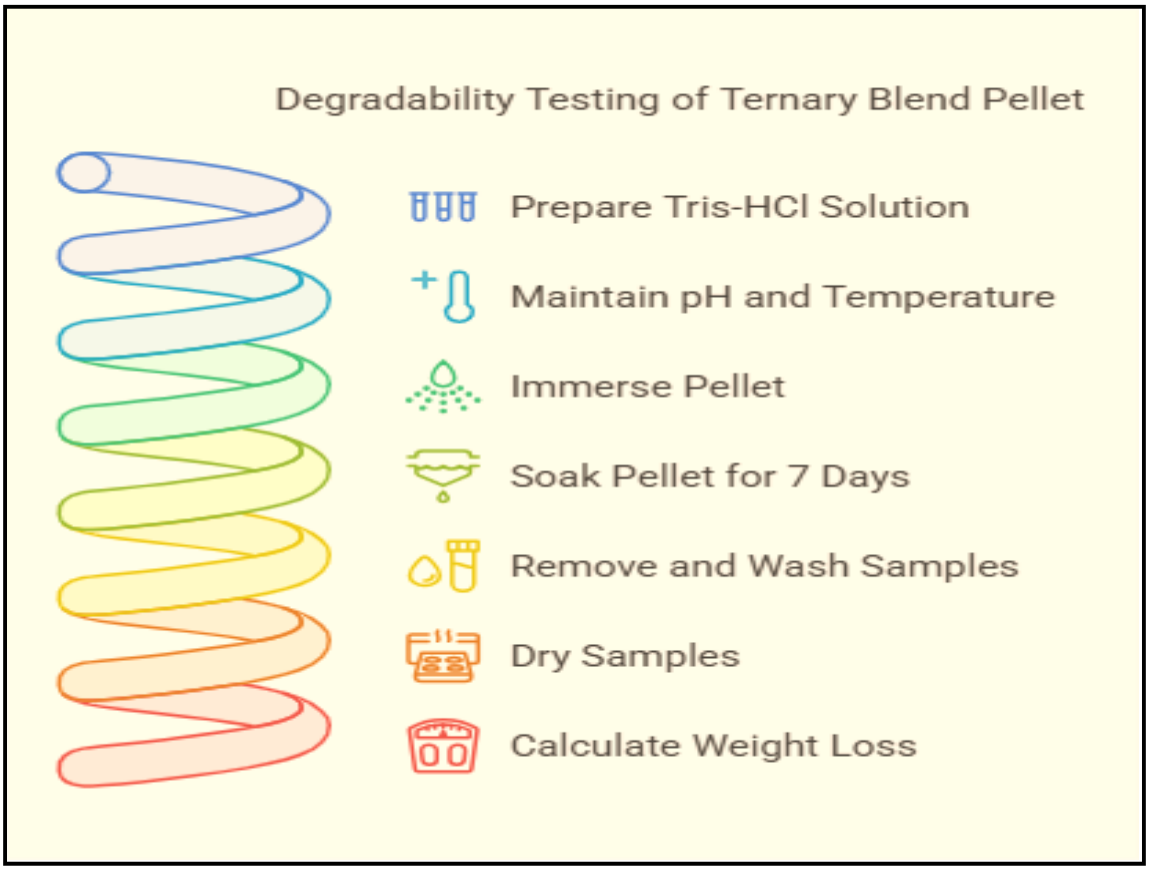

Figure 3.22: Protocol for performing biodegradation test

3.14 Statistical Analysis

Every variable was examined in triplets, and a p-value of less than 0.05 is regarded as significant. An analysis of variance (ANOVA) has been done by using software Design expert 12. The concepts of normality and homogeneity of distributional variances serve as the foundation for this method.

Chapter IV

RESULTS AND DISCUSSION

4 Results and Discussion

In this chapter, carbide lime, a waste byproduct of the acetylene industry, was utilized as a raw material for hydroxyapetite synthesis. The collected carbide lime was characterized, and its major component, calcium hydroxide, was purified using the dilution method. The purified calcium hydroxide was then analyzed using XRD. Subsequently, hydroxyapetite was synthesized from the extracted calcium hydroxide and characterized using XRD, FTIR, FESEM, and TGA analysis. Sintering additives were incorporated, followed by sintering optimization using the Taguchi L25 orthogonal array. The sintered samples were evaluated for sintered density, bulk density, relative density, porosity, and linear shrinkage. Based on the highest sintered density, selected samples underwent mechanical testing. The experimental results were further analyzed using ANOVA (Analysis of Variance) through the Taguchi method to assess the impact of various factors and their interactions on process performance. Characterization techniques such as XRD, FTIR, and FESEM were performed on the optimal ratio and other compositions for comparison. Finally, in vitro tests were conducted on the best-performing ratio to evaluate its biocompatibility, biodegradability, and cytotoxicity.

PART 1: Isolation and characterization of carbide lime from acetylene industry.

4.1 Characterization of carbide lime

4.1.1 XRD analysis of carbide lime

The X-ray diffraction (XRD) pattern of carbide lime confirms that its major crystalline component is calcium hydroxide ($Ca(OH)_2$). This is evident from the strong and sharp diffraction peaks observed at 2θ positions around 18°, 34°, and 47°, which are characteristic of $Ca(OH)_2$. These peaks highlight the well-defined crystalline nature of calcium hydroxide, formed during the hydrolysis of calcium carbide. The dominance of these peaks indicates that calcium hydroxide constitutes the bulk of the material [159].

In addition to calcium hydroxide, the XRD pattern reveals the presence of several impurities. Notably, a strong peak near 29° and a smaller peak near 43° correspond to calcium carbonate ($CaCO_3$). This phase arises due to the carbonation of calcium hydroxide, a process in which atmospheric carbon dioxide reacts with $Ca(OH)_2$ to form $CaCO_3$. A weak peak around 26° suggests the presence of silica (SiO_2), which may be introduced from raw materials or external environmental sources during processing. Furthermore, minor peaks near 25° and 45° are likely associated with residual carbon or unreacted carbide impurities, remnants of the carbide lime production process. Figure 4.1 illustrates the XRD of carbide lime [160].

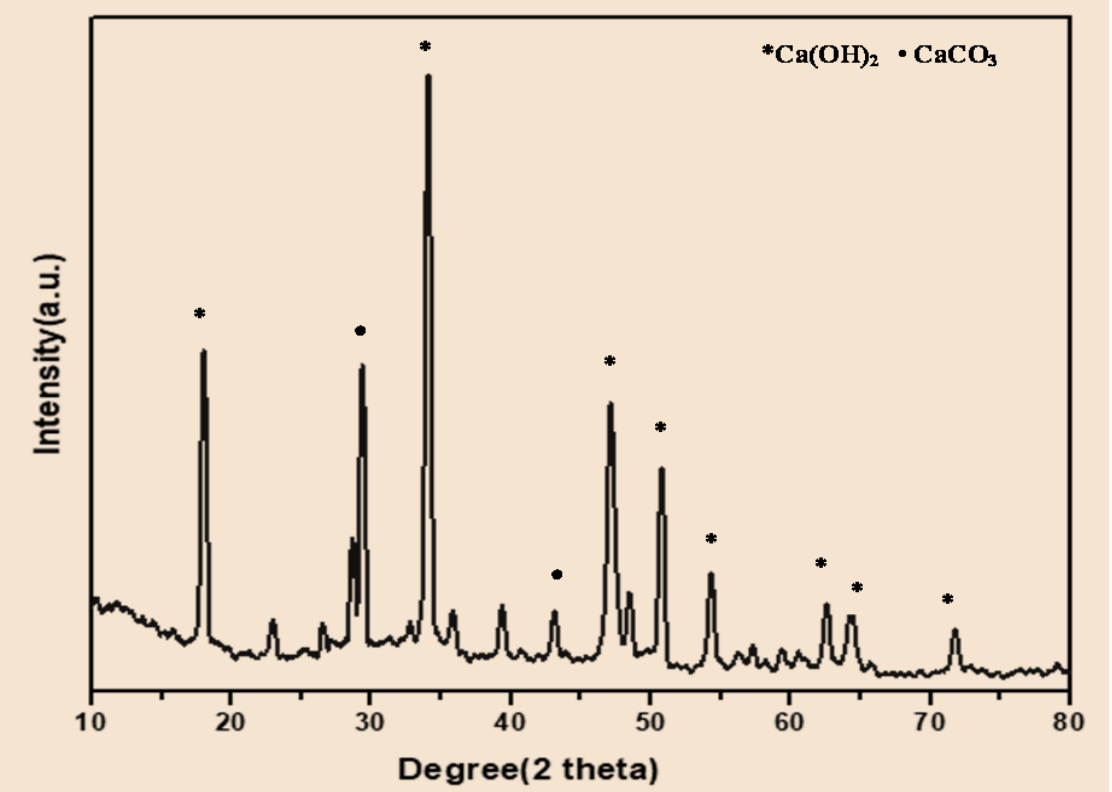

Figure 4.1: XRD of carbide lime

4.1.2 FTIR analysis of Carbide lime

The Fourier-transform infrared (FTIR) spectrum of carbide lime primarily indicates the presence of calcium hydroxide ($Ca(OH)_2$) as the main component, along with characteristic peaks corresponding to its functional groups and some impurities.

The broad and strong peak at 3642.55 cm^{-1} is attributed to the O-H stretching vibrations of hydroxyl groups in calcium hydroxide. The smaller peak at 3337.52 cm^{-1} corresponds to the hydrogen-bonded O-H stretching vibrations, likely arising from water molecules either adsorbed on the surface or present as residual moisture. The peak at 2922.86 cm^{-1} may indicate C-H stretching vibrations from trace organic impurities [161].

In the lower wavenumber region, the prominent peak at 1650.88 cm^{-1} corresponds to the H-O-H bending vibrations of water molecules, further supporting the presence of adsorbed or bound water. The sharp peak at 1416.65 cm^{-1} is indicative of carbonate (CO_3^{2-}) groups, suggesting the presence of calcium carbonate ($CaCO_3$) as an impurity. Another carbonate-related vibration is observed at 872.63 cm^{-1}, corresponding to the out-of-plane bending mode of CO_3^{2-} ions.

The peak at 1032.85 cm^{-1} is assigned to Si-O stretching vibrations, indicating the presence of silica (SiO_2) as an impurity. Additionally, peaks at 711.75 cm^{-1} and 575.07 cm^{-1} correspond to lattice vibrations associated with calcium hydroxide or other trace phases. Figure 4.2 explains the different functional groups peaks of FTIR spectra of carbide lime [162].

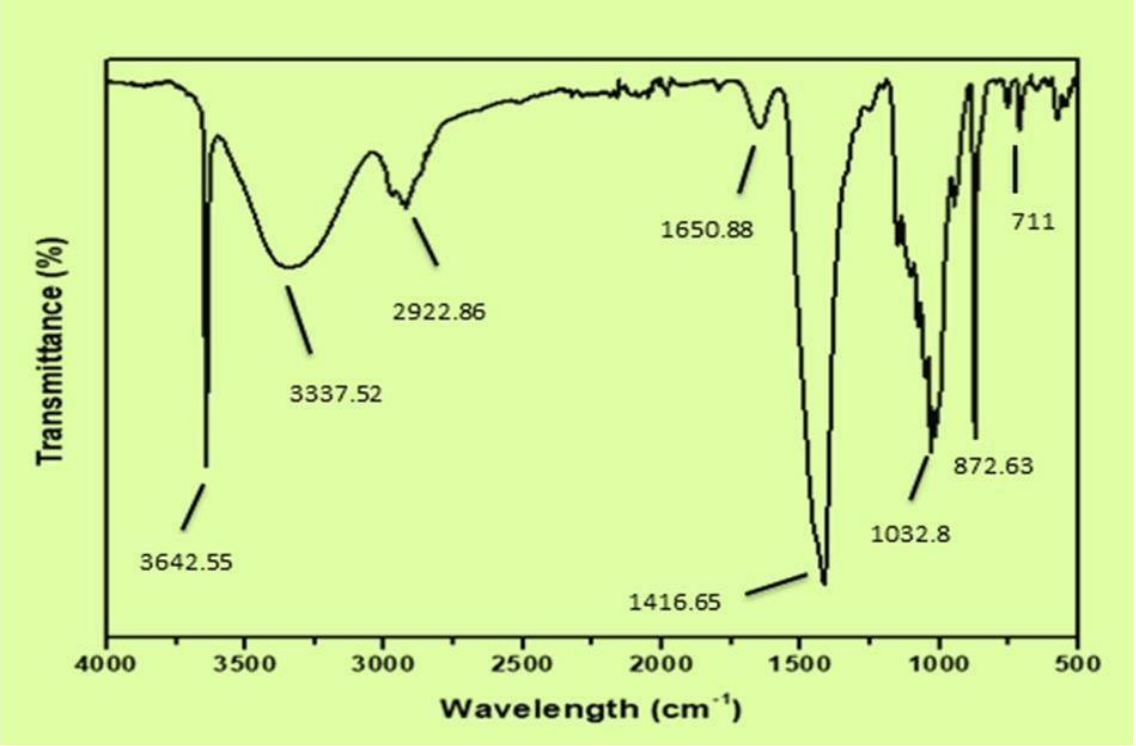

Figure 4.2: FTIR of carbide lime

4.1.3 FESEM analysis of carbide lime

The figure 4.3 provides the FESEM images and EDS analysis of carbide lime offer detailed insights into its morphology, particle structure, and elemental composition.

Figure 4.3 (A) indicates that at 20,000X magnification, the individual particles are clearly observable, exhibiting irregular shapes with rough, porous surfaces. The morphology indicates that these are finely aggregated particles, likely resulting from crystallization or precipitation processes. The particles are clustered together, suggesting strong inter-particle forces, possibly influenced by van der Waals interactions or residual moisture content [163].

These particles align with the typical properties of calcium hydroxide which is the common component of carbide lime.

Figure 4.3 (B) depicts that at a lower magnification of 10,000×, the carbide lime exhibits a heterogeneous particle distribution, featuring larger aggregates

alongside smaller dispersed particles. The larger clusters are primarily composed of calcium hydroxide, the main constituent of carbide lime. These clusters have irregular shapes with rough surfaces, reflecting their likely formation through precipitation processes. The smaller particles present are indicative of impurities or secondary phases, such as aluminum or silicon-based compounds, which are minor components within the material. The combination of calcium hydroxide and these minor phases contributes to the observed heterogeneity of the carbide lime.

Figure 4.3 (C) presents a magnified view of a specific region of carbide lime, emphasizing its microstructure for closer examination. The particles in this area exhibit a porous and irregular morphology, which is characteristic of calcium hydroxide. Elemental analysis of the selected region confirms the predominance of calcium and oxygen, validating the presence of calcium hydroxide. Furthermore, minor impurities, such as aluminum and silicon-based compounds, are also detected, likely originating from the production process or raw materials. This focused analysis highlights the combination of calcium hydroxide with secondary phases present in the material.

Figure 4.3 (D) indicates the elemental mapping of carbide lime illustrates the spatial distribution of elements within the material. The analysis reveals a predominant presence of calcium (Ca) and oxygen (O), confirming calcium hydroxide as the main constituent. The even dispersion of these elements suggests a relatively homogeneous composition across the sample. Additionally, small amounts of aluminum (Al) and silicon (Si) are detected, signifying the presence of minor impurities or secondary phases. The elemental mapping further emphasizes the coexistence of calcium hydroxide with trace secondary components.

Figure 4.3 (E) presents the EDS spectrum of carbide lime offers a detailed assessment of its elemental composition. The spectrum prominently features peaks for calcium (Ca) and oxygen (O), confirming calcium hydroxide as the primary constituent. Additionally, smaller peaks corresponding to aluminum (Al), silicon (Si), and carbon (C) suggest the presence of minor impurities or secondary phases. The EDS analysis further validates calcium hydroxide as the dominant phase, with trace elements contributing to the overall composition [164].

Overall, the analysis underscores the heterogeneous nature of carbide lime, where calcium hydroxide serves as the primary phase, while minor impurities contribute to variations in its structural and chemical properties.

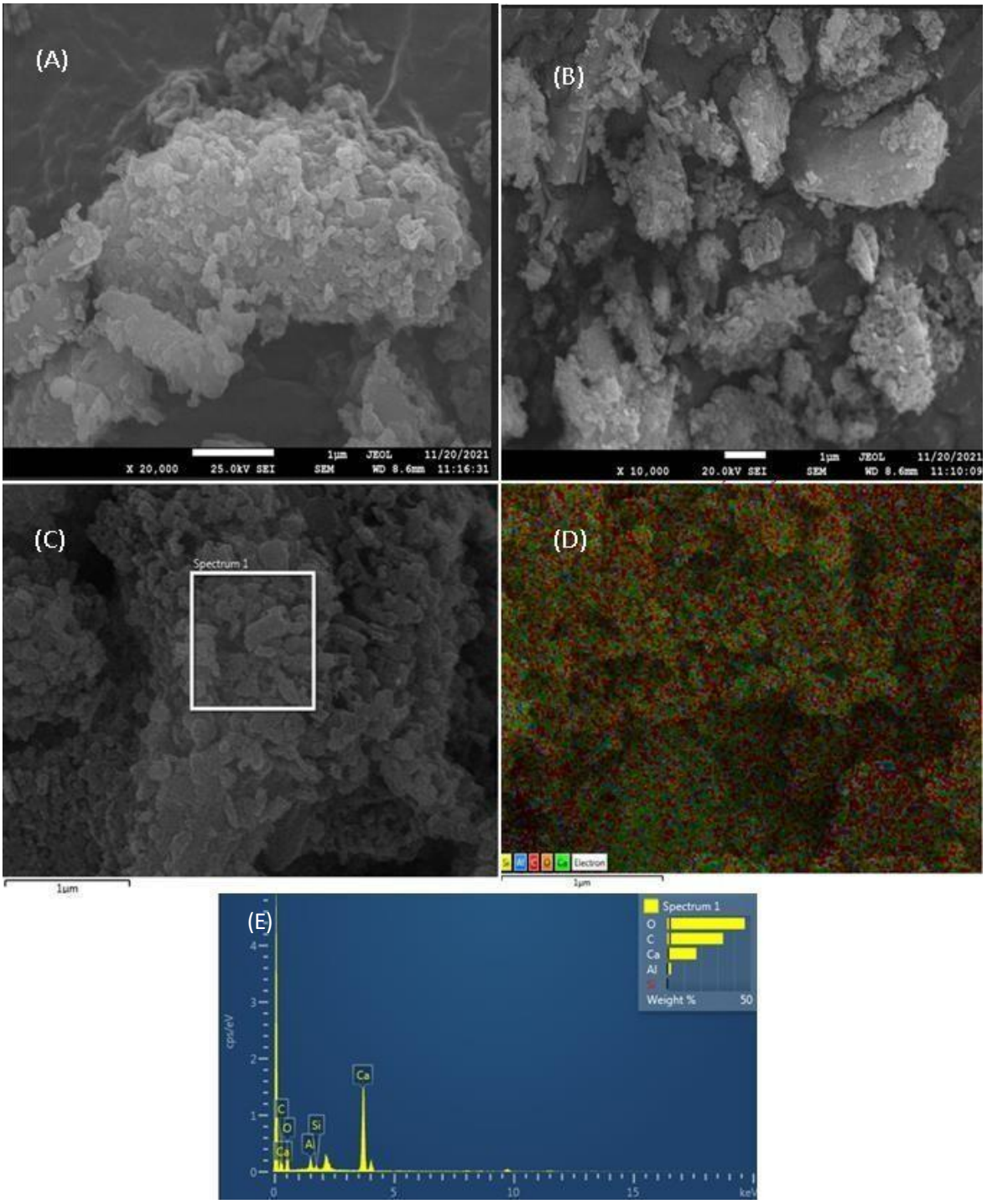

Figure 4.3: Morphology of carbide lime at 20,000X magnification (B) magnification at 10,000X magnification (C) Magnified region of carbide lime (D) Elemental mapping (E) EDS spectrum.

PART 2: Chemical synthesis and control of process parameters for the synthesis of hydroxyapetite.

4.2 Purification of calcium hydroxide from carbide lime by dilution method

Table 4.1: Purification of calcium hydroxide from carbide lime by dilution method

Water (mL)	Calcium hydroxide (Yield)(grams)	Calcium hydroxide (Yield)(grams)	Calcium hydroxide (Yield)(grams)	Calcium hydroxide (Yield)(grams)
	2 Hours	**4 Hours**	**6 Hours**	**12 Hours**
100	0.200	0.240	0.260	0.270
200	0.310	0.380	0.410	0.420
300	0.350	0.420	0.450	0.465
400	0.400	0.480	0.510	0.529
500	0.460	0.540	0.570	0.581
600	0.520	0.600	0.650	0.690
700	0.560	0.650	0.700	0.743
800	0.580	0.670	0.720	0.765
900	0.600	0.690	0.740	0.782
1000	0.610	0.700	0.750	0.781

At lower water volumes (100–500 mL), the reaction is limited by insufficient water availability, leading to incomplete dissolution of carbide lime. As a result, the conversion of calcium carbide to calcium hydroxide remains incomplete, resulting in a lower yield. With an increase in water volume to 600–1000 mL, the reaction reaches optimal conditions, where sufficient water facilitates the complete conversion of carbide lime into calcium hydroxide, leading to a maximum yield of approximately 78.2% [129].

Reaction time also plays a significant role in determining the yield of calcium hydroxide. At 2 hours, the reaction is still in progress, with incomplete conversion of carbide lime. By 4–6 hours, the yield increases as more calcium hydroxide forms. At 12 hours, the reaction reaches completion, and the yield attains its maximum value, indicating that the system has reached equilibrium. Beyond this point, extending the reaction time further does not result in a significant increase in calcium hydroxide formation.

Additionally, the possibility of side reactions such as the absorption of carbon dioxide (CO_2) from the atmosphere must be considered. Over time, calcium hydroxide can react with CO_2 to form calcium carbonate ($CaCO_3$) as follows:

$$Ca(OH)_2 + CO_2 \rightarrow CaCO_3 + H_2O$$

This reaction can lead to a slight reduction in the measurable yield of calcium hydroxide over extended durations, especially in open-air conditions where exposure to atmospheric CO_2 is significant.

PART 3: Characterization of the hydroxyapetite synthesized from carbide lime

4.3 XRD analysis of synthesized hydroxyapetite

The XRD analysis of synthesized HAp, along with the raw material carbide lime ($Ca(OH)_2$) and calcium oxide was conducted using a Bruker D8 Advance Diffractometer within a scanning range of 10–80° (2θ). Figure 4.4 (a) presents the XRD diffractograms of carbide lime ($Ca(OH)_2$) dried at 100°C (a), calcined carbide lime powder (CaO) at 800°C 4.4 (b), and synthesized HAp after calcination at 800°C (c). The characteristic diffraction peaks of $Ca(OH)_2$ were observed at 2θ values of 18.04°, 28.69°, 34.11°, 47.13°, 50.84°, 54.38°, 59.42°, 62.64°, and 64.25°, corresponding to the indexed hkl planes of (001), (100), (101), (102), (110), (111), (200), (021), and (013). These peaks confirm the presence of a hexagonal lattice structure, as referenced in the JCPDS file number 01-087-0673 [166].

The XRD analysis of CaO, obtained after the calcination of $Ca(OH)_2$, revealed distinct diffraction peaks at 2θ values of 32.20°, 37.34°, 53.86°, 64.15°, 67.37°, and 79.66°. These peaks correspond to the indexed planes (111), (200), (220), (311), (222), and (400), confirming the cubic lattice structure as referenced in JCPDS file number 00-37-1497. The XRD data validate the successful transformation of $Ca(OH)_2$ into CaO through the calcination process. Additionally, a peak at 2θ = 34.14° indicates the presence of residual $Ca(OH)_2$, which likely formed due to the reaction of CaO with atmospheric moisture, as CaO readily absorbs water from the environment, converting back into $Ca(OH)_2$ [167].

The XRD analysis of nHAp exhibited characteristic diffraction peaks at 2θ values of 10.83°, 16.84°, 19.31°, 21.76°, 25.36°, 26.45°, 28.12°, 28.92°, 29.00°, 31.77°, 32.90°, and 35.46°. These peaks correspond to the indexed hkl planes (020), (021), (111), (200), (041), (002), (012), (022), (220), (112), (221), (300), and (301), confirming a monoclinic lattice structure. This structural identification aligns with the reference JCPDS file number 01-076-0694, which is also consistent with findings reported in previous literature [168].

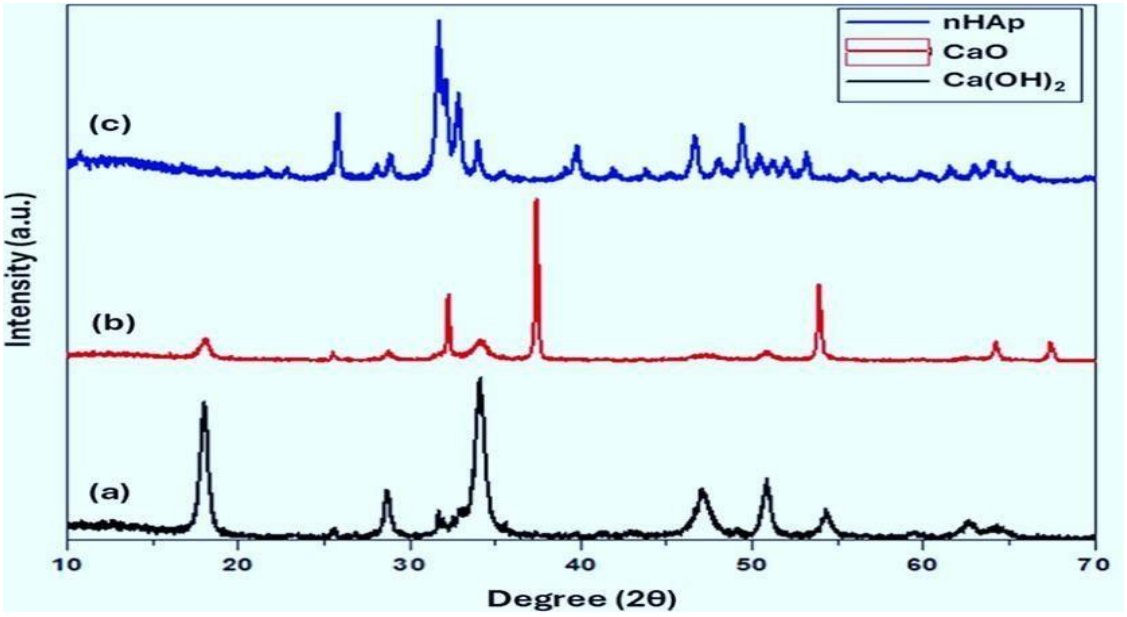

Figure 4.4: XRD of (a) Calcium hydroxide ($Ca(OH)_2$(b) Calcium oxide (CaO) (c) hydroxyapetite (HAp)

4.4 FTIR analysis of synthesized hydroxyapetite

The vibrational peaks of Ca $(OH)_2$, CaO, and synthesized HAp were examined using a Bruker Tensor 27 I.R. series FTIR instrument. FTIR spectroscopy was employed to identify the functional groups present in Ca $(OH)_2$, CaO, and synthesized HAp, as illustrated in Figure 4.5 (a–c).

The FTIR spectrum of $Ca(OH)_2$ is shown in Figure 4.5(a). A prominent band at 3642 cm^{-1} corresponds to the stretching vibration of the hydroxide (-OH) bond. The broad absorption band at 1421 cm^{-1} indicates the presence of carbonate groups (CO_3^{2-}). Additionally, the peak at 873 cm^{-1} represents the Ca–O bond, while the band at 547 cm^{-1} is associated with Ca=O bonding. These observations suggest that partial hydration may have occurred during the process [168].

The FTIR spectrum of CaO, presented in Figure 4.5 (b), exhibits a prominent band at 3642 cm^{-1}, which corresponds to the -OH group from residual hydroxide or possibly adsorbed water molecules on the surface during handling. A broad absorption band at 1456 cm^{-1} and a peak at 943 cm^{-1} indicate the presence of C–O bonds, primarily resulting from the carbonation of CaO. Additionally, strong absorption bands at 519 cm^{-1}, 618 cm^{-1}, and 679 cm^{-1} correspond to the vibrational modes of the Ca–O bond. A band at 2361 cm^{-1} is also observed, likely due to the presence of atmospheric CO_2 [169].

The FTIR spectrum of HAp, shown in Figure 4.5 (c), displays characteristic bands associated with Nano crystalline apatite. The phosphate (PO_4^{3-}) peaks appear at 564 cm^{-1} and 600 cm^{-1}. The peaks at 630 cm^{-1} and 3742 cm^{-1} correspond to the vibration and stretching of -OH groups. Additionally, a band at 962 cm^{-1} indicates the out-of-plane bending of carbonate (CO_3^{2-}) groups. The bands at 1698 cm^{-1} and 1457 cm^{-1} represent the doubly degenerate stretching of carbonate ions, while the peak at 1026 cm^{-1} corresponds to the stretching of PO_3^{2-}. Furthermore, the bands observed at 2977 cm^{-1} and 2361 cm^{-1} suggest the presence of CO_2, likely absorbed from the surrounding atmosphere [170].

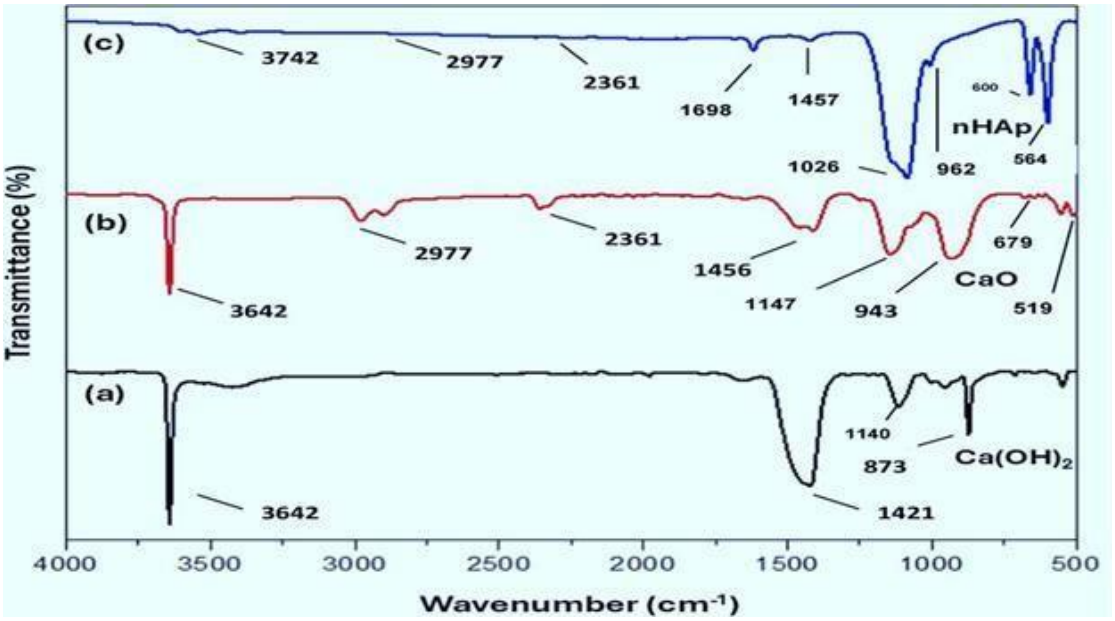

Figure 4.5: FTIR (a) Calcium hydroxide ($Ca(OH)_2$ (b) Calcium oxide (CaO) (c) hydroxyapetite (HAp).

4.5 FESEM analysis of synthesized hydroxyapetite

The average particle size and morphology of the synthesized HAp were analyzed using the FESEM (JOEL) instrument, while its elemental composition was examined through EDX spectroscopy. In Figure 4.6 (A), presents the rod shaped morphology of hydroxyapetite at 10,000X magnification Figure 4.6 (B) illustrates the closer view of rod-shaped morphology of the synthesized HAp. The particle size of the synthesized HAp was determined to be in the range of 60–102 nm, as shown in Figure 4.6 (C). Additionally, Figure 4.6 (D) presents a closer view of the synthesized hydroxyapetite (HAp), showcasing its tightly packed microstructure. The image illustrates a uniform arrangement of rod-shaped nanoparticles, a typical feature of HAp. The uniformity in particle size and shape reflects well-regulated synthesis conditions, which enhance the material's structural stability Figure 4.6 (E) depicts the elemental mapping of the synthesized hydroxyapetite (HAp), showing the spatial arrangement of essential elements within the material. The consistent distribution of calcium (Ca), phosphorus (P), and oxygen (O) underscores the homogeneity of the synthesized HAp. This uniform dispersion confirms the successful incorporation of these elements into the hydroxyapetite structure. Figure 4.6 (F) illustrates the EDX spectrum of the synthesized hydroxyapetite (HAp), offering a detailed analysis of its elemental composition. The spectrum prominently features peaks for calcium (Ca), phosphorus (P), and oxygen (O), which are the primary components of hydroxyapetite. These peaks confirm the effective transformation of precursor materials into hydroxyapetite. The calcium-to-phosphorus ratio aligns with the stoichiometric composition of hydroxyapetite, ensuring its chemical stability and structural integrity. The absence of minor peaks for trace elements highlights the high purity of the material [171].

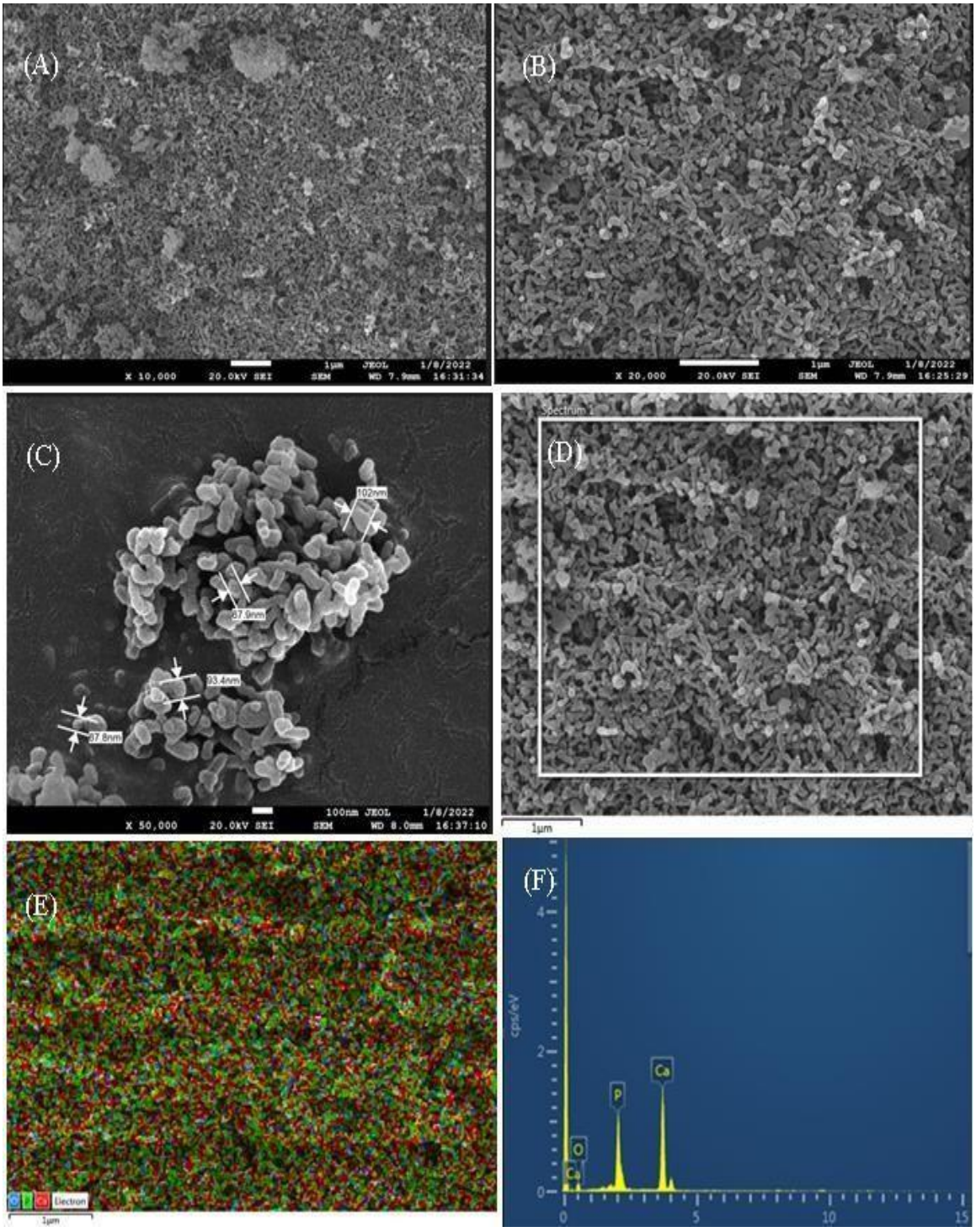

Figure 4.6: Morphology of hydroxyapetite at 10,000X (A) magnified view at 20,000X

(B) Particle size of synthesized hydroxyapetite (C) Magnified spectrum for elemental composition (D) Elemental mapping (E) EDX of elementals (F)

4.6 TGA analysis

A TGA analyzer (Perkin Elmer, USA) was used to examine the thermal decomposition behavior of carbide lime and synthesized HAp. Figure 4.7 (a) illustrates the TGA analysis of carbide lime, revealing three major weight loss stages during decomposition. The first significant weight loss of 2.05% occurred between 29°C and 390°C, primarily attributed to the release of highly volatile components, such as internal water molecules. The second notable weight reduction was observed between 390 °C and 710 °C, extending up to 800 °C, corresponding to a 31.35% loss. This stage is associated with the decomposition of hydroxides into oxides, as carbide lime primarily comprises $Ca(OH)_2$ with a minor amount of calcite. The total mass loss recorded during the decomposition process was 33.4%, closely aligning with previously reported values. Since carbide lime transitions into its oxide form during this process, it serves as a suitable precursor for HAp synthesis [171].

In Figure 4.7 (b), the thermal decomposition of HAp was approximately 15%, primarily due to the release of water and the breakdown of carbonate groups within the material. This significant weight reduction indicates a phase transformation of HAp from an amorphous to a crystalline structure. Beyond 570°C up to 990°C, no substantial weight loss was observed, highlighting the material's stability at higher temperatures. The total weight loss recorded throughout the process was around 33%. These findings confirm a stable phase transition, demonstrating the thermal stability of HAp [172].

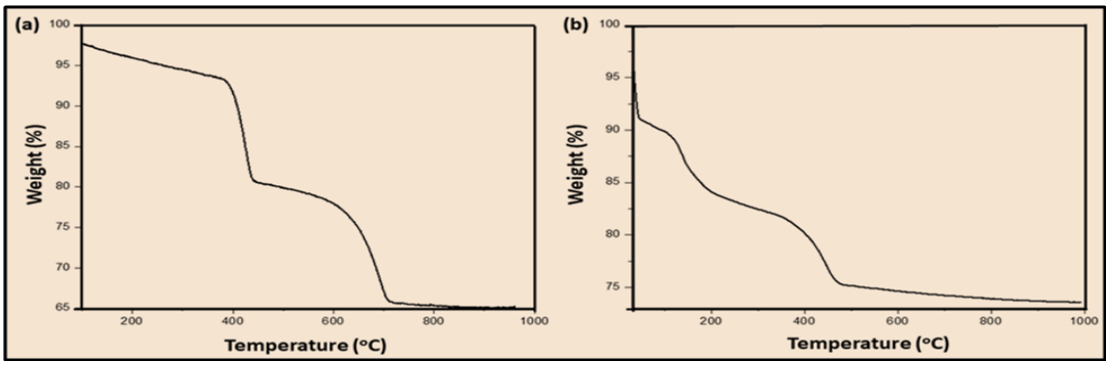

Figure 4.7: TGA curve of carbide lime (a) and calcined HAp (b).

4.7 Dynamic Light Scattering

Dynamic light scattering analysis determined the average hydrodynamic size of HAp to be 238 d.nm, as depicted in Figure 4.8. Additionally, the polydispersity index (PDI) of HAp was recorded at 0.4 [173].

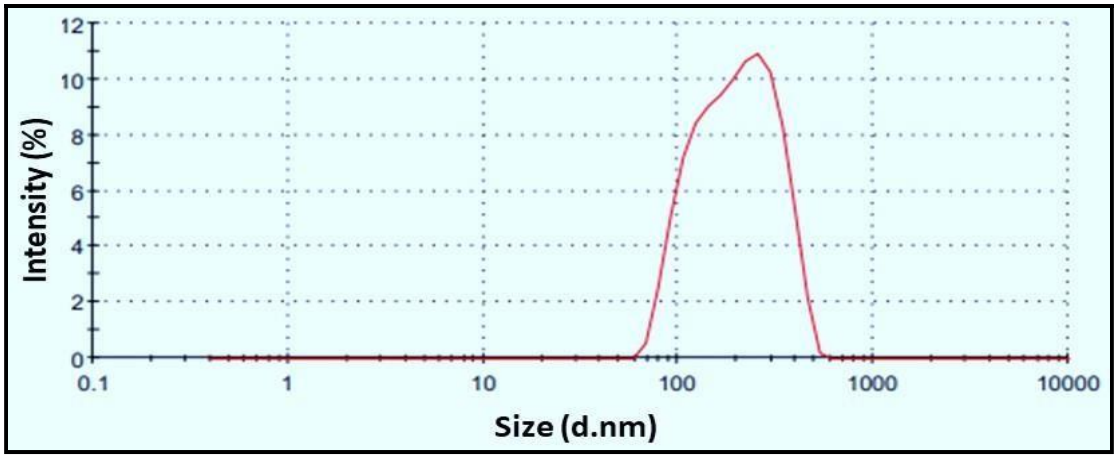

Figure 4.8: The average hydrodynamic size of HAp calculated during the DLS experiment.

PART 4: Development of mechanical strength in synthesized hydroxyapetite

4.8 Sintering of synthesized hydroxyapetite by incorporating sintering additives.

Sintering is essential in hydroxyapetite (HAp) processing to enhance its density, mechanical strength, and structural integrity for biomedical applications. It reduces porosity, improves crystallinity, and strengthens particle bonding, resulting in better bioactivity and stability. Optimizing sintering parameters ensures improved mechanical properties and controlled porosity, making HAp more suitable for bone implants and dental applications [174].

Significant factors have been selected for optimization, including different compositions of titanium dioxide and aluminum oxide, along with varying sintering temperatures (°C) and durations (hours), based on experimental data. The parameters chosen for Taguchi optimization involve aluminum oxide and titanium dioxide (weight %), sintering temperature (°C), and sintering time (hours). Additionally,

an L25 orthogonal array has been utilized, with Table presenting the experimental details and results, including sintered density (g/cm³), relative density (%), bulk density (**g/cm³), porosity (%), and linear shrinkage (%) [175].**

Table 4.2: Experimental Data as per L25 Taguchi Layout

S No	Aluminium oxide +Titanium dioxide	Temper ature	Time	Sintered Density	Relative Density	Bulk density	Porosity	Shrinkage
Units	**wt%**	**°C**	**Hours**	**g/cm^3**	**%**	**g/cm^3**	**%**	**%**
1	20+10	900	1	1.675	48.97	0.82	51.02	17.67
2	20+10	950	2	1.717	50.2	0.86	49.79	17.26
3	20+10	1000	3	1.911	55.8	1.06	44.12	15.37
4	20+10	1050	4	2.254	65.9	1.48	34.09	12.03
5	20+10	1100	5	3.121	91.25	2.84	8.74	3.58
6	22+8	900	2	1.705	49.85	0.84	50.14	17.38
7	22+8	950	3	1.766	51.6	0.91	48.36	16.78
8	22+8	1000	4	1.954	57.13	1.11	42.86	14.95
9	22+8	1050	5	2.565	75	1.92	25	9
10	22+8	1100	1	2.725	79.67	2.17	20.32	7.44
11	24+6	900	3	1.717	50.5	0.86	49.5	17.16
12	24+6	950	4	1.772	52.11	0.92	47.88	16.62
13	24+6	1000	5	2.198	64.64	1.42	35.35	12.45
14	24+6	1050	1	1.952	57.41	1.12	42.58	14.86
15	24+6	1100	2	2.725	80.14	2.18	19.85	7.28
16	26+4	900	4	1.721	50.32	0.86	49.67	17.22
17	26+4	950	5	1.788	52.28	0.93	47.71	16.57
18	26+4	1000	1	1.774	51.87	0.92	48.12	16.7
19	26+4	1050	2	1.965	57.45	1.12	42.54	14.84
20	26+4	1100	3	2.723	79.61	2.16	20.38	7.46
21	28+2	900	5	1.733	50.97	0.88	49.02	17
22	28+2	950	1	1.673	49.2	0.82	50.79	17.59
23	28+2	1000	2	1.849	54.38	1	45.61	15.87
24	28+2	1050	3	1.992	58.58	1.16	41.41	14.47
25	28+2	1100	4	2.843	83.61	2.37	16.38	6.12

4.8.1 Study of sintered density through ANOVA analysis

Sintering kinetics was used to determine the density of the ternary blend composite by firing the pellets in a muffle furnace at varying temperatures and times in accordance with the Taguchi L25 table. As an experimental output following the sintering of the composites, an ANOVA was conducted on the experimental

data. The ANOVA findings for the sintered density (g/cm^3) are shown in the table below. Initially, the information has been normalized. After normalizing the data for the sintering density, the figure 4.9 below shows that the majority of the data points appeared to be closer to the line, indicating that the data was determined to be in good agreement with the probability [176].

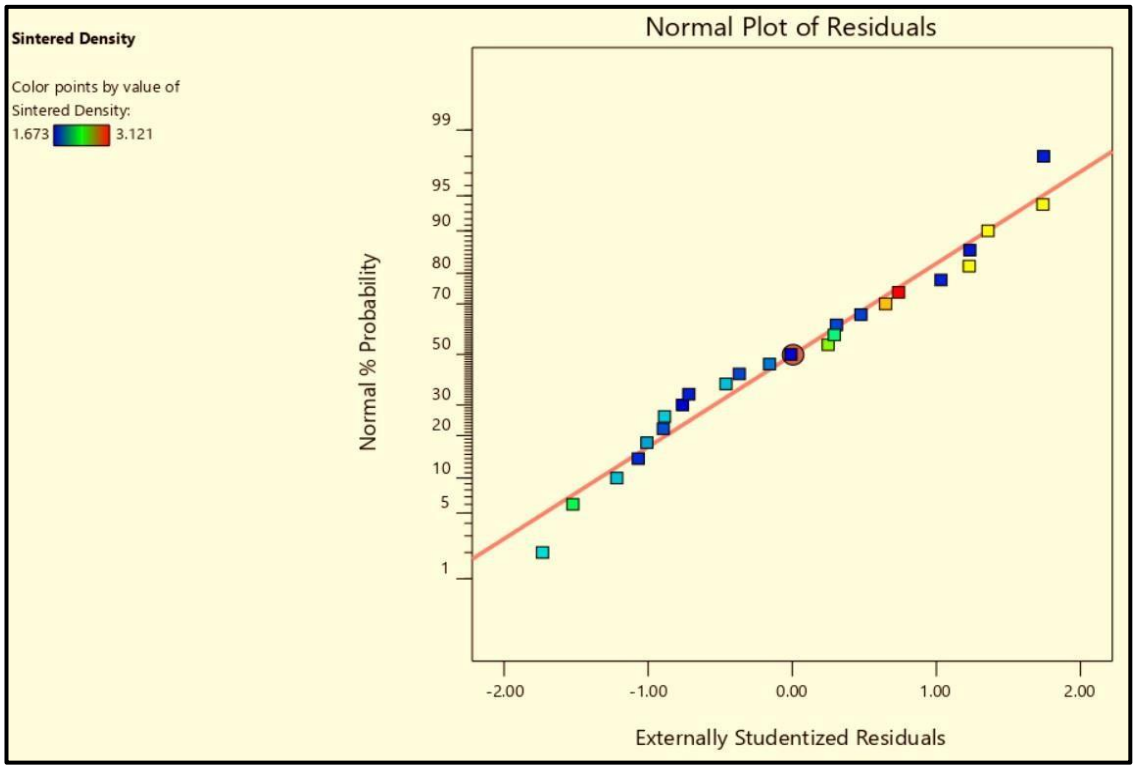

Figure 4.9: Normality plot for sintered density of composites.

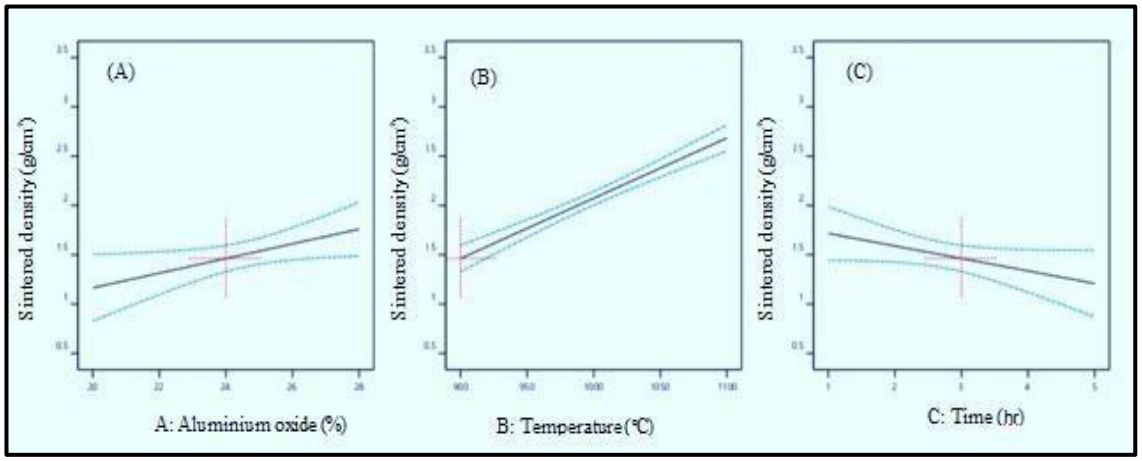

Figure 4.10: Effect of individual parameter on sintered density.

The graphs 4.10 (A) depict the influence of aluminum oxide content (%), sintering temperature (°C), and sintering time (hours) on the sintered density (g/cm³) of the material. In graph (A), increasing the aluminum oxide percentage results in a consistent rise in sintered density, demonstrating its contribution to material densification. Graph 4.10 (B) indicates that elevated sintering temperatures greatly enhance sintered density, highlighting the significance of thermal activation. Conversely, graph 4.10 (C) indicates that after reaching a certain point, extending the sintering time has a diminishing effect on density, highlighting an optimal duration for attaining maximum density. The figure shows that as the sintering temperature and time increase, porosity decreases while density increases. This is due to enhanced particle bonding and reduced pores at higher temperatures and longer durations.

Secondly, the Sintered density data was subjected to an ANOVA analysis. Analyze the mean square, F-value, and p-value for each of the parameters in Table , including the aluminum oxide composition (A), temperature (B), and time (C). Furthermore, the combined effects of temperature and time (BC), composition of aluminium oxide and time (AC), and aluminum oxide composition and temperature (AB) have been tabulated in table 4.3 [177,212].

Table 4.3: ANOVA analysis for the sintered density

S No	Source	Sum of Squares	Df	Mean Square	F-value	p-value	
1.	Model	4.18	6	0.6967	25.1	< 0.0001	Significant
2.	A-Aluminium Oxide	0.0004	1	0.0004	0.0142	0.9066	
3.	B-Temperature	3.57	1	3.57	128.49	< 0.0001	
4.	C-Time	0.0599	1	0.0599	2.16	0.1592	
5.	AB	0.2159	1	0.2159	7.78	0.0121	
6.	AC	0.2822	1	0.2822	10.17	0.0051	
7.	BC	0.2827	1	0.2827	10.18	0.0051	
8.	Residual	0.4997	18	0.0278			
9.	Total	4.68	24				

Moreover, the F-value of 25.1 indicated that the model was considered significant. The greater F- value of 0.01% probability may be attributed to noise. The model terms are significant when P-values are below 0.0500 in the given case, the model terms A, B, C, AB, AC, and BC is significant. The model terms that are not significant are revealed by a p value greater than 0.1000. Additionally, the Adeq Precision determines the signal-to-noise ratio. The ratio needs to be greater than 4, ideally. The signal strength for the previously discussed experimental run was determined to be adequate with a ratio of 17.976 [178].

4.8.1.1 Regression analysis

The regression equation for sintered density developed by the considering the significant terms is shown in equation 1 [179].

Equation 1 for Sintered Density

= -13.6554 + 0.604043 X Composition+ 0.018564 X Temperature - 2.62224 X Time - 0.00073 X Composition X Temperature + 0.041567 X composition X Time + 0.001664 X Temperature X Time.

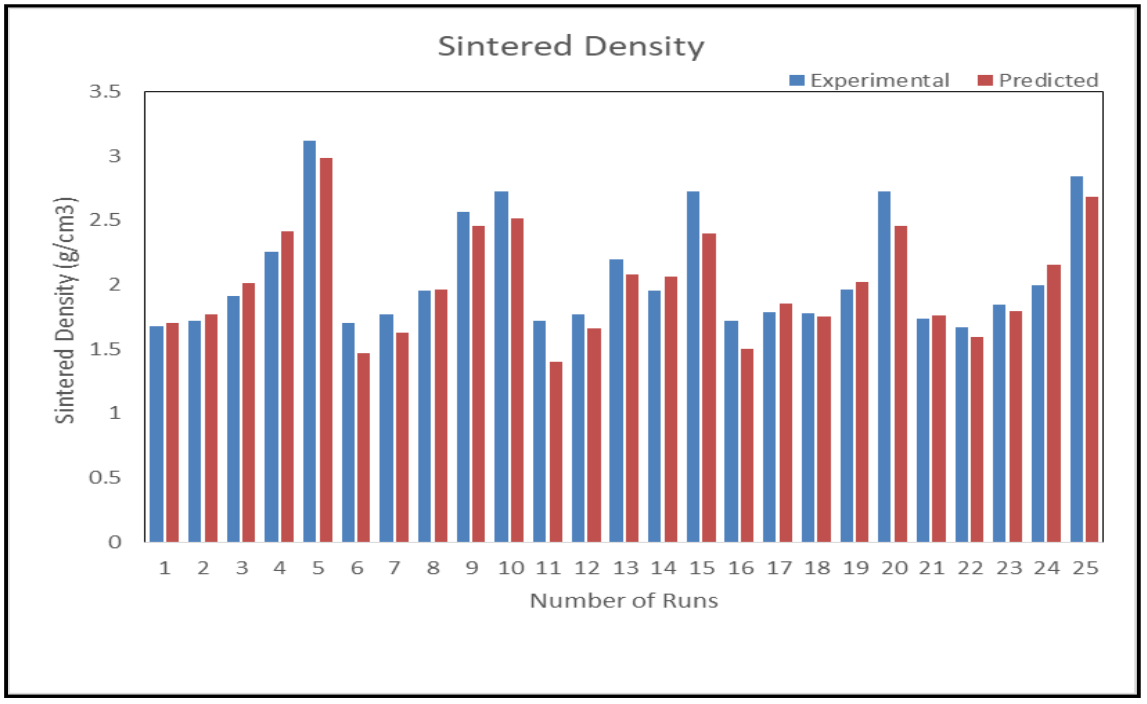

Figure 4.11: Comparison between experimental and predicted values of sintered density.

The predicted values of sintered density, calculated using the regression equation, are compared with the experimental values in the figure. The figure 4.11 shows that the deviation between the predicted and experimental values is minimal. Therefore, the regression equation can be reliably used for further calculations of sintered density based on the given input parameters.

The figure 4.12 graphs (A1, A2, B1, B2, C1, C2) provide a detailed analysis of the effects of aluminum oxide content (%), sintering temperature (°C), and sintering time (hours) on the sintered density (g/cm^3) of the material.

In figure 4.12 (A1) and (A2), the relationship between aluminum oxide weight percentage and sintering temperature is depicted. These graphs reveal that increasing sintering temperature from 900°C to 1100°C and keeping the weight percentage of aluminium oxide as 20% results in a significant improvement in sintered density. This indicated that temperature plays an important role in increasing the sintered density compared to aluminium oxide weight percentage

In figure 4.12 Graphs (B1) and (B2) examine the interaction between aluminum oxide content and sintering time. The graph illustrates that maintaining the aluminum oxide weight percentage at 20% while increasing the sintering time enhances the sintered density.

In figure 4.12 graphs (C1) and (C2) focus on the relationship between sintering temperature and sintering time. The graph illustrates that as both the sintering temperature and sintering time increase, the sintered density of the composite also improves significantly. This suggests that higher temperatures and prolonged exposure during the sintering process contribute to better particle bonding and densification, ultimately enhancing the overall density of the composite material [180].

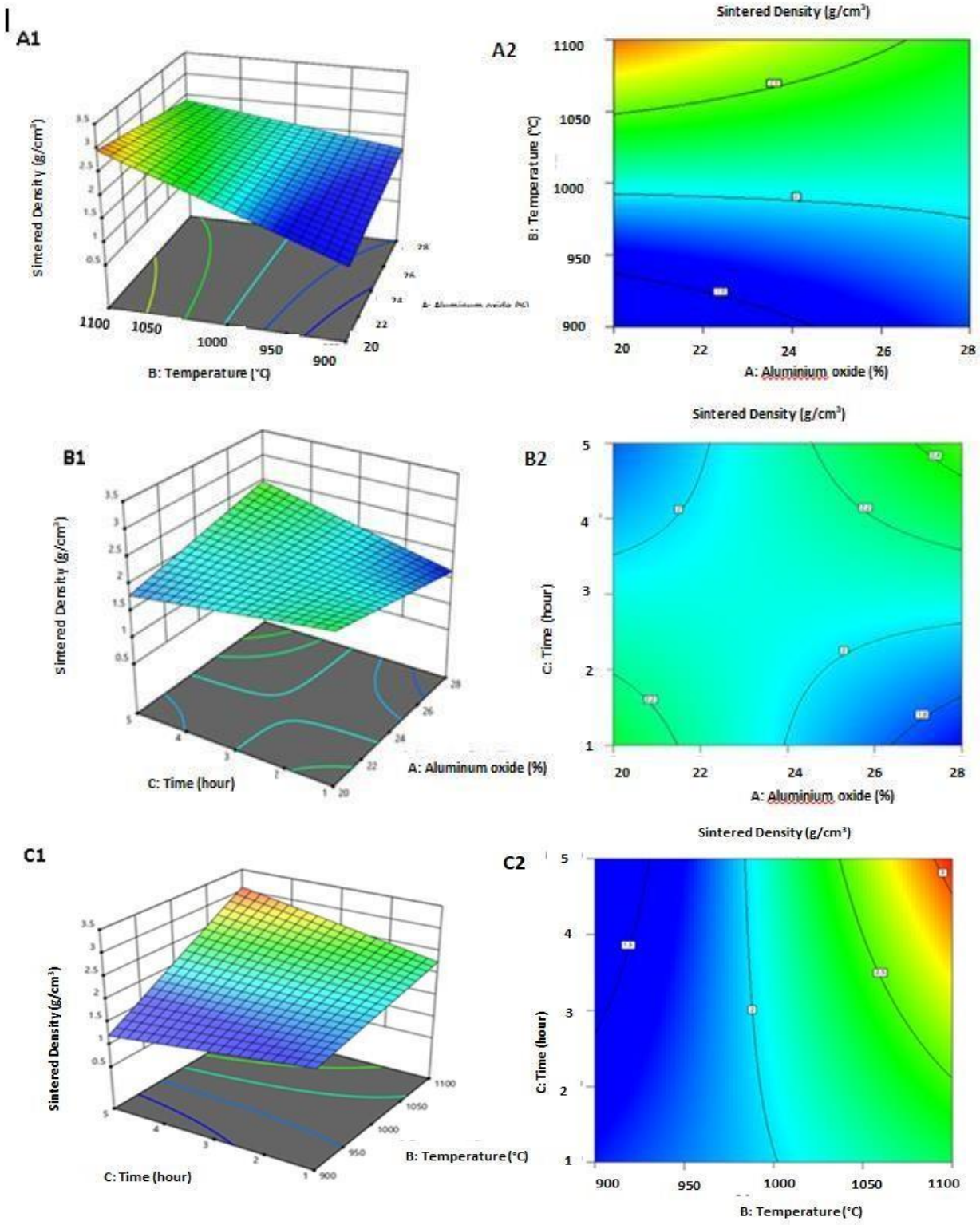

Figure 4.12: Influence of processing parameters on the sintered density of the ternary blend comprising calcined hydroxyapetite, aluminium oxide, and titanium dioxide, represented through 3D surface plots (A1, B1, C1) and contour plots (A2, B2, C2).

4.8.2 Study of Relative Density through ANOVA analysis

ANOVA was performed on the experimental data as an experimental output after the composites were sintered. The table below displays the relative density (g/cm^3) ANOVA results. First, the data has been normalized. The data was found to be in good agreement with its probability after being normalized for the relative density, as seen in the figure 4.13 below, where most of the data points seemed to be closer to the line [181].

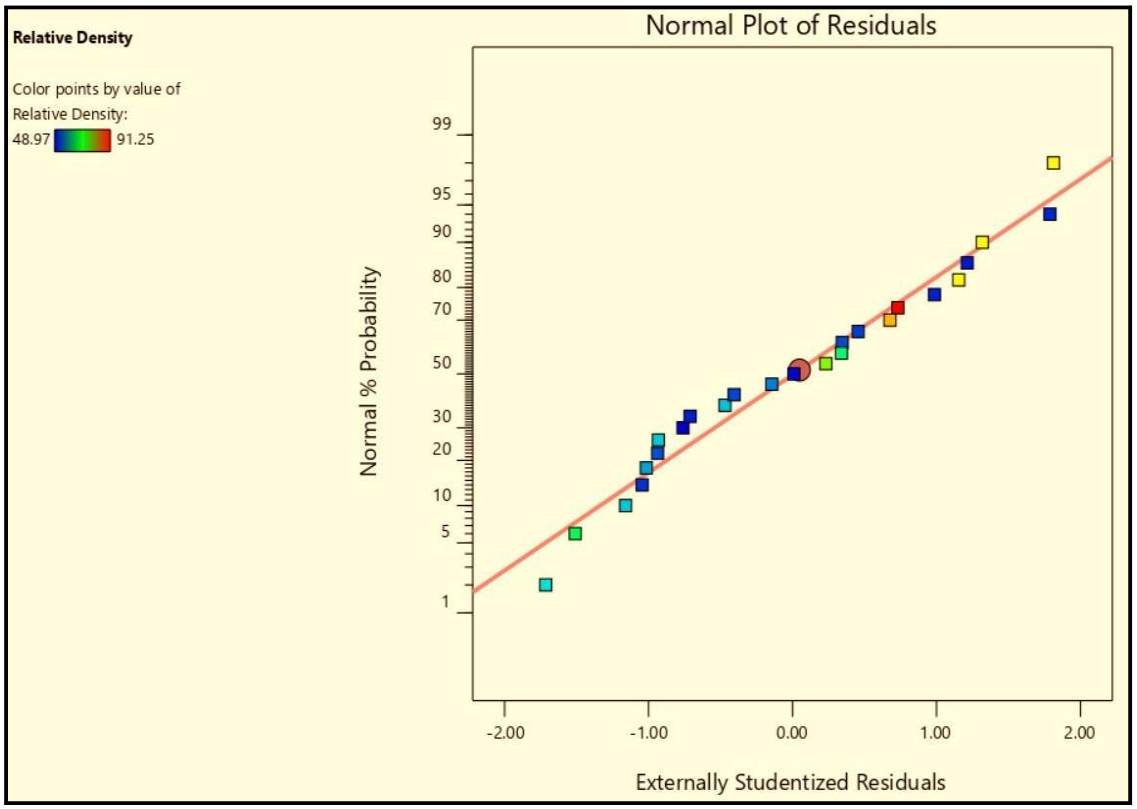

Figure 4.13: Normality plot for Relative density.

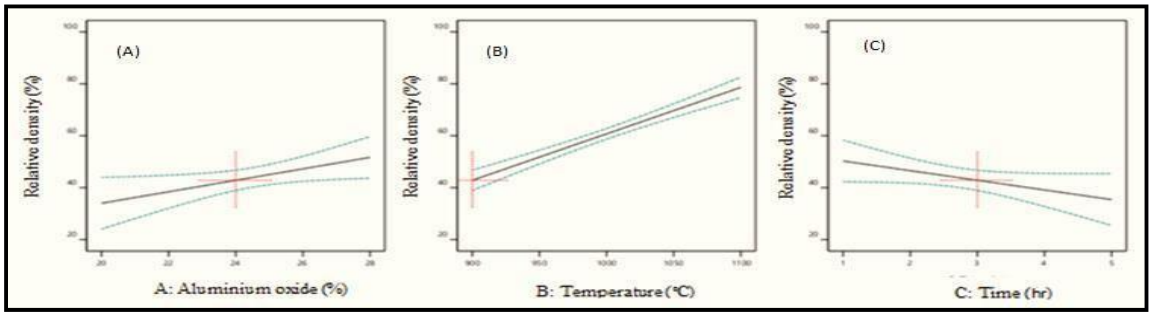

Figure 4.14: Effect of individual parameter on relative density.

The figure 4.14 graphs illustrate the impact of (A) aluminum oxide content (%), (B) sintering temperature (°C), and (C) sintering time (hours) on the relative density (%) of the material.

In graph 4.14 (A), it is observed that increasing the aluminum oxide content leads to a gradual rise in relative density. This indicates that aluminum oxide positively influences the densification process by promoting better packing and reducing voids within the material.

In Graph 4.14 (B) demonstrates that higher sintering temperatures significantly improve relative density. The increase in temperature enhances the material's ability to achieve a denser structure due to better particle fusion and reduction of porosity.

Conversely, in graph 4.14 (C) highlights the effect of sintering time on relative density. The graph shows that while moderate sintering time contributes positively to densification [184,213].

Additionally, an ANOVA analysis was performed on the relative density data. Examine the mean square, F-value, and p-value for each of the parameters listed in Table 4.4, such as the temperature (B), time (C), and aluminum oxide composition
(A). Furthermore, mentioned are the combined effects of temperature and time (BC), aluminum oxide composition and time (AC), and aluminum oxide composition and temperature (AB).

Table 4.4: ANOVA analysis for relative density

S No	Source	Sum of Squares	Df	Mean Square	F-value	p-value	
1.	Model	3580.34	6	596.72	24.83	< 0.0001	Significant
2.	A-Aluminium Oxide	1.1	1	1.1	0.0457	0.8332	
3.	B-Temperature	3063.59	1	3063.59	127.5	< 0.0001	
4.	C-Time	51.58	1	51.58	2.15	0.1601	
5.	AB	183.87	1	183.87	7.65	0.0127	
6.	AC	243.13	1	243.13	10.12	0.0052	
7.	BC	242.68	1	242.68	10.1	0.0052	
8.	Residual	432.52	18	24.03			
9.	Total	4012.87	24				

Furthermore, the model was considered significant based on the F-value of 24.83. It is possible to attribute the higher F-value of 0.01% probability to noise. P-values less than 0.0500 indicate that the model parameters are significant. The model terms A, B, C, AB, AC, and BC are important in the experiment. A p value greater than 0.1000 indicates the presence of non-significant model terms. The Adjusted R^2 was found to be 0.8922.The signal-to-noise ratio is also determined by the Adeq Precision. Ideally, the ratio should be higher than 4. With a ratio of 17.8287, the signal strength for the experimental run that was previously mentioned was found to be satisfactory [182].

4.8.2.1 Regression analysis

The regression equation for relative density developed by the considering the significant terms is shown in equation 2.

Equation 2 for Relative Density

= -398.857+ 17.64449 X Composition + 0.541925 X Temperature - 76.8782 X Time - 0.02122 X Composition X Temperature +1.22006 X Composition X Time + 0.048758 X Temperature X Time.

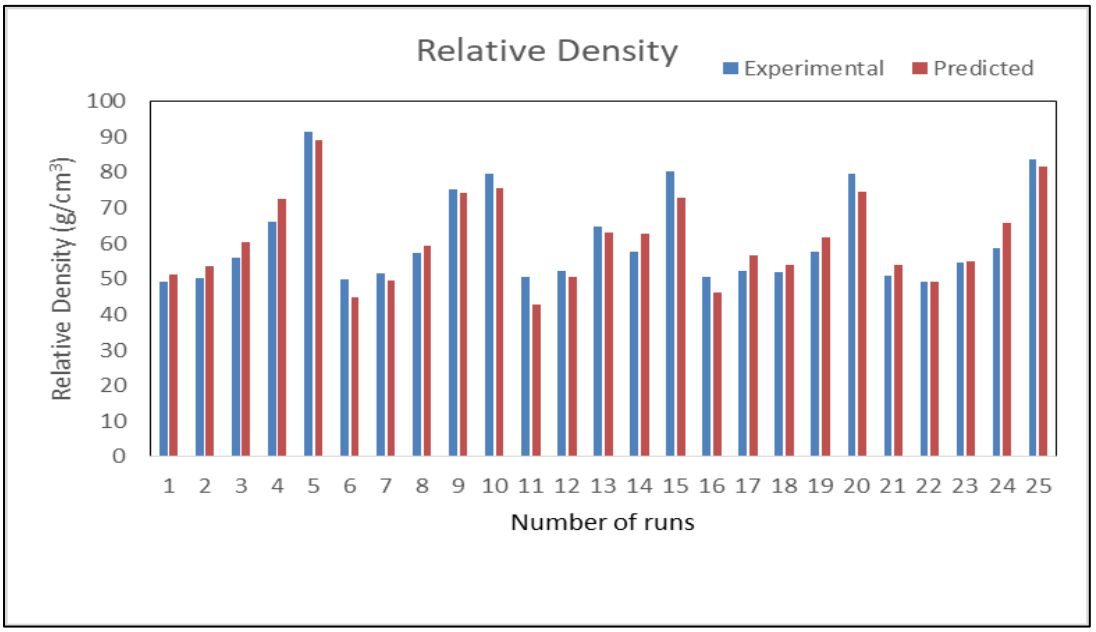

Figure 4.15: Comparison between experimental and predicted values using regression equation for relative density.

The predicted values of relative density, calculated using the regression equation, are compared with the experimental values in the figure. The figure shows that the deviation between the predicted and experimental values is minimal. Therefore, the regression equation can be reliably used for further calculations of relative density based on the given input parameters [183].

In figure 4.16 the graphs (A1, A2, B1, B2, C1, C2) provide a comprehensive visualization of the effects of aluminum oxide content (%), sintering temperature (°C), and sintering time (hours) on the relative density (%) of the material. In figure 4.16 Graphs A1 and A2 illustrate the interplay between aluminum oxide content and sintering temperature. The 3D surface plot (A1) shows that decreasing aluminum oxide percentage and increasing temperature significantly enhances the relative density, promotes densification. The corresponding 2D contour plot (A2) emphasizes the optimal conditions for achieving maximum relative density, with the gradient indicating the strong influence of these variables. In figure 4.16 (B1) and (B2), the interaction between aluminum oxide content and sintering time is examined. The surface plot (B1) highlights a steady increase in relative density with lower aluminum oxide content. The contour plot (B2) further reinforces, showing

that while higher aluminum oxide content does not has a significant effect, prolonged sintering time contribute substantially to higher relative density. In figure 4.16 Graphs C1 and C2 focus on the relationship between sintering temperature and time. The 3D plot (C1) shows that increasing the sintering temperature and sintering time leads to a substantial rise in relative density. The contour plot (C2) confirms this trend, highlighting the dominant role of temperature and time in achieving higher relative density. In conclusion, these graphs collectively underline the critical influence of aluminum oxide content, sintering temperature, and time on the relative density of the material [184].

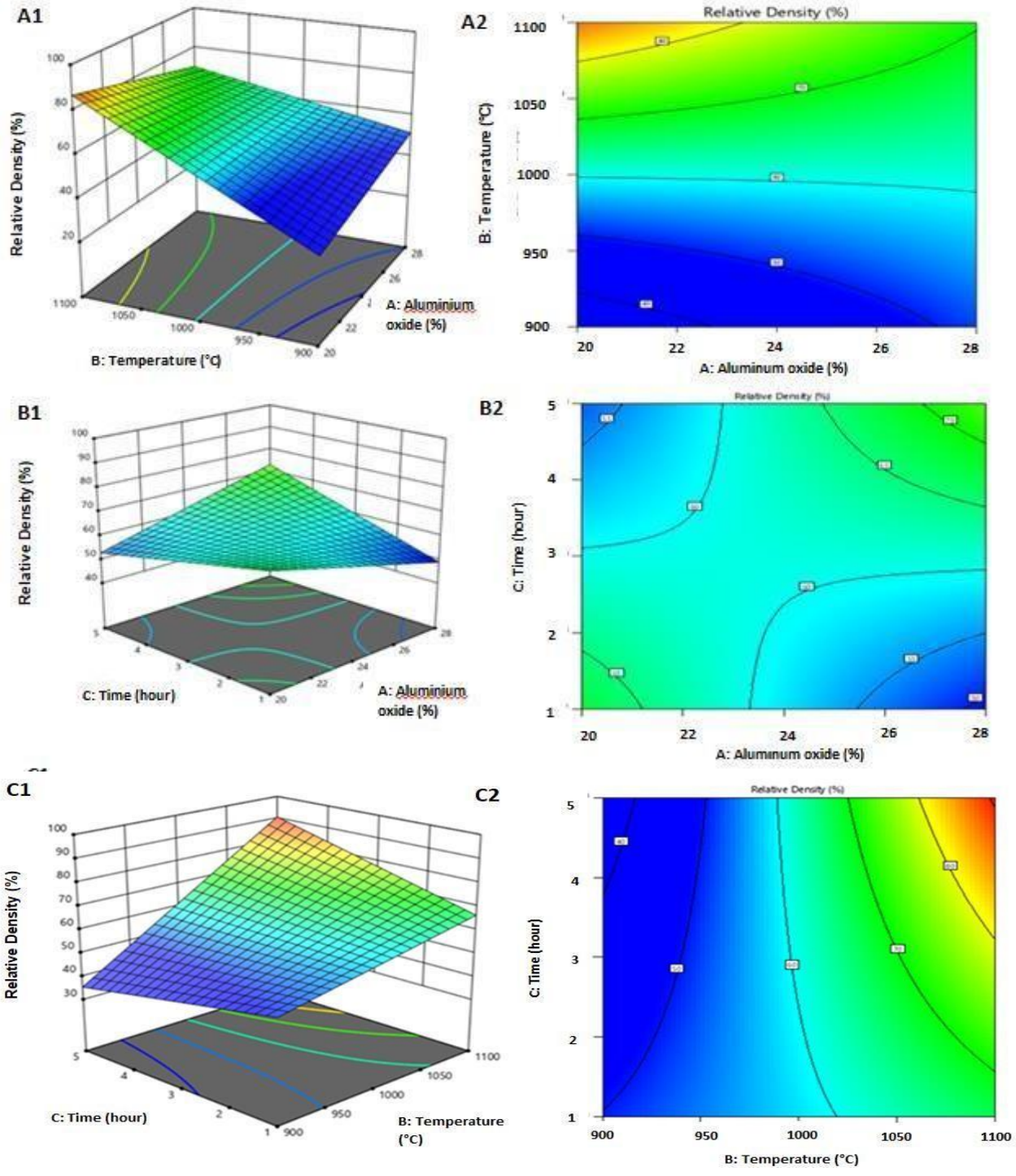

Figure 4.16: Influence of processing parameters on the relative density of the ternary blend comprising calcined hydroxyapetite, aluminum oxide, and titanium dioxide, represented through 3D surface plots (A1, B1, C1) and contour plots (A2, B2, C2).

4.8.3 ANOVA for Bulk density

An ANOVA was performed on the experimental data as an experimental outcome after the composites were sintered. The table below displays the results of the ANOVA of Bulk density (g/cm^3). First, the data was normalized. After being normalized for bulk density, the data was found to be in good agreement with its probabilities, as seen in the figure 4.17 below, where most of the data points seem to be closer to the line [185].

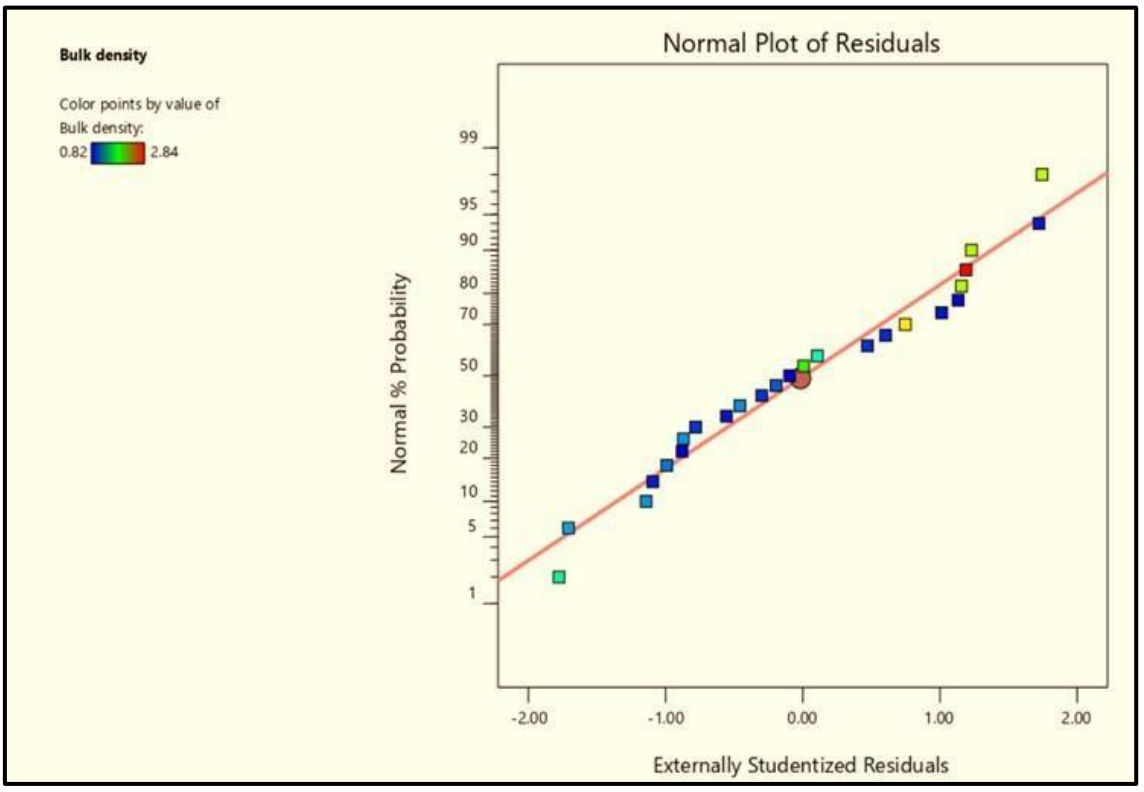

Figure 4.17: Normality plot for Bulk density for composites.

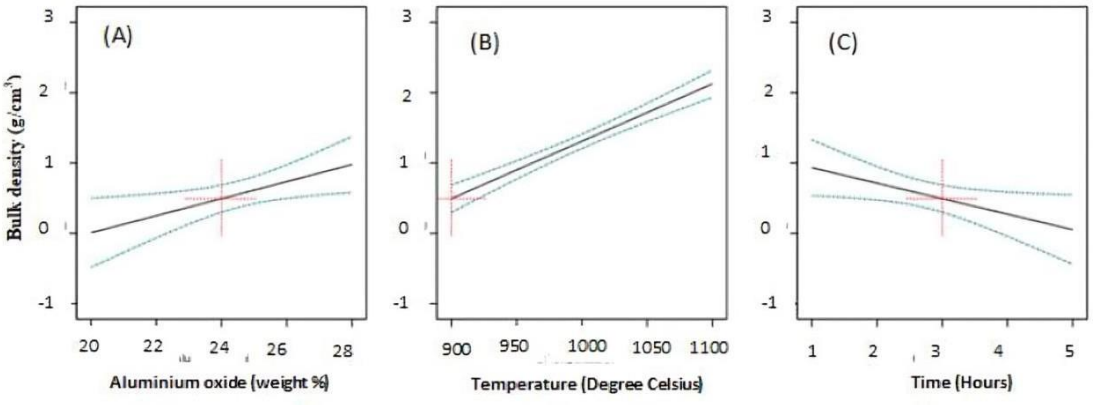

Figure 4.18: Effect of individual parameter on bulk density.

The figure 4.18 graphs (A) provide insights into the influence of aluminum oxide content (%), (B) sintering temperature (°C), and (C) sintering time (hours) on the bulk density (g/cm³) of the material.

In figure 4.18 Graph (A) shows a clear positive correlation between aluminum oxide content and bulk density. As the percentage of aluminum oxide increases, the bulk density improves steadily. This trend suggests that aluminum oxide acts as an effective densification agent, enhancing the material's structural compactness during sintering.

In figure 4.18 graph (B), the impact of sintering temperature on bulk density is evident. Higher sintering temperatures significantly increase the bulk density, underscoring the importance of thermal activation in promoting material consolidation. The elevated temperature facilitates grain growth and reduces porosity, leading to a denser material.

However, in figure 4.18 graphs (C) present a contrasting observation for sintering time. While shorter sintering times contribute positively to densification, extending the duration beyond a certain point results in a decline in bulk density. This reduction could be due to grain coarsening, over-sintering, or structural degradation, which negatively impact the material's overall density.

Moreover, an ANOVA analysis in table 4.5 was performed on the bulk density data. Analyze the aluminum oxide composition (A), temperature (B), and time (C) as well as the mean square, F-value, and p-value for each of the variables in the table. Furthermore, the combined effects of temperature and time (BC), temperature and aluminum oxide composition (AB), and time and aluminum oxide composition (AC) are examined.

Table 4.5: ANOVA analysis for Bulk density

S No	Source	Sum of Squares	Df	Mean Square	F-value	p-value	
1.	Model	7.43	6	1.24	21.07	< 0.0001	Significant
2.	A-Aluminium Oxide	0.0069	1	0.0069	0.1176	0.7357	
3.	B-Temperature	6.37	1	6.37	108.35	< 0.0001	
4.	C-Time	0.0712	1	0.0712	1.21	0.2855	
5.	AB	0.5356	1	0.5356	9.11	0.0074	
6.	AC	0.6345	1	0.6345	10.79	0.0041	
7.	BC	0.708	1	0.708	12.04	0.0027	
8.	Residual	1.06	18	0.0588			
9.	Total	8.49	24				

Additionally, the model was significant, as evidenced by the F-value of 21.07. It is possible to attribute the higher F-value of 0.01% probability to noise. A P-value below 0.0500 indicates that the model parameters are significant. The model terms A, B, C, AB, AC, and BC are essential to the experiment. When the p-value exceeds 0.1000, there are model terms that are not significant. It was discovered that the Adjusted R^2 was 0.8565. The signal-to-noise ratio is also determined by the Adeq Precision. Ideally, the ratio should be higher than 4. With a ratio of 17.840, it was found that the signal strength for the experiment run that was previously described was good [186,214].

4.8.3.1 Regression analysis

The regression equation for bulk density developed by the considering the significant terms is shown in equation 3.

Equation Regression equation 3 for Bulk Density

= -22.2394 + 0.965045 X Composition + 0.027745 X Temperature – 4.08617 X Time – 0.00115 X Composition X Temperature + 0.062327 X Composition X Time + 0.002633 X Temperature X Time.

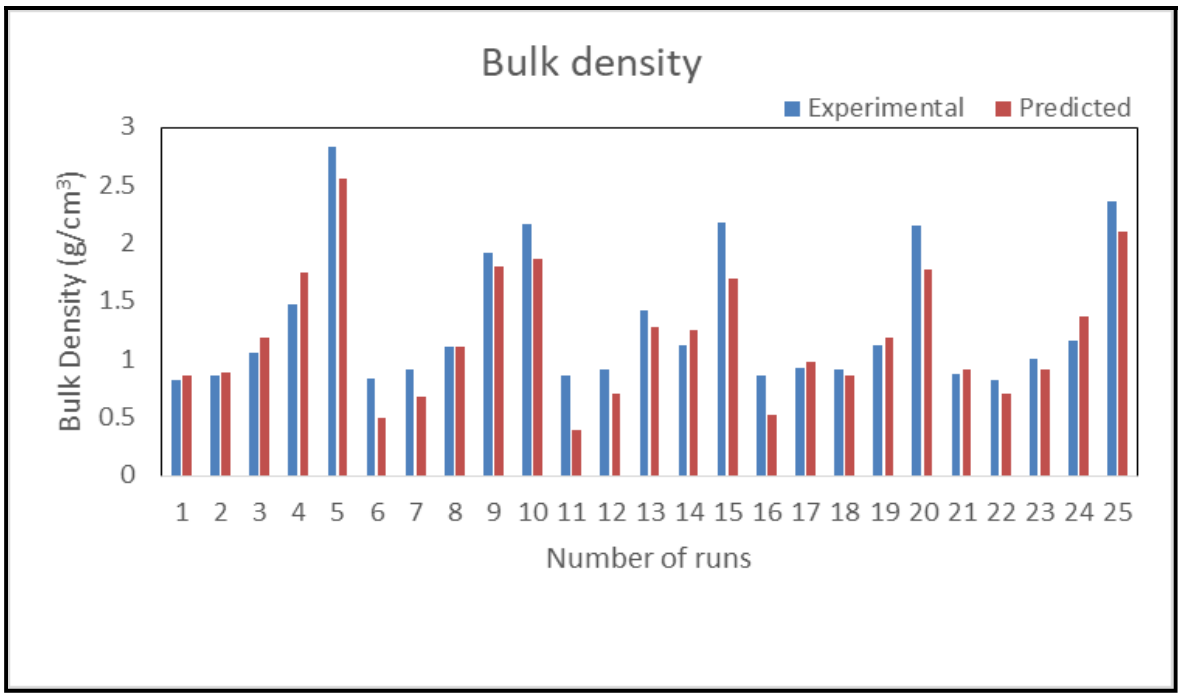

Figure 4.19: Comparison between experimental and predicted values using regression equation for bulk density.

The predicted values of bulk density, calculated using the regression equation, are compared with the experimental values in the figure. The figure shows that the deviation between the predicted and experimental. Therefore, the regression equation can be reliably used for further calculations of bulk density based on the given input parameters [187].

The figure 4.20 below provides the graphs presents a comprehensive analysis of how bulk density (g/cm³) is influenced by three key factors: aluminum oxide percentage, temperature (°C), and sintering time (hours). It consists of three sets of visualizations, each containing a 3D surface plot and a corresponding contour plot.

In figure 4.20 graphs (A1 and A2) examines the effect of aluminum oxide percentage and temperature on bulk density. The 3D surface plot (A1) shows a

clear increasing trend in bulk density with increasing temperature and decreasing aluminum oxide content. This suggests that higher sintering temperatures and lower aluminum oxide percentages promote densification. The contour plot (A2) provides a top-down view; this indicates that a combination of high temperature and lower aluminum oxide results in optimal material density.

In figure 4.20 graphs (B1 and B2) investigates the impact of aluminum oxide percentage and sintering time on bulk density. The 3D plot (B1) reveals that while sintering time and lower content of aluminium oxide has a positive effect on bulk density. The surface plot appears more gradual, indicating that while prolonged sintering contributes to densification. The contour plot (B2) confirms this observation, showing a more uniform distribution of bulk density across different sintering times. This suggests that while increasing sintering time and lowering the aluminium oxide weight percentage can enhance bulk density.

In figure 4.20 graphs (C1 and C2) focuses on the relationship between temperature and sintering time and their combined effect on bulk density. The 3D surface plot (C1) demonstrates that temperature has the most substantial impact on increasing bulk density, with sintering time playing a supporting role. The steep incline in the surface plot indicates that as temperature rises, bulk density increases significantly. The contour plot (C2) further supports this conclusion, with the highest bulk density values concentrated in the upper-right region, where both temperature and sintering time are at their peak. This confirms that temperature is the most dominant factor in achieving high bulk density [188].

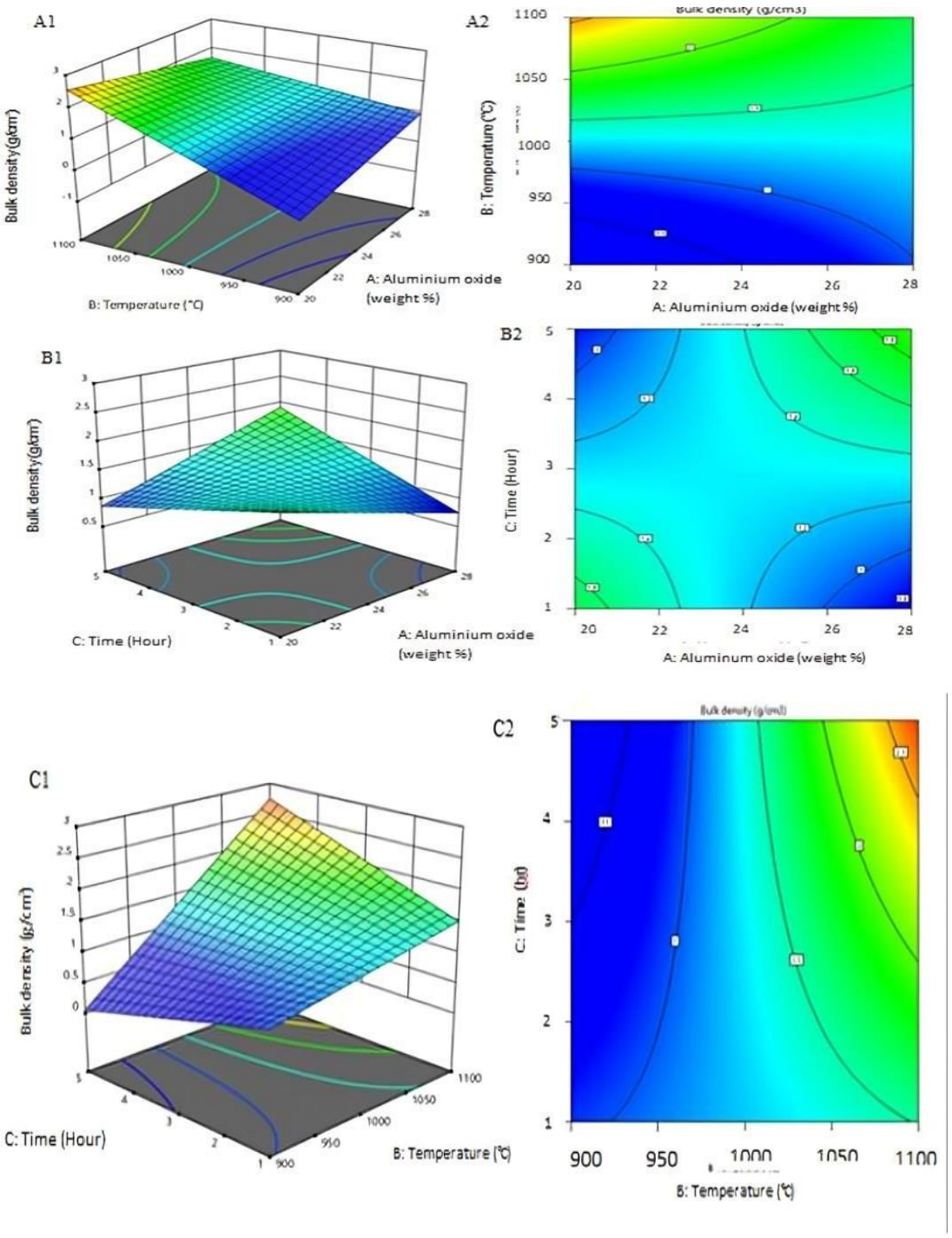

Figure 4.20: Influence of processing parameters on the bulk density of the ternary blend comprising calcined hydroxyapetite, aluminum oxide, and titanium dioxide,represented through 3D surface plots (A1, B1,C1) and contour plots (A2, B2, C2).

4.8.4 ANOVA analysis for Porosity

Once the composites were sintered, the experimental data was subjected to an ANOVA as an experimental outcome. The Porosity (%) ANOVA findings are shown in the table below. The data has first been normalized. As can be seen in the figure

4.21 below, where the majority of the data points appear to be closer to the line, the data was found to be in good agreement with its probabilities after being normalized for porosity [189].

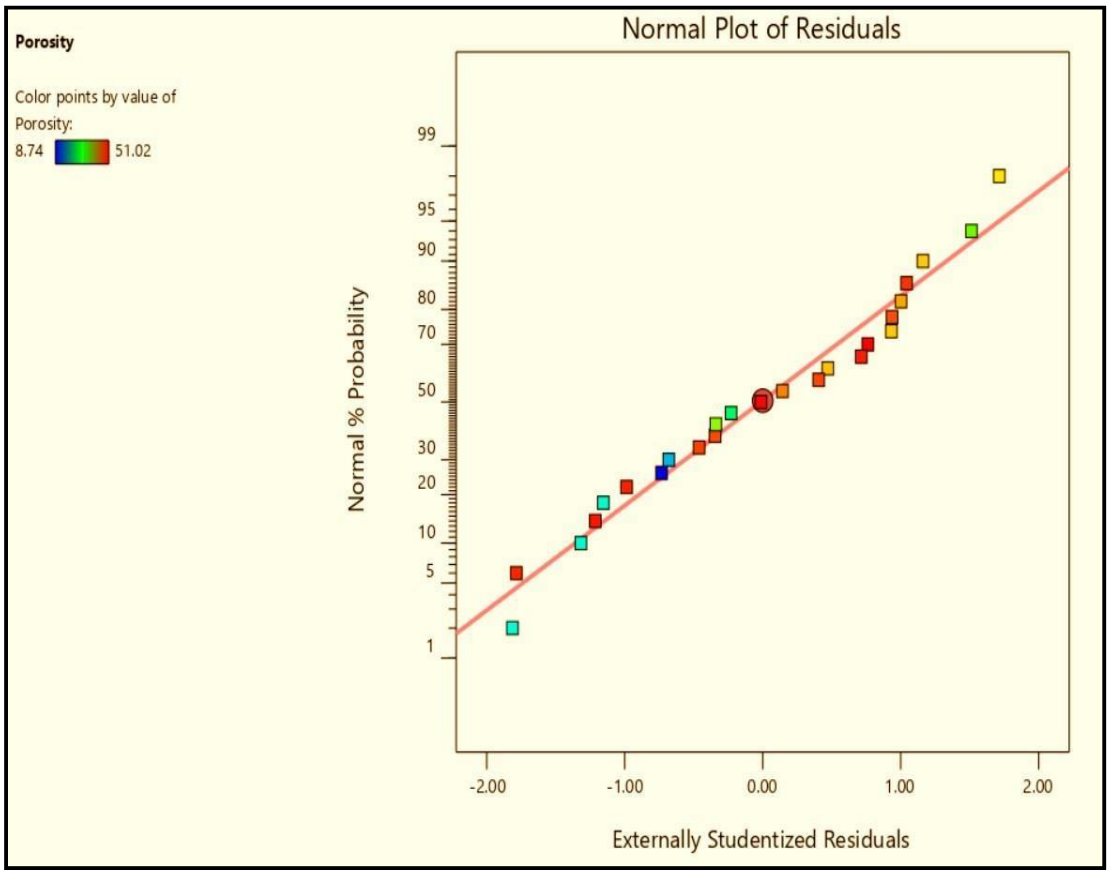

Figure 4.21: Normality plot for porosity of composites.

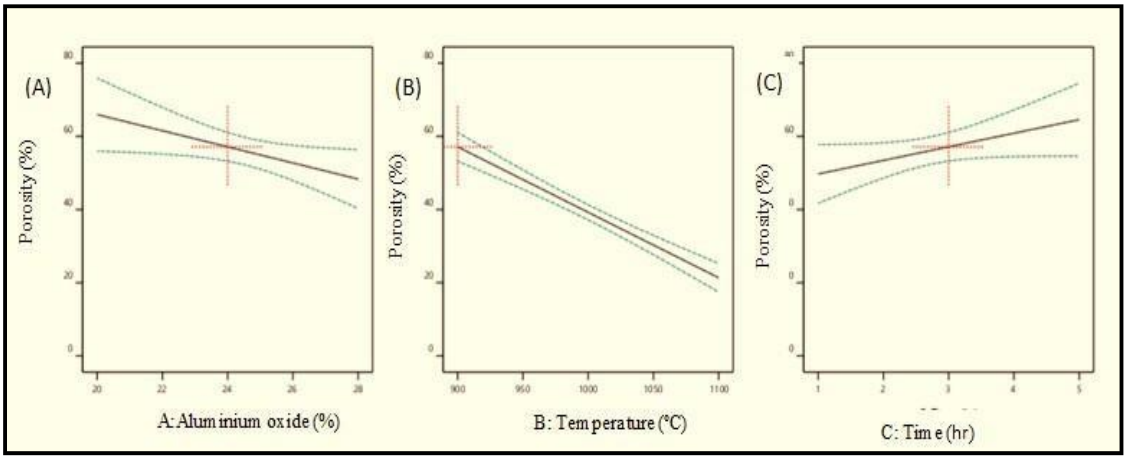

Figure 4.22: Effect of individual parameter on Porosity

In figure 4.22images presents three line graphs labeled (A), (B), and (C), each illustrating the effect of different parameters on porosity (%). The x-axis in each graph represents a specific variable—aluminum oxide percentage in (A), temperature in (B), and sintering time in (C)—while the y-axis represents porosity percentage. Each graph features a central trend line with confidence intervals indicated by the dashed lines.

In figure 4.22 graph (A), the relationship between aluminum oxide percentage and porosity shows a decreasing trend, indicating that higher aluminum oxide content leads to lower porosity. This suggests that increasing aluminum oxide enhances material densification, thereby reducing the overall porosity of the structure. The confidence interval remains relatively narrow, indicating a more predictable effect.

In figure 4.22 graphs (B) displays the effect of temperature on porosity. The trend line shows a clear negative correlation, meaning that as the temperature increases, porosity decreases. This aligns with the expected behavior in sintering processes, where higher temperatures facilitate densification, leading to lower porosity. The confidence interval remains consistent, further confirming the reliability of this trend.

In contrast, figure 4.22 graph (C) illustrates the impact of sintering time on porosity.

Unlike the previous two graphs, this trend line shows a slight increase in porosity with increasing sintering time. This could indicate that excessive sintering time may lead to grain growth and pore coalescence, which can contribute to increased porosity.

Furthermore, the porosity data were subjected to an ANOVA analysis. Examine at the mean square, F-value, and p-value for each of the variables in Table 2, including the aluminum oxide composition (A), temperature (B), and time (C). Additionally, the combined effects of time and temperature (BC), aluminum oxide composition and time (AC), and aluminum oxide composition and temperature (AB) are discussed in table 4.6.

Table 4.6: ANOVA analysis for Porosity.

S No	Source	Sum of Squares	Df	Mean Square	F-value	p-value	
1.	Model	3579.72	6	596.62	24.87	< 0.0001	Significant
2.	A-Aluminium Oxide	1.04	1	1.04	0.0433	0.8375	
3.	B-Temperature	3062.67	1	3062.67	127.66	< 0.0001	
4.	C-Time	51.64	1	51.64	2.15	0.1596	
5.	AB	183.49	1	183.49	7.65	0.0127	
6.	AC	242.76	1	242.76	10.12	0.0052	
7.	BC	242.13	1	242.13	10.09	0.0052	
8.	Residual	431.84	18	23.99			
9.	Total	4011.55	24				

Further, the F-value of 24.87 indicated that the model was significant. The greater F-value of 0.01% probability can be assigned to noise. The model parameters are considered significant if the P-value is less than 0.0500. In the experiment, the model terms A, B, C, AB, AC, and BC are crucial. Model terms that are not significant are present when the p-value is higher than 0.1000. In comparison to the Predicted R^2 of 0.7880, it was found that the Adjusted R^2 of 0.8565 was less than 0.2. The Adeq Precision also determines the signal-to-noise ratio. The ratio should ideally be greater than 4. The signal strength for the previously discussed experimental run was determined to be good with a ratio of 17.840 [190,215].

4.8.4.1 Regression analysis

The regression equation for porosity developed by the considering the significant terms is shown in equation 4.

Regression equation 4 for Porosity

= 498.4693 - 17.623 X Composition - 0.54154 X Temperature + 76.79948 X Time
+0.021198 X Composition X Temperature - 1.21912 X Composition X Time - 0.0487 X Temperature X Time.

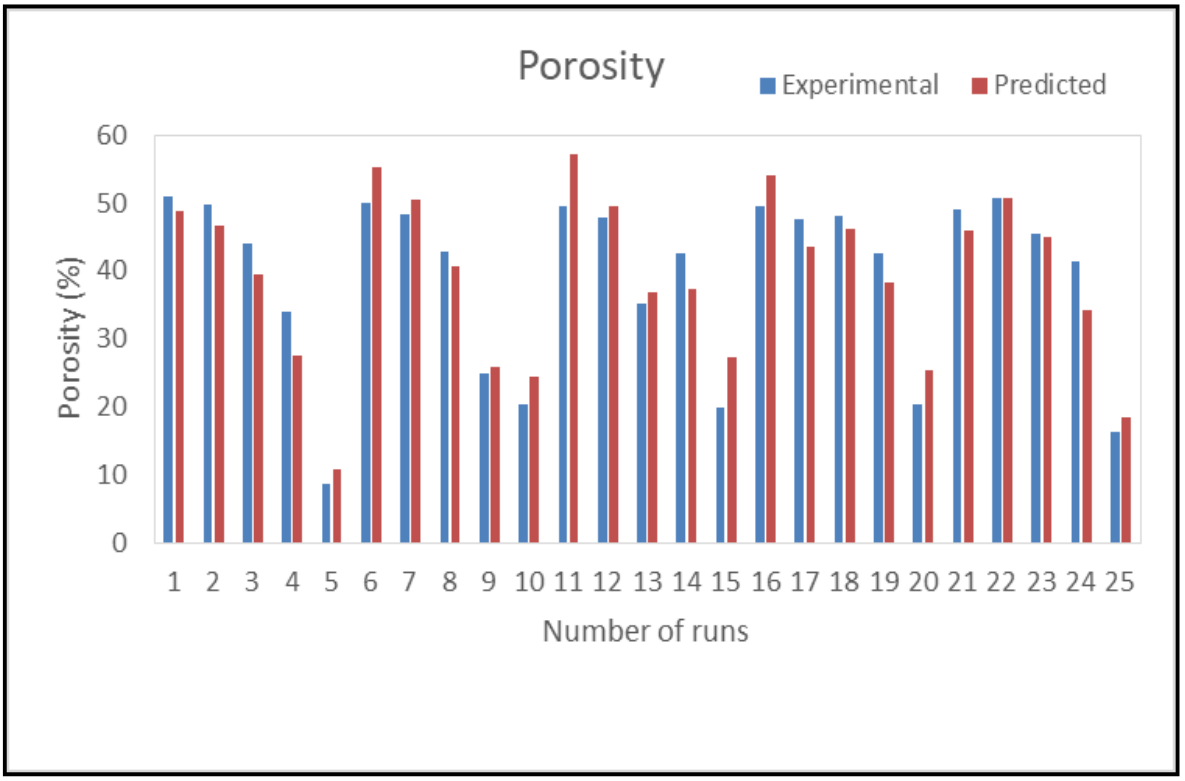

Figure 4.23: Comparison between experimental and predicted values using regression equation for porosity.

The predicted values of porosity, calculated using the regression equation, are compared with the experimental values in the figure. The figure shows that the deviation between the predicted and experimental is minimal. Therefore, the regression equation can be reliably used for further calculations of porosity based on the given input parameters [191].

The figure 4.24 consists of three sets of 3D surface plots and corresponding contour plots, labeled as A1, A2, B1, B2, C1, and C2, illustrating the effect of different parameters on porosity (%). Each row represents the relationship between porosity and two independent variables: aluminum oxide percentage, temperature, and sintering time.

In Figure 4.24 A1 and A2, the effect of aluminum oxide content and temperature on porosity is analyzed. The 3D surface plot (A1) demonstrates that porosity decreases as temperature increases and aluminum oxide content rises. This suggests that higher temperatures promote densification, leading to lower porosity, while aluminum oxide contributes to reducing pore formation. The corresponding contour plot (A2) confirms this trend, with a gradient indicating lower porosity at elevated temperatures and aluminum oxide concentrations.

Figure 4.24 B1 and B2 examine the impact of aluminum oxide content and sintering time on porosity. The surface plot (B1) shows a more complex interaction, where porosity remains relatively stable at lower sintering times but slightly decreases as sintering time increases, especially at lower aluminum oxide concentrations. The contour plot (B2) provides a clearer representation, highlighting areas of low porosity associated with longer sintering times and lower aluminum oxide content.

In Figure 4.24 C1 and C2, the relationship between temperature and sintering time on porosity is depicted. The 3D surface plot (C1) reveals a strong inverse correlation between temperature and time, where porosity significantly decreases at higher temperatures. Sintering time has a same impact as temperature which influences porosity variations. The contour plot (C2) corroborates this observation, with red areas representing high porosity at lower temperatures, transitioning to blue regions where porosity is reduced at higher temperatures [192].

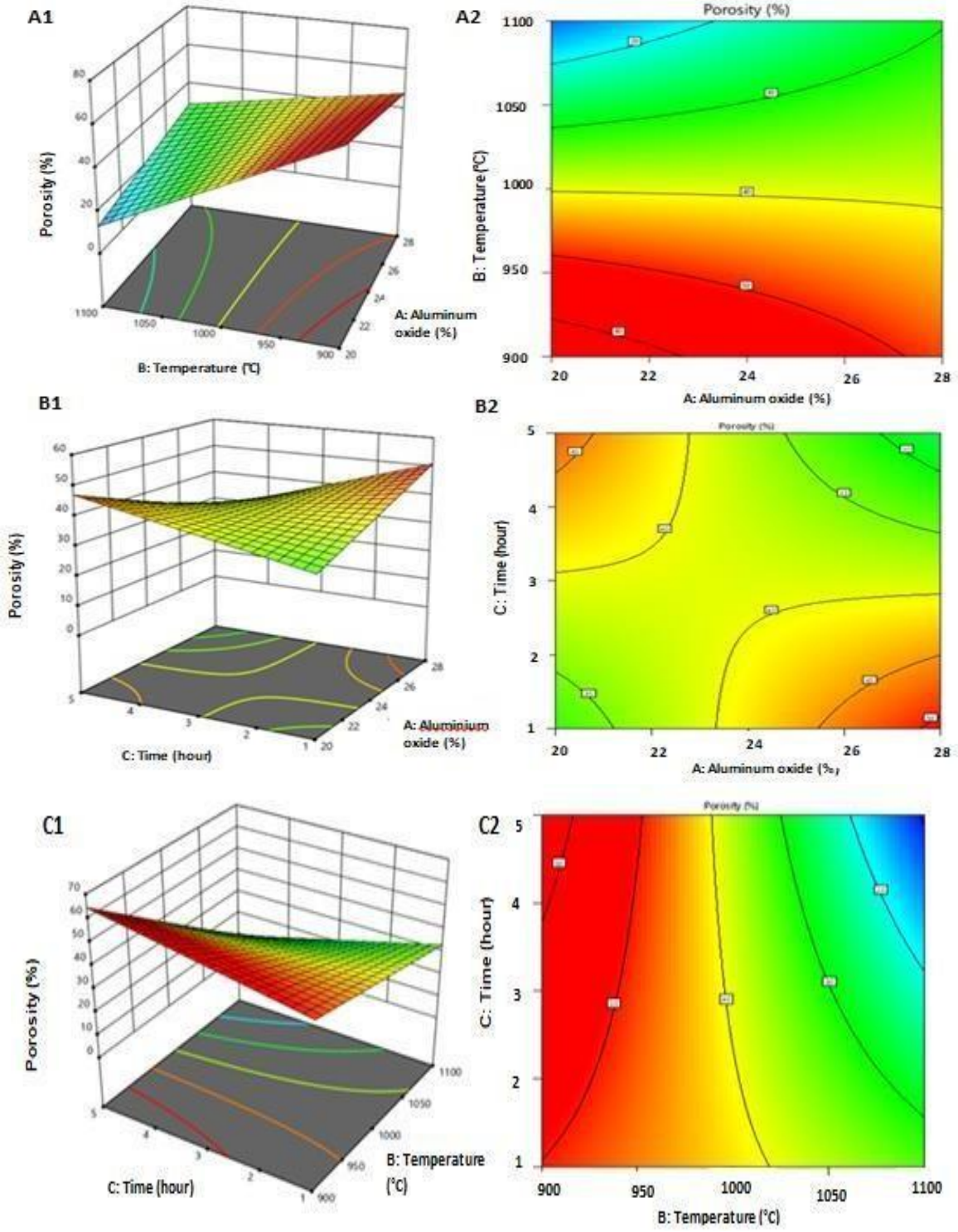

Figure 4.24: Influence of processing parameters on the porosity of the ternary blend comprising calcined hydroxyapetite, aluminum oxide, and titanium dioxide, represented through 3D surface plots (A1, B1, C1) and contour plots (A2, B2, C2).

4.8.5 ANOVA analysis for linear shrinkage

Following the sintered composites, an ANOVA was performed on the experimental data as an experimental result. The table below displays the Linear Shrinkage (%) ANOVA results. The first step was to normalize the data. The data was found to be in good agreement with its probabilities after being normalized for linear shrinkage, as shown in the figure4.25 below, where most of the data points seem to be closer to the line [193].

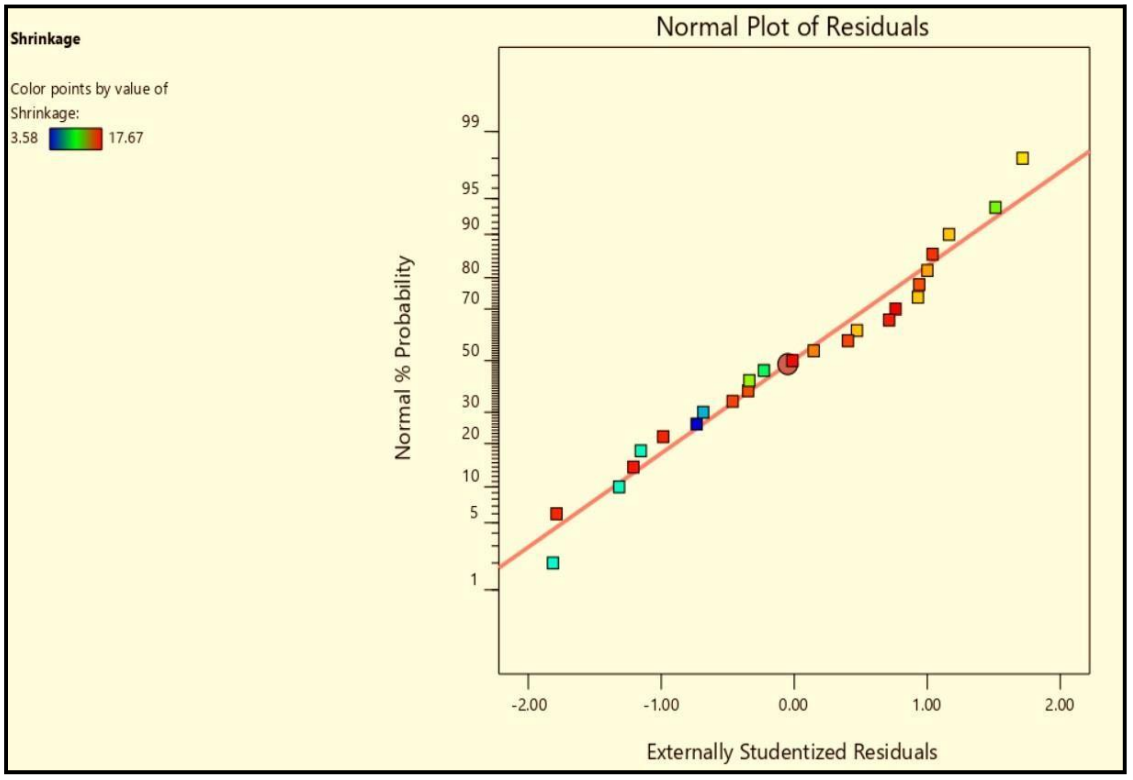

Figure 4.25: Normal plot for shrinkage for the composites.

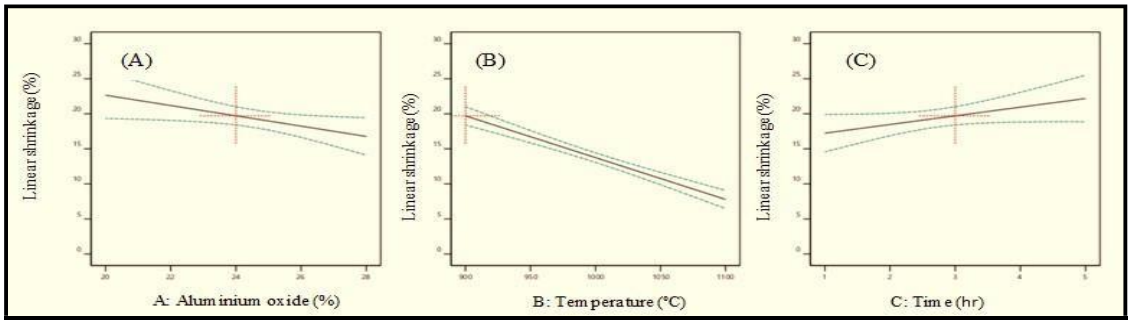

Figure 4.26: Effect of individual factor parameter on linear shrinkage.

In figure 4.26, contains three graphs labeled (A), (B), and (C), depicting the relationship between linear shrinkage (%) and three independent variables: aluminum oxide content, temperature, and sintering time. Each graph shows a trend line with confidence intervals, illustrating how these factors influence the shrinkage of the material.

In Figure 4.26 (A), the effect of aluminum oxide content on linear shrinkage is presented. The graph shows a decreasing trend, indicating that as the aluminum oxide percentage increases, linear shrinkage reduces. This suggests that higher aluminum oxide content may contribute to structural stability, limiting excessive shrinkage during processing.

Figure 4.26 (B) examines the influence of temperature on linear shrinkage. The plot demonstrates a noticeable decline in shrinkage as temperature increases. This suggests that higher sintering temperatures facilitate material densification, leading to reduced shrinkage. The confidence intervals indicate a consistent trend, reinforcing the inverse relationship between temperature and shrinkage.

Figure 4.26 (C) presents the relationship between sintering time and linear shrinkage. Unlike the other two graphs, this one shows a slight increasing trend, meaning that longer sintering durations contribute to higher shrinkage. This is likely due to prolonged exposure to high temperatures, allowing the material to contract further. However, the effect appears to be less pronounced compared to temperature.

Moreover, an ANOVA analysis was performed on the linear shrinkage data. For every variable in Table 2, such as the aluminum oxide composition (A), temperature (B), and time (C), analyze the mean square, F-value, and p-value. Furthermore, the combined effects of temperature and time (BC), temperature and aluminum oxide composition (AB), and time and aluminum oxide composition (AC) are examined.

Table 4.7: ANOVA analysis of linear shrinkage.

S No	Source	Sum of Squares	df	Mean Square	F-value	p-value	
1.	Model	397.51	6	66.25	24.84	< 0.0001	significant
2.	A-Aluminium Oxide	0.1175	1	0.1175	0.0441	0.8361	
3.	B-Temperature	340.11	1	340.11	127.54	< 0.0001	
4.	C-Time	5.73	1	5.73	2.15	0.1598	
5.	AB	20.38	1	20.38	7.64	0.0128	
6.	AC	26.96	1	26.96	10.11	0.0052	
7.	BC	26.9	1	26.9	10.09	0.0052	
8.	Residual	48	18	2.67			
9.	Total	445.51	24				

In addition, the model was significant, as demonstrated by the F-value of 24.84. It is possible to attribute the higher F-value of 0.01% probability to noise. A P-value below 0.0500 indicates that the model parameters are significant. The model terms A, B, C, AB, AC, and BC are essential to the experiment. When the p-value exceeds 0.1000, there are model terms that are not significant. The Adjusted R2 was 0.8563 the signal-to-noise ratio is also determined by the Adeq Precision. Ideally, the ratio should be higher than 4. With a ratio of 17.8306, the signal strength for the experimental run that was previously described was found to be good [194].

4.8.5.1 Regression analysis

The regression equation for linear shrinkage developed by the considering the significant terms is shown in equation 5.

Regression equation 5 for linear shrinkage

=166.7761- 5.87292 X Composition - 0.18046 X Temperature +25.5957 X Time
+0.007064 X Composition X Temperature -0.40629 X Composition X Time - 0.01623 X Temperature X Time.

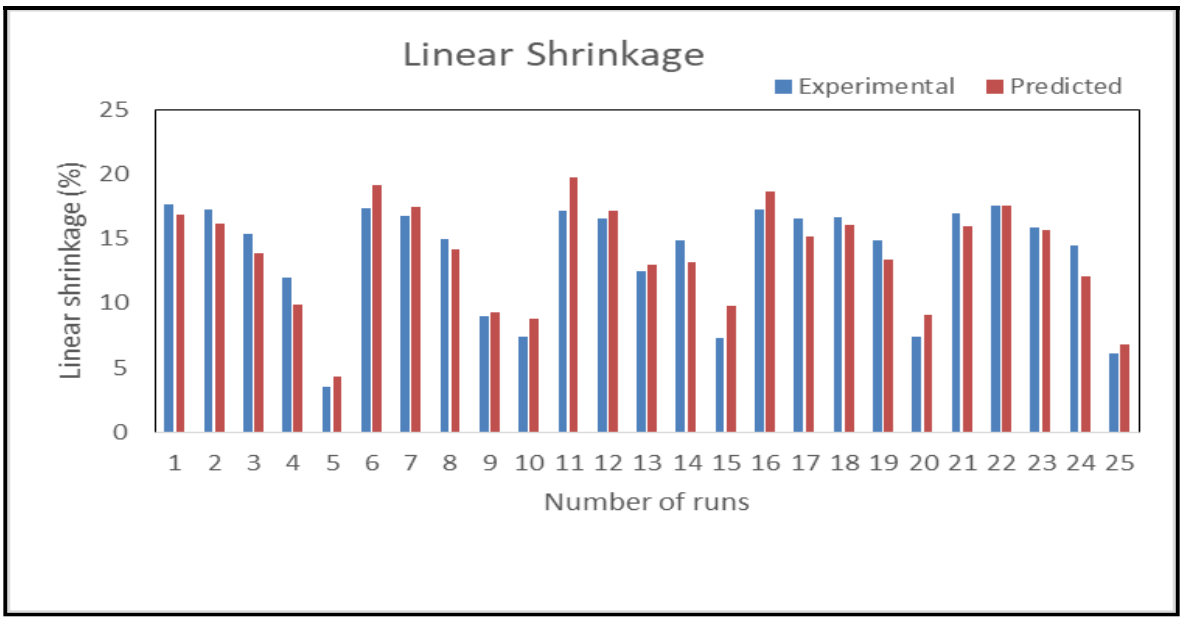

Figure 4.27: Comparison between the experimental and predicted values of linear shrinkage using regression equation.

The predicted values of linear shrinkage, calculated using the regression equation, are compared with the experimental values in the figure. The figure shows that the deviation between the predicted and experimental is minimal. Therefore, the regression equation can be reliably used for further calculations of linear shrinkage based on the given input parameters [195].

The provided image consists of three sets of 3D surface plots and contour plots, illustrating the effects of aluminum oxide content, temperature, and sintering time on shrinkage (%).

In Figure 4.28 (A1), the surface plot shows that shrinkage increases with temperature and lower aluminum oxide content. The contour plot in Figure 4.28 (A2) confirms this trend, highlighting higher shrinkage at elevated temperatures and lower aluminum oxide levels.

Figure 4.28 (B1) examines lower aluminum oxide content and higher sintering time, shows reduction in shrinkage. The contour plot in Figure 4.28 (B2) further supports this observation, with shrinkage decreasing as aluminum oxide content increases.

Figure 4.28 (C1) explores the effect of sintering time and temperature, revealing that temperature and time both play a same role on the influence of shrinkage. The contour plot in Figure 4.28 (C2) shows high shrinkage at higher temperatures, while lower shrinkage is observed at reduced temperatures [196].

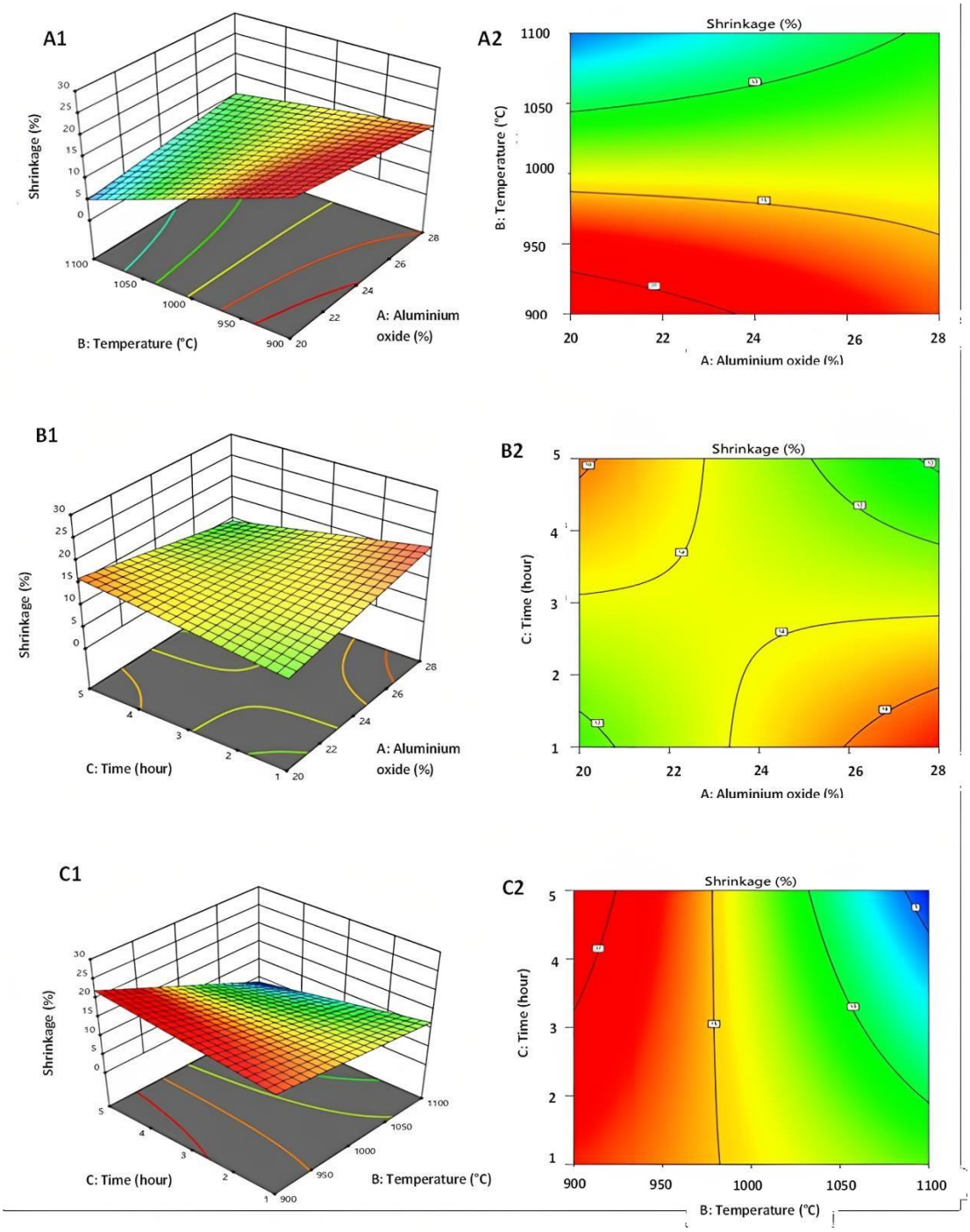

Figure 4.28: Influence of processing parameters on the linear shrinkage of the ternary blend comprising calcined hydroxyapetite, aluminum oxide, and titanium dioxide, represented through 3D surface plots (A1, B1, C1) and contour plots (A2, B2, C2)

4.9 Characterization of ternary blend

4.9.1 XRD analysis of the ternary blend

The XRD diffraction results of the composite of titanium dioxide (TiO_2), aluminum oxide (Al_2O_3), and hydroxyapetite (HAp) sintered at varying temperatures indicated the formation of secondary phases that significantly enhance the material's mechanical properties are shown in figure 4.29. The composite's composition changes is different at all sintering temperatures as Taguchi L25 orthogonal array was applied for optimization of the ratio's : The ratio is 70% HAp, 28% Al_2O_3, and 2% TiO_2 at 900°C, 70% HAp, 26% Al_2O_3, and 4% TiO_2 at 950°C, 70% HAp, 24% Al_2O_3, and 6% TiO_2 at 1000°C, 70% HAp, 22% Al_2O_3, and 8% TiO_2 at 1050°C, 70% HAp, and 70% HAp, 20% Al_2O_3, and 10% TiO_2 at 1100°C at constant time for 5 hours each.

The X-ray diffraction (XRD) patterns displayed in the graph correspond to samples sintered at various temperatures ranging from 900°C to 1100°C, with peaks labeled for different crystalline phases. The dominant peaks across all sintering temperatures indicate the presence of hydroxyapetite (HAp) as the primary phase, with characteristic diffraction peaks appearing at approximately 25.8°, 31.8°, 32.2°, and 34.0° (2θ). These peaks confirm the retention of the HAp phase even at higher sintering temperatures.

Additionally, the presence of secondary phases is evident, including aluminum oxide (Al_2O_3), titanium dioxide (TiO_2) in both anatase and rutile forms, calcium titanate ($CaTiO_3$), β-tricalcium phosphate (β-TCP), and calcium aluminate ($CaAl_2O_4$). The Al_2O_3 phase is identified by peaks around 35.1° and 43.2°, contributing to improved mechanical strength. The anatase and rutile TiO_2 phases are observed at 25.3°, 37.8°, and 48.0°, with the anatase phase gradually transitioning into rutile at higher temperatures, particularly beyond 1000°C, due to thermal stability changes.

With increasing sintering temperature, the decomposition of HAp results in the formation of β-TCP and $CaAl_2O_4$, particularly noticeable around 30.5° and 33.8°, which signifies a structural transformation that may enhance bioactivity. The formation of $CaTiO_3$ at 38.2° suggests interactions between calcium from HAp and TiO_2, leading to a stable phase at elevated temperatures [197].

Furthermore, the effect of temperature on peak crystallinity is evident, as higher sintering temperatures lead to sharper and more intense diffraction peaks**,** indicating increased crystallinity. At 900°C**,** the peaks appear broader and less intense, suggesting a lower degree of crystallinity and possible residual amorphous content. As the temperature increases to 1000°C and beyond, the peaks become sharper and more defined**,** confirming enhanced crystallinity.

Overall, the XRD analysis indicates that while HAp remains the primary phase, secondary phase transformations occur with increasing sintering temperature, including the conversion of anatase to rutile TiO_2 and the formation of β-TCP and $CaAl_2O_4$. These secondary phases can influence the material's mechanical properties and bioactivity, making the ternary composite suitable for biomedical applications such as bone regeneration [198].

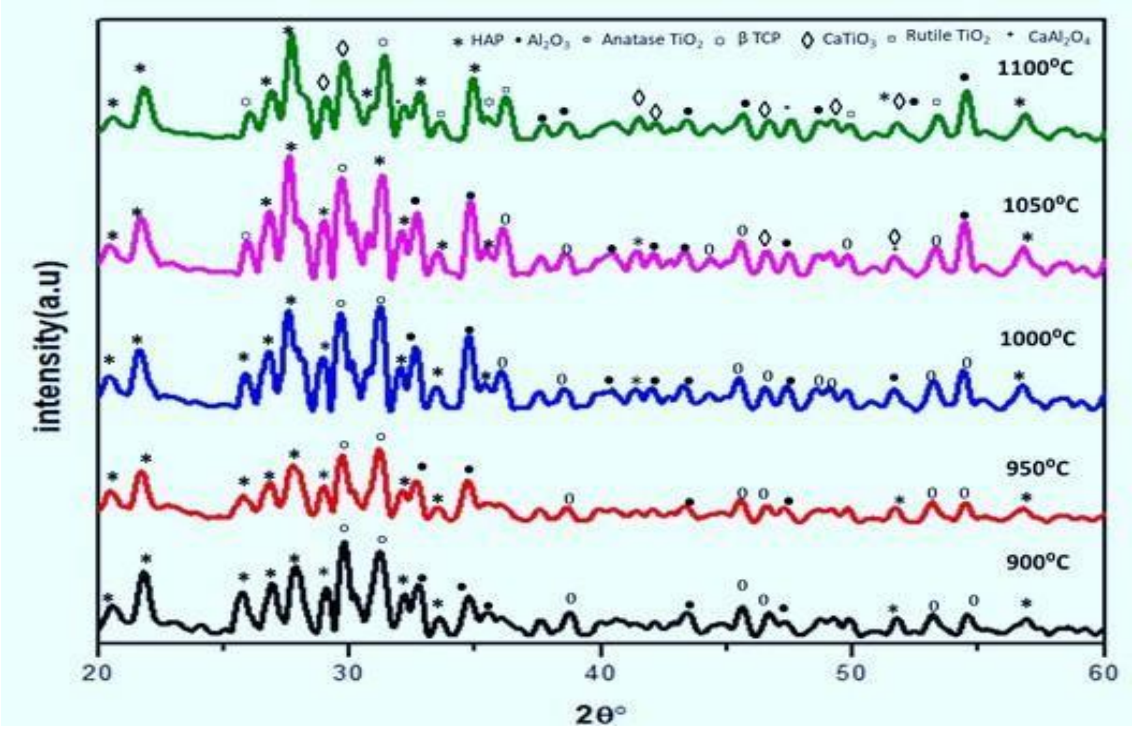

Figure 4.29: XRD graphs of different composite sintered at different temperature for 5 hours

4.9.2 FTIR analysis of Ternary blend

The FTIR spectrum shown in figure 4.30 corresponds to a ternary composite consisting of aluminum oxide (Al_2O_3), titanium dioxide (TiO_2), and hydroxyapetite (HAp), sintered at 1100°C for 5 hours. The observed peaks confirm the presence of the primary phases along with secondary phases that formed due to sintering at high temperatures.

The band observed at 2973 cm^{-1} is the presence of CO_2, likely absorbed from the surrounding. The strong absorption bands in the region 1000–1200 cm^{-1}, particularly at1209.76 cm^{-1}, 1186.0 cm^{-1}, and 1156.32 cm^{-1}, indicate the presence of phosphate (PO_4^{3-}) stretching vibrations, which confirm the retention of hydroxyapetite even after high-temperature sintering. Additionally, the peaks at 972.5 cm^{-1}and1062.56 cm^{-1} correspond to P-O bending vibrations, further supporting the presence of HAp [199].

Secondary phase formation is evident in the spectrum. The absorption peaks around
611.56 cm^{-1},724.79 cm^{-1}, and 493.23 cm^{-1} correspond to Ti-O vibrations, indicating the presence of both anatase and rutile phases of TiO_2. The transformation of anatase into rutile is expected at high sintering temperatures, and the appearance of these peaks confirms the phase transition. Peaks observed at 1100.86 cm^{-1} and 1136.79 cm^{-1} suggest the formation of calcium aluminates ($CaAl_2O_4$), which typically form as a reaction product between Al_2O_3 and Ca^{2+} from HAp at elevated temperatures.

Furthermore, the absorption bands at 556.30 cm^{-1} and 525.92 cm^{-1} correspond to Al-O stretching vibrations, confirming the presence of aluminum oxide, which remains stable during sintering. The peak at 450.34 cm^{-1} may also be attributed to lattice vibrations of aluminum-titanium compounds, suggesting possible interaction between Al_2O_3 and TiO_2 at high temperatures [200].

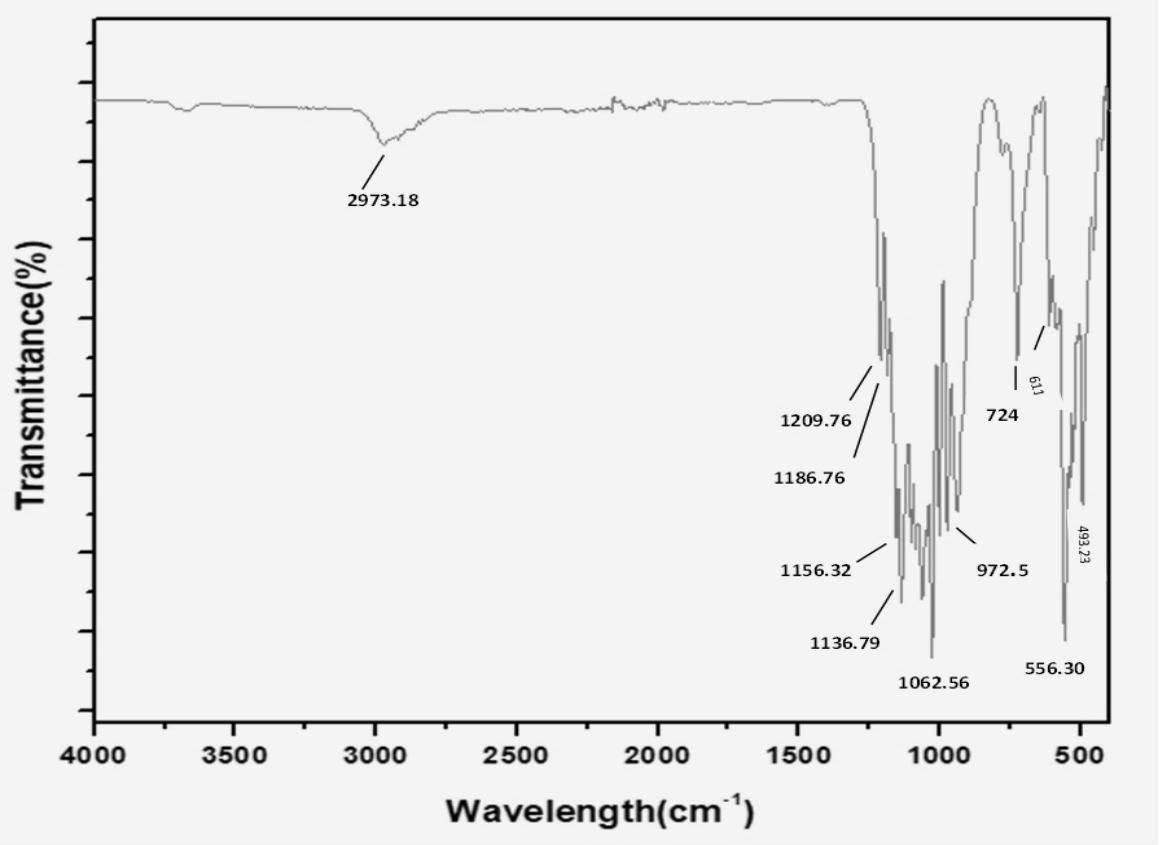

Figure 4.30: FTIR spectrum of the Ternary blend sintered at 1100℃ for 5 hours.

4.9.3 FESEM analysis of Ternary blend

The figure 4.31 consists of five Scanning Electron Microscope (SEM) micrographs (A–E) and an Energy Dispersive X-ray Spectroscopy (EDS) spectrum (F), which illustrate the effect of sintering temperature on the microstructure and density of the composite material. The micrographs correspond to different sintering temperatures, specifically 900℃ (A), 950℃ (B), 1000℃ (C), 1050℃ (D), and 1100℃ (E). The EDS spectrum (F) provides elemental composition analysis, indicating the presence of key elements such as phosphorus (P), calcium (Ca), aluminum (Al), oxygen (O), and titanium (Ti).

As the sintering temperature increases, significant changes in the microstructure are observed. At 900°C (A), the composite exhibits a porous structure with loosel packed particles, indicating lower densification. As the temperature increases to 950°C (B) and 1000°C (C), the porosity reduces, and the particles begin to coalesce, improving the densification of the composite. At 1050°C (D), the material shows a further reduction in porosity, with a more compact and interconnected grain structure, suggesting enhanced densification and improved mechanical properties [201].

At the highest temperature, 1100°C (E), the microstructure appears highly compact, with minimal porosity and well-formed grain boundaries. This indicates the highest density achieved in the composite, which correlates with increased mechanical strength. However, excessive sintering at high temperatures can also lead to grain coarsening, which may affect certain material properties. The EDS spectrum (F) confirms the presence of essential elements contributing to the composite's structural integrity [202].

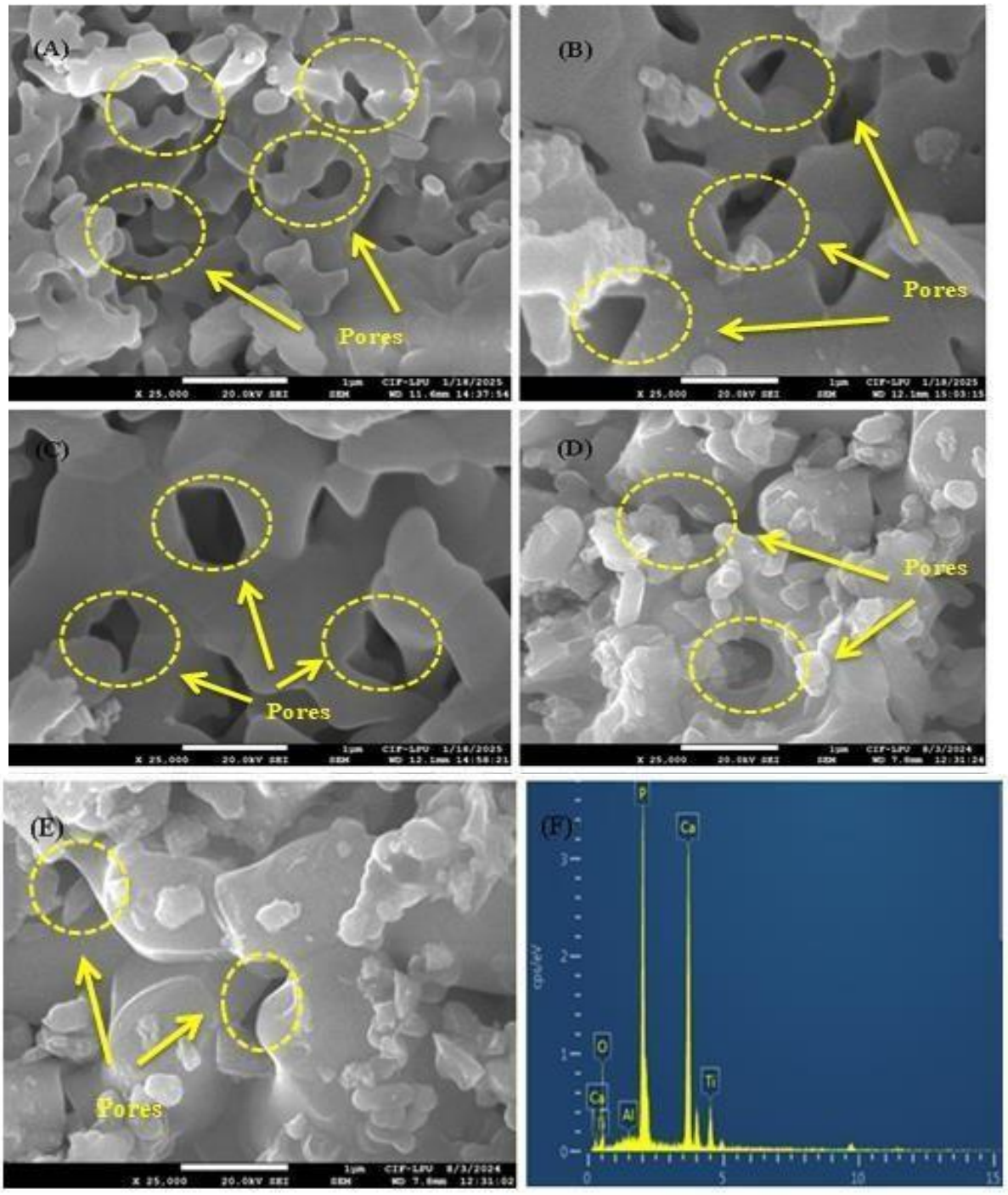

Figure 4.31: FESEM of ternary blend sintered at different temperature and at constant time 5 hours (A) 900°C (B) 950°C (C) 1000°C (D) 1050°C (E) 1100°C (F) EDX of ternary blend.

4.10 Mechanical Testing

Based on the Taguchi L25 orthogonal array results, the optimal ternary blend composition was identified as 20% aluminum oxide, 10% titanium dioxide, and 70% hydroxyapetite, sintered at 1100°C for 5 hours. Mechanical testing was performed to assess the mechanical strength, accompanied by a comparative analysis of four other ternary blends sintered at 1100°C for 1, 2, 3, and 4 hours. The synthesized hydroxyapetite was used as a control to facilitate comparison of the results. This comparison aimed to assess the influence of sintering duration on the material's mechanical strength and overall properties.

The graph in figure 4.32 illustrates the compressive strength (MPa) of a ternary blend of hydroxyapetite (HAp), aluminum oxide (Al_2O_3), and titanium dioxide (TiO_2) sintered at 1100°C for different durations ranging from 1 to 5 hours. The results indicate a significant improvement in mechanical properties with increasing sintering time.

At zero hours, the synthesized hydroxyapetite, used as a control without sintering, exhibited a compressive strength of 12.62 MPa. After 1 hour, the compressive strength increased to 18.72 MPa, followed by a gradual rise to 22.45 MPa at 2 hours and 28.91 MPa at 3 hours. A significant increase was observed at 4 hours, where the compressive strength reached 41.75 MPa, with only a slight increment to 42.25 MPa at 5 hours.

This trend suggests that prolonged sintering enhances the densification, phase transformation, and crystallinity of the material, leading to improved compressive strength. However, the slight difference between 4 and 5 hours indicates that after a certain sintering duration, the improvement in strength stabilizes, possibly due to grain coarsening or saturation in densification [203].

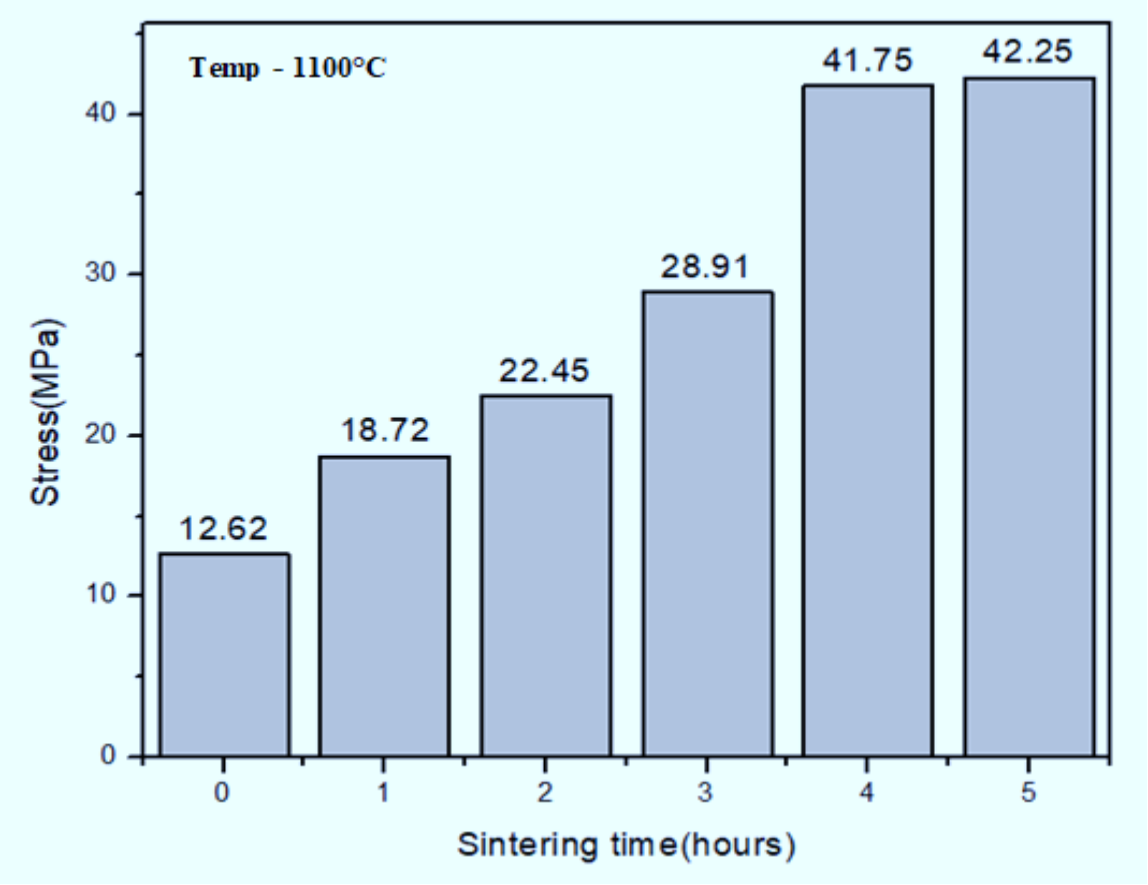

Figure 4.32: Compressive strength of ternary blend at constant temperature and at different time.

PART 5: In vitro study of the hydroxyapetite and study of its biocompatibility.

4.11 Invitro studies

4.11.1 Cytotoxicity test

The bar graph in figure 4.33 illustrates the effect of different concentrations of synthesized hydroxyapetite (HAP) and a ternary blend on cell viability (%). The control group exhibits 100% cell viability, serving as a baseline. As the concentration increases from 10 to 500 µg/mL, cell viability decreases for both materials. However, the ternary blend consistently shows higher cell viability compared to synthesized HAp across all concentrations, indicating better biocompatibility. At lower concentrations (10–100 µg/mL), cell viability remains above 60% for both materials, whereas at higher concentrations (200–500 µg/mL), a significant decline is observed,

with synthesized HAp exhibiting a more pronounced reduction. The results suggest that while both materials are cytocompatible at lower concentrations, the ternary blend maintains superior cell viability, making it a potentially more favorable biomaterial [204,209].

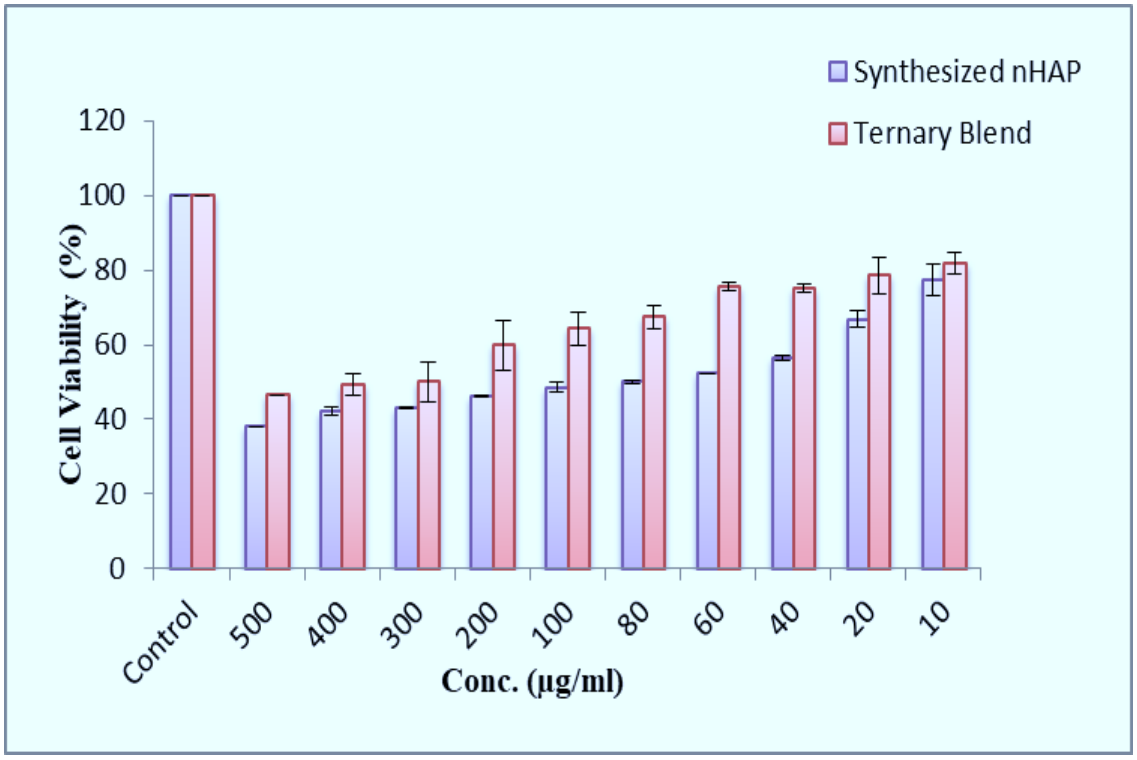

Figure 4.33: MTT assay for synthesized hydroxyapetite and ternary blend showing the percentage of cell viability.

4.11.2 Biocompatibility test

4.11.2.1 Mechanism of apatite layer formation in SBF

The development of an apatite layer on hydroxyapetite (HA) in synthetic Body Fluid (SBF) occurs through ion exchange, nucleation, precipitation, and crystal growth**.** When HA is submerged in SBF, its surface attracts Ca^{2+} and PO_4^{3-} ions, leading to their accumulation and the formation of a supersaturated state. This initiates the nucleation of amorphous calcium phosphate (ACP)**,** which then precipitates onto the HAp surface. Gradually, this precipitate undergoes structural transformation, crystallizing into an apatite layer that mimics natural bone mineral. This bioactive

coating enhances osteoconductivity and bone bonding**,** making HAp a valuable material for applications like bone implants and biomedical coatings. Figure 4.34 illustrates the mechanism of apatite layer formation on HAp [205].

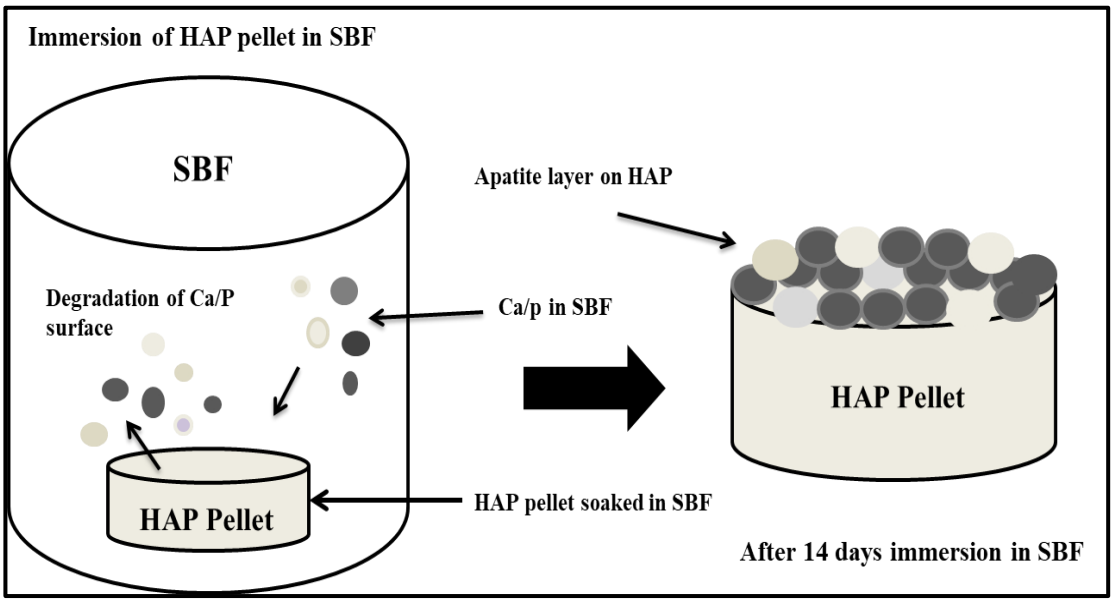

Figure 4.34: Mechanism of Apatite Layer Deposition on Hydroxyapetite (HAp) in Synthetic Body Fluid (SBF).

4.11.2.2 Biocompatibility of synthesized hydroxyapetite

Figure 4.35 presents the SEM images of the HAp surface after being soaked in SBF for varying durations, specifically 7, 14, and 21 days. Throughout the experiment, the SBF was maintained at a constant pH of 7.4 and a temperature of 37°C. The pH variations were monitored at regular intervals from day 0 to day 21. The SEM images in Figure 4.35 specifically capture the surface morphology of the HAp pellet on day 14.

The images 4.35 reveal the presence of tiny, agglomerated particles on the surface of HAp. Notably, as the soaking duration increased from 7 to 14 days, both the size and quantity of these agglomerates visibly grew on the HAp pellet's surface. Additionally, an appetite-like layer formed, characterized by small, clustered particles, indicating clear signs of mineralization. These findings confirm that the HAp synthesized using

carbide lime exhibited significant bioactivity in SBF, as evidenced by the progressive formation of the mineralized layer [206].

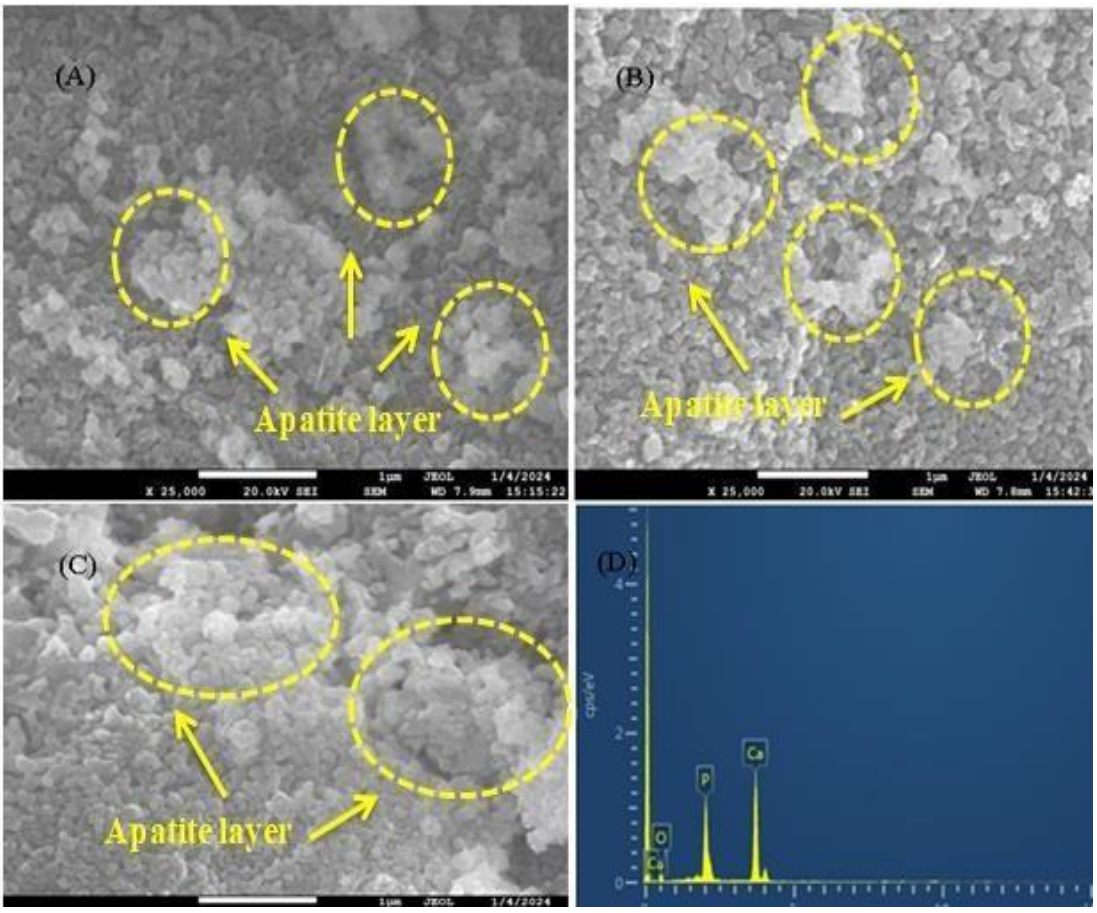

Figure 4.35: SBF of calcined hydroxyapetite (A) 7 days (B) 14 days (C) 21 days (D) EDX of calcined HAp.

4.11.2.3 Biocompatibility of Ternary blend

Figure 4.36 displays SEM images of the ternary blend surface following immersion in SBF for different time periods—7, 14, and 21 days. Throughout the study, the SBF conditions were maintained at a stable pH of 7.4 and a temperature of 37°C, with pH variations recorded periodically from day 0 to day 21. In figure 4.36 A, B, and C corresponds to soaking durations of 7, 14, and 21 days, respectively, and depicts the formation of small, agglomerated particles on the surface of the ternary blend. As the immersion period extended from 7 to 14 days, both the size and

number of these agglomerates increased noticeably. Furthermore, a distinct apatite-like layer began to form, consisting of clustered particles, providing strong evidence of mineralization. These observations indicate that the ternary blend pellets demonstrated notable bioactivity in SBF, as reflected by the continuous development of the mineralized layer over time [207]

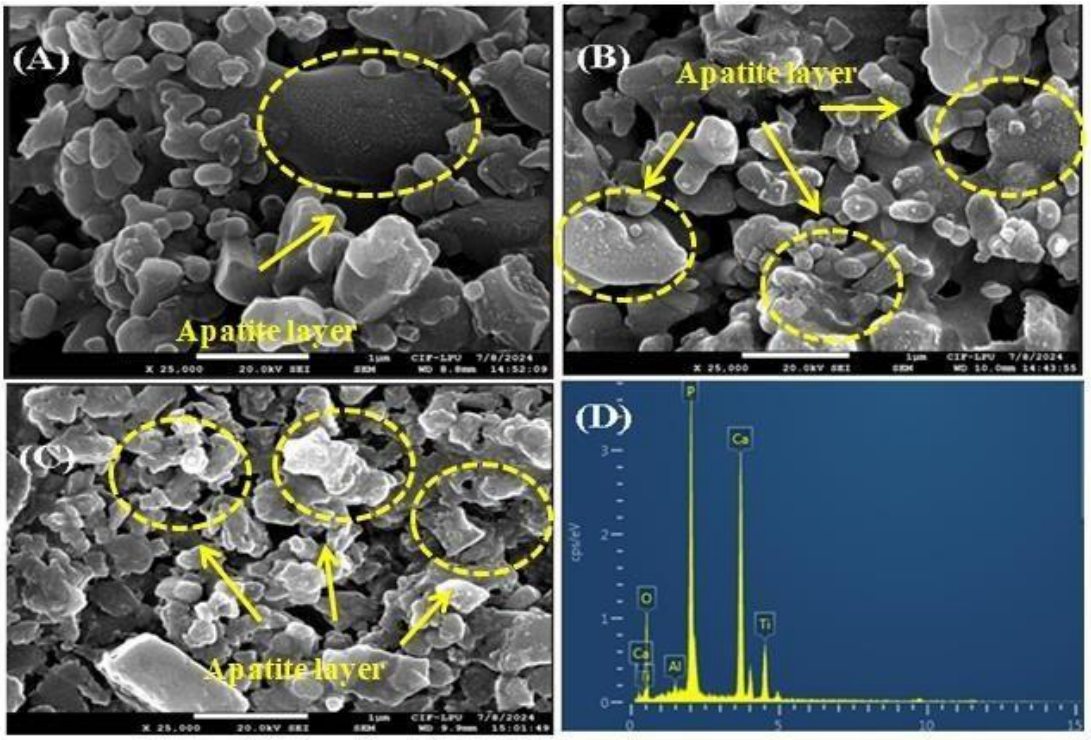

Figure 4.36: SBF of ternary blend of hydroxyapetite (A) 7 days (B) 14 days (C) 21 days (D) EDX of ternary blend of hydroxyapetite.

4.11.3 Biodegradation test

The biodegradation of the HAp and ternary blend pellets was analyzed in a tris-HCl solution. The calcined samples were immersed in tris-HCl for 7 days, maintaining a temperature of 37 °C and an initial pH of 7.4. During soaking, the loss of calcium ions led to a pH rise from 7.4 to 8.4, confirming the biodegradation of the synthesized HAp. Throughout the degradation process, the total calcium loss for the HAp pellet was 1.8%, while the ternary blend pellet exhibited a higher calcium loss of 3.09% [208].

Chapter V

SUMMARY AND CONCLUSION

5.1 **Summary**

The issue of environmental pollution caused by the release of industrial waste, along with the high cost of hydroxyapetite as a biomaterial, is effectively addressed in this thesis titled "Utilization of Carbide Lime for the Synthesis of Hydroxyapetite and Study of Its Biocompatibility." In this research, carbide lime, a byproduct of the acetylene industry and primarily composed of calcium hydroxide, was utilized as the key raw material for hydroxyapetite synthesis. This study proposes the development of a cost-effective biomaterial derived from industrial waste with enhanced mechanical strength and biocompatibility. The selection of raw materials and sintering additives to improve the mechanical properties was based on a comprehensive review of the literature. Carbide lime was chosen as the main raw material, while aluminum oxide and titanium dioxide were incorporated as sintering additives to strengthen the material's mechanical properties. This study successfully demonstrated the sustainable utilization of carbide lime as a precursor for the synthesis of hydroxyapetite, which is a valuable material for biomedical applications. The carbide lime was purified using the dilution method to obtain a high-quality precursor, and hydroxyapetite was synthesized via the wet chemical precipitation method. To improve the mechanical strength of hydroxyapetite, sintering additives such as aluminum oxide and titanium dioxide were incorporated in varying ratios. Aluminum oxide was varied at 20%, 22%, 24%, 26%, and 28% by weight, while titanium dioxide was varied at 10%, 8%, 6%, 4%, and 2% by weight, with hydroxyapetite content kept constant at 70%. The optimization of these parameters was done using the Taguchi L25 orthogonal array.

Extensive characterization techniques were employed to analyze the synthesized hydroxyapetite and its composites. X-ray diffraction (XRD) was performed to confirm the crystalline structure of the hydroxyapetite and to identify phase changes after incorporating sintering additives. Fourier-transform infrared spectroscopy (FTIR) analysis confirmed the presence of functional groups characteristic of hydroxyapetite, ensuring the successful synthesis of the material. Field emission scanning electron microscopy (FESEM) revealed the morphology of the

hydroxyapetite, showing needle-shaped structures, which are indicative of high

bioactivity. The incorporation of sintering additives resulted in a more compact microstructure, enhancing the mechanical properties. Thermo gravimetric analysis (TGA) was used to study the thermal stability of the synthesized hydroxyapetite. Particle size analysis was conducted to determine the uniformity and size distribution of the synthesized hydroxyapetite particles, which further supported the material's suitability for biomedical applications.

Sintering was performed at various temperatures (900°C, 950°C, 1000°C, 1050°C, and 1100°C) and durations (1, 2, 3, 4, and 5 hours) to enhance the material's properties. Higher sintering temperatures and longer durations contributed to significant improvements in mechanical strength, density, and structural stability, making the material suitable for biomedical applications.

Further, in vitro testing of the optimized sample, including cell viability tests, simulated body fluid (SBF) tests, and biodegradation studies, confirmed its potential as a biocompatible and bioactive material. The cell viability tests demonstrated that the material supports cellular proliferation and attachment, while the SBF tests indicated excellent bioactivity with the formation of an appetite layer. The biodegradation studies revealed a controlled degradation rate, making it suitable for gradual integration with natural bone during implantation.

Overall, this study highlights the potential of utilizing industrial waste (carbide lime) for the development of high-performance hydroxyapetite-based biomaterials. The findings, supported by comprehensive characterization and biological evaluation, provide a strong foundation for the use of optimized hydroxyapetite composites in biomedical implants. This approach offers sustainability, cost-effectiveness, and excellent biological performance.

5.2 Conclusion

Based on the comprehensive experimental analysis, the optimal composition for achieving superior mechanical strength, biocompatibility, and overall material performance was determined to be 20% aluminum oxide, 10% titanium dioxide, and 70% hydroxyapetite. This composition was identified through systematic optimization using the Taguchi L25 method, which enabled the evaluation of various combinations of sintering additives and their effects on the material's properties. The material was sintered under the optimal conditions of 1100°C for 5 hours, resulting in significant enhancements in mechanical strength, density, and structural stability. These improvements are attributed to the synergistic effect of aluminum oxide and titanium dioxide as sintering additives, which contributed to the densification and reinforcement of the hydroxyapetite matrix.

The optimized composition underwent extensive characterization, including XRD, FTIR, FESEM, TGA, and particle size analysis, confirming its crystalline structure, thermal stability, and uniform morphology with needle-shaped hydroxyapetite particles. These characteristics are crucial for ensuring the material's suitability for biomedical applications. Additionally, the optimized material was subjected to *in vitro* tests, including cell viability assays, synthetic body fluid interaction studies, and biodegradation tests. The results demonstrated excellent biocompatibility, bioactivity through apatite layer formation, and controlled biodegradability, making the material highly suitable for biomedical implants.

This study highlights that the selected ratio of raw materials and sintering conditions not only maximizes the mechanical and biological performance of hydroxyapetite but also addresses the dual challenges of industrial waste management and the high cost of biomaterials. By utilizing carbide lime, an industrial byproduct, as the primary raw material, this research provides solution for developing advanced biomaterials.

5.3 Scope, Limitations and Future commercial Prospects

The scope of the present research comprised the synthesis of hydroxyapetite (HAP) using carbide lime, an industrial by-product, as a calcium precursor. The study focused on optimizing synthesis parameters to maintain the ideal Ca/P molar ratio and evaluating the physicochemical and *in vitro* biological properties of the resulting material. Large-scale production and *in vivo* studies were beyond the defined scope of this work and are proposed for future research.

The present study successfully demonstrated the utilization of carbide lime as a sustainable and economical precursor for the synthesis of hydroxyapetite with desirable structural and biological characteristics. The synthesized HAP exhibited excellent *in vitro* biocompatibility, confirming its potential for biomedical applications. Although *in vivo* testing was not performed within the current scope, this focus allowed for a comprehensive understanding of the synthesis process and *in vitro* performance.

Future investigations will extend to *in vivo* evaluations, which require ethical approval and infrastructural readiness, to validate and strengthen the current findings. The encouraging outcomes of this study establish a solid foundation for further biological and clinical research.

From a commercialization standpoint, the proposed method provides a feasible pathway for converting industrial waste into high-value biomaterials. With further optimization for large-scale synthesis, assurance of raw material consistency, and compliance with biomedical regulatory standards, this approach holds significant potential for industrial adoption offering both environmental benefits and sustainable economic value.

BIBLIOGRAPHY

1. Carvalho, F. P. (2017). Mining industry and sustainable development: time for change. *Food and Energy security*, *6*(2), 61-77.

2. Dong, Q. G., Li, J., Kang, Z. Q., Anwar, M. I., Asad, M., Miao, B., ... & Younas,A. (2024). Unlocking the potential: A comprehensive review on blast furnace slag and silica analog adsorbents for sustainable industrial and pharmaceutical pollution control and resource utilization. *Emerging Contaminants*, 100387.

3. Akhtar, A., & Sarmah, A. K. (2018). Construction and demolition waste generation and properties of recycled aggregate concrete: A global perspective. *Journal of Cleaner Production*, *186*, 262-281.

4. Artiola, J. F. (2019). Industrial waste and municipal solid waste treatment and disposal. In *Environmental and pollution science* (pp. 377-391).Academic Press.

5. Hossain, A., Krupnik, T. J., Timsina, J., Mahboob, M. G., Chaki, A. K., Farooq, M., ...& Hasanuzzaman, M. (2020). Agricultural land degradation: processes and problems undermining future food security. In *Environment, climate, plant and vegetation growth* (pp. 17-61). Cham: Springer International Publishing.

6. Ilić, T., Elert, K., Ruiz-Agudo, E., & Rodriguez-Navarro, C. (2024, April). Potential Use of Carbide Lime Waste in Construction: A Comprehensive Analysis. In *RILEM Spring Convention and Conference* (pp. 35-43). Cham: Springer Nature Switzerland.

7. Vijayan, D. S., & Parthiban, D. (2020). Effect of Solid waste based stabilizing material for strengthening of Expansive soil-A review. *Environmental Technology & Innovation*, *20*, 101108.

8. Kareem, R. O., Bulut, N., & Kaygili, O. (2024). Hydroxyapetite biomaterials: a comprehensive review of their properties, structures, medical applications, and

fabrication methods. *J. Chem. Rev*, *6*(1), 1-26.

9. Torres-Romero, S., Mendoza-Acosta, A., Flores-Cortez, M. R., Gamez-Serna, F., Váldez-Robles, A. S., & Soto-Robles, C. A. Hydroxyapetite Production Techniques: Overview Of Precipitation, Sol-Gel, Hydrothermal, And Thermal Decomposition Methods.

10. Jaffar, F. H., Othman, M. H. D., Ismail, N. J., Puteh, M. H., Kurniawan, T. A., Bakar, S. A., & Abdullah, H. (2024). Hydroxyapetite-based materials for adsorption, and adsorptive membrane process for heavy metal removal from wastewater: Recent progress, bottleneck and opportunities. *Journal of the Taiwan Institute of Chemical Engineers*, *164*, 105668.

11. Yelten-Yilmaz, A., & Yilmaz, S. (2018). Wet chemical precipitation synthesis of hydroxyapetite (HA) powders. *Ceramics International*, *44*(8), 9703-9710.

12. Kuppusamy, S., Palanisami, T., Megharaj, M., Venkateswarlu, K., & Naidu, R. (2016). Ex-situ remediation technologies for environmental pollutants: a critical perspective. *Reviews of Environmental Contamination and Toxicology Volume 236*, 117-192.

13. Basu, B., Kalidindi, S. R., Keshavan, N., & Poddar, K. (2022). Structural Biomaterials for Affordable Health Care. In *Future Landscape of Structural Materials in India* (pp. 133-147). Singapore: Springer Nature Singapore.

14. Verma, R., Mishra, S. R., Gadore, V., & Ahmaruzzaman, M. (2023). Hydroxyapetite-based composites: excellent materials for environmental remediation and biomedical applications. *Advances in Colloid and Interface Science*, *315*, 102890.

15. Varadavenkatesan, T., Vinayagam, R., Pai, S., Kathirvel, B., Pugazhendhi, A., & Selvaraj, R. (2021). Synthesis, biological and environmental applications of hydroxyapetite and its composites with organic and inorganic coatings. *Progress in*

Organic Coatings, *151*, 106056.

16. Arokiasamy, P., Abdullah, M. M. A. B., Abd Rahim, S. Z., Luhar, S., Sandu, A. V., Jamil, N. H., & Nabiałek, M. (2022). Synthesis methods of hydroxyapetite from natural sources: A review. *Ceramics International*, *48*(11), 14959-14979.

17. Salehuddin, F., Zain, A. S. M., Kaharudin, K. E., Hanim, A. R., Hazura, H., & Idris, S. K. (2019, July). Comparisons in L32 2k-Factorial and L25 Taguchi for the 16 nm FinFET Statistical Optimization Applications. In *Intelligent Manufacturing and Mechatronics: Proceedings of the 2nd Symposium on Intelligent Manufacturing and Mechatronics–SympoSIMM 2019, 8 July 2019, Melaka, Malaysia* (p. 419). Springer.

18. Das, R., Ambardekar, V., & Bandyopadhyay, P. P. (2021). Titanium dioxide and its applications in mechanical, electrical, optical, and biomedical fields. *Titanium Dioxide-Advances and Applications*.

19. Salimi, E. (2021). Development of bioactive sodium alginate/sulfonated polyether ether ketone/hydroxyapetite nanocomposites: synthesis and in-vitro studies. *Carbohydrate Polymers*, *267*, 118236.

20. Huang, Y. C., Hsiao, P. C., & Chai, H. J. (2011). Hydroxyapetite extracted from fish scale: Effects on MG63 osteoblast-like cells. *Ceramics international*, *37*(6), 1825-1831.

21. Kylchbekov, S. (2023). Bioactivity and Structural Properties of Hydroxyapetite on Ti6A| 4V and Si (100) Surfaces by Pulsed Laser Deposition.

22. Eliaz, N., & Metoki, N. (2017). Calcium phosphate bioceramics: a review of their history, structure, properties, coating technologies and biomedical applications. *Materials*, *10*(4), 334.

23. Waghmare, G., Waghmare, K., Bagde, S., Deshmukh, M., Kashyap, D. N., & Shahu, V. T. (2024). Materials evolution in dental implantology: a comprehensive review. *J. Adv. Res. Appl. Mech*, *123*, 75-100.

24. Mondal, S., Dorozhkin, S. V., & Pal, U. (2018). Recent progress on fabrication and drug delivery applications of nanostructured hydroxyapetite. *Wiley Interdisciplinary Reviews: Nanomedicine and Nanobiotechnology*, *10*(4), e1504.

25. Naahidi, S., Jafari, M., Edalat, F., Raymond, K., Khademhosseini, A., & Chen, P. (2013). Biocompatibility of engineered nanoparticles for drug delivery. *Journal of controlled release*, *166*(2), 182-194.

26. Bandyopadhyay, A., Mitra, I., Goodman, S. B., Kumar, M., & Bose, S. (2023). Improving biocompatibility for next generation of metallic implants. *Progress in materials science*, *133*, 101053.

27. Ma, X., Wei, H., & Luo, Z. (2024). Development and prospect of the acetylene production chain based on the process systems engineering: a focus on the polyvinyl chloride production. *Reviews in Chemical Engineering*.

28. Rautela, R., Sharma, A., Prakash Ranjan, V., Rathika, K., Pratap, V., Ram Yadav, B., & Kumar, S. (2024). Turning Solid Waste into Catalysts: A Path for Environmental Solutions. *ChemPlusChem*, *89*(12), e202400246.

29. Porras-Herrera, D. R., Herrera-Hernández, H., Miranda-Hernández, J. G., Castillo-Robles, J. A., Armendariz-Mireles, E. N., Calles-Arriaga, C. A., & Rocha-Rangel, E. (2024). Innovative Bioceramic Based on Hydroxyapetite with Titanium Nanoparticles as Reinforcement for Possible Medical Applications. *Journal of Manufacturing and Materials Processing*, *8*(6), 296.

30. Kattimani, V. S., Kondaka, S., & Lingamaneni, K. P. (2016). Hydroxyapetite–- Past, present, and future in bone regeneration. *Bone and Tissue Regeneration Insights*, *7*, BTRI-S36138.

31. Yelten-Yilmaz, A., & Yilmaz, S. (2018). Wet chemical precipitation synthesis of hydroxyapetite (HA) powders. *Ceramics International*, *44*(8), 9703-9710.

32. Monmaturapoj, N. (2008). Nano-size hydroxyapetite powders preparation by wet- chemical precipitation route. *Journal of Metals, Materials and Minerals*, *18*(1), 15-20.

33. Agrawal, K., Singh, G., Puri, D., & Prakash, S. (2011). Synthesis and characterization of hydroxyapetite powder by sol-gel method for biomedical application. *J. Miner. Mater.Charact. Eng*, *10*(8), 727-734.

34. Kim, I. S., & Kumta, P. N. (2004). Sol–gel synthesis and characterization of nanostructured hydroxyapetite powder. *materials science and Engineering: B*, *111*(2- 3), 232-236.

35. Hui, P., Meena, S. L., Singh, G., Agarawal, R. D., & Prakash, S. (2010).

Synthesis of hydroxyapetite bio-ceramic powder by hydrothermal method. *Journal of Minerals & Materials Characterization & Engineering*, *9*(8), 683-692.

36. Fitriyana, D. F., Ismail, R., Santosa, Y. I., Nugroho, S., Hakim, A. J., & Al Mulqi,
M. S. (2019, October). Hydroxyapetite synthesis from clam shell using hydrothermal method: A review. In *2019 International Biomedical Instrumentation and Technology Conference (IBITeC)* (Vol. 1, pp. 7-11).IEEE.

37. Wei, G., Gong, C., Hu, K., Wang, Y., & Zhang, Y. (2019). Biomimetic hydroxyapetite on graphene supports for biomedical applications: a review. *Nanomaterials*, *9*(10), 1435.

38. Habibovic, P., Barrère, F., Van Blitterswijk, C. A., de Groot, K., & Layrolle, P. (2002). Biomimetic hydroxyapetite coating on metal implants. *Journal of the American Ceramic Society*, *85*(3), 517-522.

39. Guo, X., Yan, H., Zhao, S., Li, Z., Li, Y., & Liang, X. (2013). Effect of calcining temperature on particle size of hydroxyapetite synthesized by solid-state reaction at room temperature. *Advanced Powder Technology*, *24*(6), 1034-1038.

40. Koonawoot, R., Saelee, C., Thiansem, S., & Punyanitya, S. (2012). Synthesis control and characterization of hydroxyapetite ceramic using a solid state reaction.In *1st Mae Fah Luang University International Conference* (pp. 2-6).

41. Hassan, M. N., Mahmoud, M. M., Abd El-Fattah, A., & Kandil, S. (2016). Microwave-assisted preparation of Nano-hydroxyapetite for bone substitutes. *Ceramics International*, *42*(3), 3725-3744.

42. Sözügeçer, S., & Bayramgil, N. P. (2021). Preparation and characterization of polyacrylic acid-hydroxyapetite nanocomposite by microwave-assisted synthesis method. *Heliyon*, *7*(6).

43. Kong, L. B., Ma, J., & Boey, F. (2002). Nanosized hydroxyapetite powders derived from coprecipitation process. *Journal of materials science*, *37*, 1131-1134.

44. Danilchenko, S. N., Kalinkevich, O. V., Pogorelov, M. V., Kalinkevich, A. N., Sklyar, A. M., Kalinichenko, T. G., ... & Sukhodub, L. F. (2011). Characterization and in vivo evaluation of chitosan-hydroxyapetite bone scaffolds made by one step coprecipitation method. *Journal of biomedical materials research Part A*, *96*(4), 639- 647.

45. Wang, M. C., Hon, M. H., Chen, H. T., Yen, F. L., Hung, I. M., Ko, H. H., &
Shih, W. J. (2013). Process parameters on the crystallization and morphology of

hydroxyapetite powders prepared by a hydrolysis method. *Metallurgical and Materials Transactions A*, *44*, 3344-3352.

46. Monma, H., Ueno, S., & Kanazawa, T. (1981). Properties of hydroxyapetite prepared by the hydrolysis of tricalcium phosphate. *Journal of Chemical technology and biotechnology*, *31*(1), 15-24.

47. Djošić, M. S., Mišković-Stanković, V. B., Milonjić, S., Kačarević-Popović, Z. M., Bibić, N., & Stojanović, J. (2008). Electrochemical synthesis and characterization of hydroxyapetite powders. *Materials Chemistry and Physics*, *111*(1), 137-142.

48. Nur, A., Setyawan, H., Widjaja, A., & Lenggoro, I. W. (2014). Electrochemical processes for the formation of hydroxyapetite powders. *Bulletin of Chemical Reaction Engineering & Catalysis*, *9*(3), 168-175.

49. Wakiya, N., Yamasaki, M., Adachi, T., Inukai, A., Sakamoto, N., Fu, D., ...& Suzuki, H. (2010). Preparation of hydroxyapetite–ferrite composite particles by ultrasonic spray pyrolysis. *Materials Science and Engineering: B*, *173*(1-3), 195-198.

50. Cho, J. S., & Rhee, S. H. (2013). Formation mechanism of nano-sized hydroxyapetite powders through spray pyrolysis of a calcium phosphate solution containing polyethylene glycol. *Journal of the European Ceramic Society*, *33*(2), 233- 241.

51. Trommer, R. M., Santos, L. A., & Bergmann, C. P. (2009). Nanostructured hydroxyapetite powders produced by a flame-based technique. *Materials Science and Engineering: C*, *29*(6), 1770-1775.

52. Pawłowski, L. (2018). Synthesis, properties and applications of hydroxyapetite. *Ind. Chem. Oxides Emerg.Appl*, 311.

53. Poinern, G. E., Brundavanam, R. K., Mondinos, N., & Jiang, Z. T. (2009). Synthesis and characterisation of nanohydroxyapetite using an ultrasound assisted method. *Ultrasonics sonochemistry*, *16*(4), 469-474.

54. Ingole, V. H., Hany Hussein, K., Kashale, A. A., Ghule, K., Vuherer, T., Kokol, V., ... & Ghule, A. V. (2017). Ultrasound-assisted green economic synthesis of hydroxyapetite nanoparticles using eggshell biowaste and study of mechanical and biological properties for orthopedic applications. *Journal of Biomedical Materials Research Part A*, *105*(11), 2935-2947.

55. Liu, Y., Ding, C., He, L., Yang, X., Gou, Y., Xu, X., ...& Li, J. (2018).

Bioinspired heptapeptides as functionalized mineralization inducers with enhanced hydroxyapetite affinity. *Journal of Materials Chemistry B*, *6*(13), 1984-1994.

56. wiu, J., Zhang, Z., Yu, X., Pan, H., Jiang, W., Xu, X., & Tang, R. (2011).Mechanism of promoted dipeptide formation on hydroxyapetite crystal surfaces. *Chinese Science Bulletin*, *56*, 633-639.

57. Karunakaran, G., Kumar, G. S., Cho, E. B., Sunwoo, Y., Kolesnikov, E., & Kuznetsov, D. (2019). Microwave-assisted hydrothermal synthesis of mesoporous carbonated hydroxyapetite with tunable nanoscale characteristics for biomedical applications. *Ceramics International*, *45*(1), 970-977.

58. Kumar, G. S., Karunakaran, G., Girija, E. K., Kolesnikov, E., Van Minh, N., Gorshenkov, M. V., & Kuznetsov, D. (2018). Size and morphology-controlled synthesis of mesoporous hydroxyapetite nanocrystals by microwave-assisted hydrothermal method. *Ceramics International*, *44*(10), 11257-11264.

59. Wang, Y. J., Lai, C., Wei, K., Chen, X., Ding, Y., & Wang, Z. L. (2006).Investigations on the formation mechanism of hydroxyapetite synthesized by thesolvothermal method. *Nanotechnology*, *17*(17), 4405.

60. Chen, R., & Shen, J. (2020). The synthesis of hydroxyapetite crystals with various morphologies via the solvothermal method using double surfactants. *Materials Letters*, *259*, 126881.

61. Nayak, A. K. (2010). Hydroxyapetite synthesis methodologies: an overview. *International Journal of ChemTech Research*, *2*(2), 903-907.

62. Mohd, P. A., NAS, A. H., & RH, M. N. (2019). H., Abdullah, HZ, Idris, MI & Lee. *TC*, 233-239.

63. Kumar, G. S., Girija, E. K., Thamizhavel, A., Yokogawa, Y., & Kalkura, S. N. (2010). Synthesis and characterization of bioactive hydroxyapetite–calcite nanocomposite for biomedical applications. *Journal of colloid and interface science*, *349*(1), 56-62.

64. Mobasherpour, I., Heshajin, M. S., Kazemzadeh, A., & Zakeri, M. (2007). Synthesis of nanocrystalline hydroxyapetite by using precipitation method. *Journal of Alloys and Compounds*, *430*(1-2), 330-333.

65. Yelten-Yilmaz, A., & Yilmaz, S. (2018). Wet chemical precipitation synthesis of hydroxyapetite (HA) powders. *Ceramics International*, *44*(8), 9703-9710.

66. Pham Minh, D., Rio, S., Sharrock, P., Sebei, H., Lyczko, N., Tran, N. D., ...& Nzihou, A. (2014). Hydroxyapetite starting from calcium carbonate and orthophosphoric acid: synthesis, characterization, and applications. *Journal of Materials Science*, *49*, 4261-4269.

67. Mohd, P. A., NAS, A. H., & RH, M. N. (2019). H., Abdullah, HZ, Idris, MI & Lee. *TC*, 233-239.

68. Santos, M. H., Oliveira, M. D., Souza, L. P. D. F., Mansur, H. S., & Vasconcelos,
W. L. (2004). Synthesis control and characterization of hydroxyapetite prepared by wet precipitation process. *Materials Research*, *7*, 625-630.

69. Sirait, M., Sinulingga, K., Siregar, N., & Siregar, R. S. D. (2020, February). Synthesis of hydroxyapetite from limestone by using precipitation method. In *Journal of Physics: Conference Series* (Vol. 1462, No. 1, p. 012058). IOP Publishing.

70. Habibie, S., Wargadipura, A. H. S., Gustiono, D., Herdianto, N., Riswoko, A., Nikmatin, S., & Clarke, S. (2017). Production and characterization of hydroxyapetite bone substitute material performed from Indonesian limestone. *Int. J. Biomed. Eng. Sci*, *4*(1), 11-23.

71. Siva Rama Krishna, D., Siddharthan, A., Seshadri, S. K., & Sampath Kumar, T. S. (2007). A novel route for synthesis of nanocrystalline hydroxyapetite from eggshell waste. *Journal of Materials Science: Materials in Medicine*, *18*, 1735-1743.

72. Kareem, Z., & Eyiler, E. (2024). Synthesis of hydroxyapetite from eggshells via wet chemical precipitation: a review. *RSC advances*, *14*(30), 21439-21452.

73. Santhosh, S., & Prabu, S. B. (2012). Synthesis and characterisation of nanocrystalline hydroxyapetite from sea shells. *International Journal of Biomedical Nanoscience and Nanotechnology*, *2*(3-4), 276-283.

74. Plumbum, I. (2017). Synthesis and characterization of hydroxyapetite from bulk seashells and its potential usage as lead ions adsorbent. *Malaysian Journal of Analytical Sciences*, *21*(3), 571-584.

75. Pon-On, W., Suntornsaratoon, P., Charoenphandhu, N., Thongbunchoo, J., Krishnamra, N., & Tang, I. M. (2016). Hydroxyapetite from fish scale for potential use as bone scaffold or regenerative material. *Materials Science and Engineering: C*, *62*, 183-189.

76. Deb, P., Barua, E., Lala, S. D., & Deoghare, A. B. (2019). Synthesis of hydroxyapetite from Labeo rohita fish scale for biomedical application. *Materials*

Today: Proceedings, *15*, 277-283.

77. Geethakarthi, A. (2022). Synthesis of Hydroxyapetite Nanoparticle from Papermill Sludge. *Textile Wastewater Treatment: Sustainable Bio-nano Materials and Macromolecules, Volume 1*, 311-328.

78. Yatongchai, C., & Thavornyutikarn, B. (2021). Conversion of lime mud waste to hydroxyapetite biomaterials. *Materials Chemistry and Physics*, *266*, 124544.

79. Bensalah, H., Bekheet, M. F., Younssi, S. A., Ouammou, M., & Gurlo, A. (2018). Hydrothermal synthesis of nanocrystalline hydroxyapetite from phosphogypsum waste. *Journal of environmental chemical engineering*, *6*(1), 1347-1352.

80. Nasrellah, H., Yassine, I., Hatimi, B., Joudi, M., Chemaa, A., El Gaini, L., ...& Bakasse, M. (2017). New synthesis of hydroxyapetite from local phosphogypsum. *J. Mater. Environ. Sci*, *83*, 168-3174.

81. Chouchane, T., Abedghars, M. T., Chouchane, S., & Boukari, A. (2024). Synthesis of hydroxyapetite-zeolite from blast furnace slag and its application for the removal of copper, lead and copper-lead mixture by adsorption. *Advances in Environmental Technology*, *10*(4), 339-359.

82. Li, C., Li, X., Yu, Y., Zhang, Q., Li, L., Zhong, H., & Wang, S. (2022). A novel conversion for blast furnace slag (BFS) to the synthesis of hydroxyapetite-zeolite material and its evaluation of adsorption properties. *Journal of Industrial and Engineering Chemistry*, *105*, 63-73.

83. Chen, C., Wang, L., Xu, Y., & Wang, F. (2024). Production of hydroxyapetite utilizing calcium and phosphorus in sewage sludge incineration ash. *Process Safety and Environmental Protection*, *191*, 2513-2521.

84. Júnior, P. W. P. M., de Souza Miranda, F., Prado, E. S. A. P., Essiptchouk, A. M., Cruz, A. C., & Petraconi Filho, G. (2024). Dairy sludge characteristics and its degradation during thermal treatment and thermal plasma treatment. *Environmental Technology*, 1-17.

85. Pujiyanto, E., Widyo Laksono, P., & Triyono, J. (2014). Synthesis and characterization of hydroxyapetite powder from natural gypsum rock. *Advanced Materials Research*, *893*, 56-59.

86. Furuta, S., Katsuki, H., & Komarneni, S. (1998). Porous hydroxyapetite monoliths from gypsum waste. *Journal of Materials Chemistry*, *8*(12), 2803-2806.

87. Navarro, M., Michiardi, A., Castano, O., & Planell, J. A. (2008). Biomaterials in orthopaedics. *Journal of the royal society interface*, *5*(27), 1137-1158.

88. Farag, M. M. (2023). Recent trends on biomaterials for tissue regeneration applications. *Journal of Materials Science*, *58*(2), 527-558.

89. Ajmal, S., Hashmi, F. A., & Imran, I. (2022). Recent progress in development and applications of biomaterials. *Materials Today: Proceedings*, *62*,

385-391.

90. Woo, R. K., Jenkins, D. D., & Greco, R. S. (2004). Biomaterials: Historical overview and current directions. In *Nanoscale Technology in Biological Systems* (pp. 21-44).CRC Press.

91. Bezzi, G., Celotti, G., Landi, E., La Torretta, T. M. G., Sopyan, I., & Tampieri, A. (2003). A novel sol–gel technique for hydroxyapetite preparation. *Materials Chemistry and Physics*, *78*(3), 816-824.

92. Aminzare, M., Eskandari, A., Baroonian, M. H., Berenov, A., Hesabi, Z. R., Taheri, M., & Sadrnezhaad, S. K. (2013). Hydroxyapetite nanocomposites: Synthesis, sintering and mechanical properties. *Ceramics International*, *39*(3), 2197-2206.

93. Ratha, I., Datta, P., Balla, V. K., Nandi, S. K., & Kundu, B. (2021). Effect of doping in hydroxyapetite as coating material on biomedical implants by plasma spraying method: A review. *Ceramics International*, *47*(4), 4426-4445.

94. Li, H., Khor, K. A., Chow, V., & Cheang, P. (2007). Nanostructural characteristics, mechanical properties, and osteoblast response of spark plasma sintered hydroxyapetite. *Journal of Biomedical Materials Research Part A: An Official Journal of The Society for Biomaterials, The Japanese Society for Biomaterials, and The Australian Society for Biomaterials and the Korean Society for Biomaterials*, *82*(2), 296-303.

95. Xihua, Z., Changxia, L., Musen, L., Yunqiang, B., & Junlong, S. (2009). Fabrication of hydroxyapetite/diopside/alumina composites by hot-press sintering process. *Ceramics International*, *35*(5), 1969-1973.

96. Nosrati, H., Mamoory, R. S., Le, D. Q. S., & Bünger, C. E. (2020). Fabrication of gelatin/hydroxyapetite/3D-graphene scaffolds by a hydrogel 3D-printing method. *Materials Chemistry and Physics*, *239*, 122305.

97. Mysore, T. H. M., Patil, A. Y., Hegde, C., Sudeept, M. A., Kumar, R., Soudagar,
M. E. M., & Fattah, I. M. R. (2024). Apatite insights: From synthesis to biomedical applications. *European Polymer Journal*, 112842.

98. Sivaperumal, V. R., Mani, R., Nachiappan, M. S., & Arumugam, K. (2017). Direct hydrothermal synthesis of hydroxyapetite/alumina nanocomposite. *Materials characterization*, *134*, 416-421.

99. Cannillo, V., Lusvarghi, L., & Sola, A. (2008). Production and characterization of plasma-sprayed TiO2–hydroxyapetite functionally graded

coatings. *Journal of the European Ceramic Society*, *28*(11), 2161-2169.

100. Sivaperumal, V. R., Mani, R., Polisetti, V., Aruchamy, K., & Oh, T. (2022). Synthesis of hydroxyapetite (HAp)-zirconia nanocomposite powder and evaluation of its biocompatibility: An in vitro study. *Applied Sciences*, *12*(21), 11056.

101. Taherian, M., Rojaee, R., Fathi, M., & Tamizifar, M. (2014). Effect of different sol-gel synthesis processes on microstructural and morphological characteristics of hydroxyapetite-bioactive glass composite nanopowders. *Journal of Advanced Ceramics*, *3*, 207-214.

102. Subramaniyan, M., Karuppan, S., Helaili, S., & Ahmad, I. (2024). Structural, mechanical, and in-vitro characterization of hydroxyapetite loaded PLA composites. *Journal of Molecular Structure*, *1306*, 137862.

103. Ningrum, E. O., Pratiwi, E. L., Shaffitri, I. L., Putra, A. F. P., Karisma, A. D., & Suprapto, S. (2022). Production of bone implant filaments from blue crab shells (Portunus pelagicus) in various synthesis conditions and blending ratios of hydroxyapetite (HAp)-polycaprolactone (PCL). In *IOP Conference Series: Earth and Environmental Science* (Vol. 963, No. 1, p. 012021). IOP Publishing.

104. Zhou, D., Qi, C., Chen, Y. X., Zhu, Y. J., Sun, T. W., Chen, F., & Zhang, C. Q.
(2017). Comparative study of porous hydroxyapetite/chitosan and whitlockite/chitosan scaffolds for bone regeneration in calvarial defects. *International journal of nanomedicine*, 2673-2687..

105. Zahid, A. (2009). *Synthesis and comparative study of HAP/SS316L Functinally Graded material used in Biomedical Implants* (Doctoral dissertation, Ghulam Ishaq Khan Institute of Engineering Sciences and Technology).

106. Khanra, A. K., Jung, H. C., Yu, S. H., Hong, K. S., & Shin, K. S. (2010).
Microstructure and mechanical properties of Mg-HAP composites. *Bulletin of Materials Science*, *33*, 43-47.

107. Kaviya, M., Ramakrishnan, P., Mohamed, S. B., Ramakrishnan, R., Gimbun, J., Veerabadran, K. M., ...& Sridhar, T. M. (2021). Synthesis and characterization of nano-hydroxyapetite/graphene oxide composite materials for medical implant coating applications. *Materials Today: Proceedings*, *36*, 204-207.

108. Farokhi, M., Mottaghitalab, F., Samani, S., Shokrgozar, M. A., Kundu, S. C., Reis, R. L., ...& Kaplan, D. L. (2018). Silk fibroin/hydroxyapetite composites for bone tissue engineering. *Biotechnology advances*, *36*(1), 68-91.

109. Mukherjee, S., Kundu, B., Chanda, A., & Sen, S. (2015). Effect of functionalisation of CNT in the preparation of HAp–CNT biocomposites. *Ceramics international*, *41*(3), 3766-3774.

110. Ng, K. H., & Abdullah, H. Z. (2015). Preliminary Studies of the Effects of Polyethylene Glycol/Hydroxyapetite Powder-Binder System for 3D Printing Application. *Advanced Materials Research*, *1087*, 345-349.

111. Tajitsu, Y., Fukuda, K., & Takaki, T. (2008, July). High Ionic Conductivity of Transparent Film of Hydroxyapetite and Poly (vinyl alcohol) Nanocomposite.In *Macromolecular symposia* (Vol. 268, No. 1, pp. 14-18). Weinheim: WILEY-VCH Verlag.

112. Tajitsu, Y., Fukuda, K., & Takaki, T. (2008, July). High Ionic Conductivity of Transparent Film of Hydroxyapetite and Poly (vinyl alcohol) Nanocomposite.In *Macromolecular symposia* (Vol. 268, No. 1, pp. 14-18). Weinheim: WILEY-VCH Verlag.

113. Davis, K. (2010). Material Review: Alumina (Al 2 O 3). *School of Doctoral Studies European Union Journal*, (2).

114. Hassanpour, P., Panahi, Y., Ebrahimi-Kalan, A., Akbarzadeh, A., Davaran, S., Nasibova, A. N. & Kavetskyy, T. (2018). Biomedical applications of aluminium oxide nanoparticles. *Micro & Nano Letters*, *13*(9), 1227-1231.

115. Shirai, T., Watanabe, H., Fuji, M., & Takahashi, M. (2010). *Structural properties and surface characteristics on aluminum oxide powders* (Doctoral dissertation, Nagoya Institute of Technology).

116. Kalmodia, S., Goenka, S., Laha, T., Lahiri, D., Basu, B., & Balani, K. (2010). Microstructure, mechanical properties, and in vitro biocompatibility of spark plasma sintered hydroxyapetite–aluminum oxide–carbon nanotube composite. *Materials Science and Engineering: C*, *30*(8), 1162-1169.

117. Kalmodia, S., Goenka, S., Laha, T., Lahiri, D., Basu, B., & Balani, K. (2010). Microstructure, mechanical properties, and in vitro biocompatibility of spark plasma sintered hydroxyapetite–aluminum oxide–carbon nanotube composite. *Materials Science and Engineering: C*, *30*(8), 1162-1169.

118. Saber-Samandari, S., Yekta, H., Ahmadi, S., & Alamara, K. (2018). The role of titanium dioxide on the morphology, microstructure, and bioactivity of grafted cellulose/hydroxyapetite nanocomposites for a potential application in bone repair. *International journal of biological macromolecules*, *106*, 481-488.

119. Racovita, A. D. (2022). Titanium dioxide: structure, impact, and

toxicity. *International journal of environmental research and public health*, *19*(9), 5681.

120. Saber-Samandari, S., Yekta, H., Ahmadi, S., & Alamara, K. (2018). The role of titanium dioxide on the morphology, microstructure, and bioactivity of grafted cellulose/hydroxyapetite nanocomposites for a potential application in bone repair. *International journal of biological macromolecules*, *106*, 481-488.

121. Chung, J. H., Kim, Y. K., Kim, K. H., Kwon, T. Y., Vaezmomeni, S. Z., Samiei, M., ... & Akbarzadeh, A. (2016). Synthesis, characterization, biocompatibility of hydroxyapetite–natural polymers nanocomposites for dentistry applications. *Artificial cells, nanomedicine, and biotechnology*, *44*(1), 277-284.

122. Fox, K., Tran, P. A., & Tran, N. (2012). Recent advances in research applications of nanophase hydroxyapetite. *ChemPhysChem*, *13*(10), 2495-2506.

123. Kolmas, J., Krukowski, S., Laskus, A., & Jurkitewicz, M. (2016). Synthetic hydroxyapetite in pharmaceutical applications. *Ceramics International*, *42*(2), 2472-2487.

124. Mahmoodi, M., Hashemi, P. M., & Imani, R. (2015). Fabrication of TiO2-Al2O3-HA Nanobiocomposite by Sintering and Evalution of in Vitro Bioactivity and Cell Toxicity for Orthopedic Applications.

125. Dong, H., Liu, H., Zhou, N., Li, Q., Yang, G., Chen, L., & Mou, Y. (2020).
Surface modified techniques and emerging functional coating of dental implants. *Coatings*, *10*(11), 1012.

126. Navarro, M., & Planell, J. A. (2010). Bioactive composites based on calcium phosphates for bone regeneration. *Key Engineering Materials*, *441*, 203-233.

127. Teixeira, J. M. D. C., Alburquerque, J. S. V., Duarte, E. B., Silva, S. A., & Nogueira, R. E. F. Q. (2019). In vitro drug release study from hydroxyapetite-alumina composites. *Journal of Sol-Gel Science and Technology*, *89*, 521-530.

128. Saldanha, R. B., Scheuermann Filho, H. C., Mallmann, J. E. C., Consoli, N. C., & Reddy, K. R. (2018). Physical–mineralogical–chemical characterization of carbide lime: An environment-friendly chemical additive for soil stabilization. *Journal of Materials in Civil Engineering*, *30*(6), 06018004.

129. Chukwudebelu, J. A., Igwe, C. C., Taiwo, O. E., & Tojola, O. B. (2013). Recovery of pure slaked lime from carbide sludge: Case study of Lagos state, Nigeria. *African Journal of Environmental Science and Technology*, *7*(6), 490-496.

130. Tang, P., Javadi, A. A., & Vinai, R. (2024). Sustainable utilisation of calcium- rich industrial wastes in soil stabilisation: Potential use of calcium carbide residue. *Journal of Environmental Management*, *357*, 120800.

131. Cahyaningrum, S. E., Herdyastuty, N., Devina, B., & Supangat, D. (2018, January). Synthesis and characterization of hydroxyapetite powder by wet precipitation method. In *IOP Conference Series: Materials Science and Engineering* (Vol. 299, p. 012039). IOP Publishing.

132. Shaltout, A. A., Allam, M. A., & Moharram, M. A. (2011). FTIR spectroscopic, thermal and XRD characterization of hydroxyapetite from new natural sources. *Spectrochimica Acta Part A: Molecular and Biomolecular Spectroscopy*, *83*(1), 56-60.

133. Epp, J. (2016). X-ray diffraction (XRD) techniques for materials characterization.In *Materials characterization using nondestructive evaluation (NDE) methods* (pp. 81-124). Woodhead Publishing.

134. Magalhães, S., Goodfellow, B. J., & Nunes, A. (2021). FTIR spectroscopy in biomedical research: How to get the most out of its potential. *Applied Spectroscopy Reviews*, *56*(8-10), 869-907.

135. Alyamani, A. M. O. L., & Lemine, O. M. (2012). FE-SEM characterization of some nanomaterial. In *Scanning electron microscopy*. IntechOpen.

136. Abd Mutalib, M., Rahman, M. A., Othman, M. H. D., Ismail, A. F., & Jaafar, J. (2017).Scanning electron microscopy (SEM) and energy-dispersive X-ray (EDX) spectroscopy.In *Membrane characterization* (pp. 161-179).Elsevier.

137. Saadatkhah, N., Carillo Garcia, A., Ackermann, S., Leclerc, P., Latifi, M., Samih, S., ...& Chaouki, J. (2020). Experimental methods in chemical engineering: Thermogravimetric analysis—TGA. *The Canadian Journal of Chemical Engineering*, *98*(1), 34-43.

138. Bhattacharjee, S. (2016). DLS and zeta potential–what they are and what they are not?. *Journal of controlled release*, *235*, 337-351.

139. Muralithran, G., & Ramesh, S. J. C. I. (2000). The effects of sintering temperature on the properties of hydroxyapetite. *Ceramics International*, *26*(2), 221-230.

140. Safronova, T. V., Putlyaev, V. I., Shekhirev, M. A., Tretyakov, Y., Kuznetsov, A. V., & Belyakov, A. V. (2009). Densification additives for hydroxyapetite ceramics. *Journal of the European Ceramic Society*, *29*(10), 1925-1932.

141. Kacker, R. N., Lagergren, E. S., & Filliben, J. J. (1991). Taguchi's orthogonal arrays are classical designs of experiments. *Journal of research of the National Institute of Standards and Technology*, *96*(5), 577.

142. Ilyas, S., Ru'an, C. H. I., Lee, J. C., & Bhatti, H. N. (2012). One step bioleaching of sulphide ore with low concentration of arsenic by Aspergillus niger and Taguchi orthogonal array optimization. *Chinese Journal of Chemical Engineering*, *20*(5), 923- 929.

143. Kim, J. H., Yanagisawa, K., Onda, A., Sasabe, E., & Yamamoto, T. (2015). Densification behavior of hydroxyapetite green pellets prepared by different methods. *Journal of the Ceramic Society of Japan*, *123*(1444), 1097-1101.

144. Somani, V. (2006). Alumina-aluminum Titanate-titania Nanocomposite: Synthesis, Sintering Studies, Assessment Of Bioactivity And Its Mechanical And Electrical Properties.

145. Pires, I., Gouveia, B., Rodrigues, J., & Fonte, R. (2014).Characterization of sintered hydroxyapetite samples produced by 3D printing. *Rapid Prototyping Journal*, *20*(5), 413-421.

146. Gunawan, G., Arifin, A., Yani, I., & Indrajaya, M. (2019, September). Characterization of porous hydroxyapetite-alumina composite scaffold produced via powder compaction method. In *IOP Conference Series: Materials Science and Engineering* (Vol. 620, No. 1, p. 012107). IOP Publishing.

147. Karna, S. K., & Sahai, R. (2012). An overview on Taguchi method. *International journal of engineering and mathematical sciences*, *1*(1), 1-7.

148. Chen, W. H., Uribe, M. C., Kwon, E. E., Lin, K. Y. A., Park, Y. K., Ding, L., & saw, L. H. (2022). A comprehensive review of thermoelectric generation optimization by statistical approach: Taguchi method, analysis of variance (ANOVA), and response surface methodology (RSM). *Renewable and Sustainable Energy Reviews*, *169*, 112917.

149. Shaltout, A. A., Allam, M. A., & Moharram, M. A. (2011). FTIR spectroscopic, thermal and XRD characterization of hydroxyapetite from new natural sources. *Spectrochimica Acta Part A: Molecular and Biomolecular Spectroscopy*, *83*(1), 56-60.

150. Epp, J. (2016). X-ray diffraction (XRD) techniques for materials characterization.In *Materials characterization using nondestructive evaluation (NDE) methods* (pp. 81-124). Woodhead Publishing.

151. Berthomieu, C., & Hienerwadel, R. (2009). Fourier transform infrared

(FTIR) spectroscopy. *Photosynthesis research*, *101*, 157-170.

152. Deng, H., Hu, X., Li, H. A., Luo, B., & Wang, W. (2016).Improved pore-structure characterization in shale formations with FESEM technique. *Journal of Natural Gas Science and Engineering*, *35*, 309-319.

153. Liu, D. M. (1997). Influence of porosity and pore size on the compressive strength of porous hydroxyapetite ceramic. *Ceramics International*, *23*(2), 135-139.

154. Huerta, E., Corona, J. E., Oliva, A. I., Avilés, F., & González-Hernández, J. (2010). Universal testing machine for mechanical properties of thin materials. *Revista mexicana de física*, *56*(4), 317-322.

155. Yamamura, Hirochi, et al. "Physico-chemical characterization and biocompatibility of hydroxyapetite derived from fish waste." *Journal of the Mechanical Behavior of Biomedical Materials* 80 (2018): 137-142.

156. Fathi, M. H., Hanifi, A., & Mortazavi, V. (2008). Preparation and bioactivity evaluation of bone-like hydroxyapetite nanopowder. *Journal of materials processing technology*, *202*(1-3), 536-542.

157. Malash, A. E., Al-Esnawy, A. A., Ereiba, K. T., Bakr, A. M., & Abdraboh, A. S. (2025). An In Vitro Study of the Effects of Methotrexate Loaded Biocomposite Beads on MG63 Osteoblast Cells. *Scientific Reports*, *15*(1), 2231.

158. Zhong, Q., Li, W., Su, X., Li, G., Zhou, Y., Kundu, S. C., ...& Cai, Y. (2016).
Degradation pattern of porous CaCO3 and hydroxyapetite microspheres in vitro and in vivo for potential application in bone tissue engineering. *Colloids and Surfaces B: Biointerfaces*, *143*, 56-63.

159. Cardoso, F. A., Fernandes, H. C., Pileggi, R. G., Cincotto, M. A., & John, V. M. (2009). Carbide lime and industrial hydrated lime characterization. *Powder Technology*, *195*(2), 143-149.

160. Saldanha, R. B., Scheuermann Filho, H. C., Mallmann, J. E. C., Consoli, N. C., & Reddy, K. R. (2018). Physical–mineralogical–chemical characterization of carbide lime: An environment-friendly chemical additive for soil stabilization. *Journal of Materials in Civil Engineering*, *30*(6), 06018004.

161. Subramaniam, K., Munusamy, S., Pua, F. L., Nasir, M. A. M., Othman, R., & Jaafar, S. N. S. (2018). Utilization of carbide lime waste as base catalyst for biodiesel production. *International Journal of Engineering & Technology*, *7*(4.35), 700-704.

162. Hua, L. H., Pua, F. L., Othman, R., Hin, T. Y. Y., & Nabihah, S.

(2021).Synthesis of Carbide Lime Derived Strong Base Catalyst for Biodiesel Production. *Solid State Phenomena*, *317*, 251-256.

163. Ilić, T., Elert, K., Ruiz-Agudo, E., & Rodriguez-Navarro, C. (2024, April). Potential Use of Carbide Lime Waste in Construction: A Comprehensive Analysis. In *RILEM Spring Convention and Conference* (pp. 35-43). Cham: Springer Nature Switzerland.

164. Dueramae, S., Tangchirapat, W., & Jaturapitakkul, C. (2018). Strength and heat generation of concrete using carbide lime and fly ash as a new cementitious material without Portland cement. *Advanced Powder Technology*, *29*(3), 672-681.

165. Delhomme, F., Prud'Homme, E., Julliot, C., Guillot, T., Amziane, S., & Marceau, S. (2022). Effect of hemp on cement hydration: Experimental characterization of the interfacial transition zone. *Results in Chemistry*, *4*, 100440.

166. Nurfiana, F., Kadarwati, A., & Putra, S. (2020). Synthesis and characterization of hydroxyapetite from duck eggshell modified silver by gamma radiolysis method. In *Journal of Physics: Conference Series* (Vol. 1436, No. 1, p. 012099). IOP Publishing.

167. Heakal, F. E. T., Sarhan, Y. B., Maamoun, M. A., Bakry, A. M., Abdel-Monem,
Y. K., & Ghayad, I. M. (2021). Hydrothermal microwave-assisted fabrication of nanohydroxyapetite powder and optimization of its nanocomposite coatings on magnesium alloy for orthopedic applications. *ACS omega*, *7*(1), 1021-1034.

168. Kaur, N., Kumar, R., Kesari, K. K., Gupta, P. K., & Singh, A. (2025). Synthesis and characterization of nano-hydroxyapetite from carbide lime waste through a green conversion approach. *Nano-Structures & Nano-Objects*, *41*, 101433.

169. Jeyakumar, S. J., Sindhya, A., Jothibas, M., Pugalendhi, P., & Sathiyamoorthy,
K. (2023). Preparation and analysis of pure and surface modified nanohydroxyapetite derived from eggshells and its in-vitro studies for bone graft applications. *Ceramics International*, *49*(11), 18708-18727.

170. Bandyopadhyay, A., Mitra, I., Goodman, S. B., Kumar, M., & Bose, S. (2023). Improving biocompatibility for next generation of metallic implants. *Progress in materials science*, *133*, 101053.

171. Niu, S., Liu, M., Lu, C., Li, H., & Huo, M. (2014). Thermogravimetric analysis of carbide slag: A potential transesterification catalyst validation. *Journal of Thermal Analysis and Calorimetry*, *115*, 73-79.

172. Moharram, M. A., & Allam, M. A. (2007). Study of the interaction of poly

(acrylic acid) and poly (acrylic acid-poly acrylamide) complex with bone powders and hydroxyapetite by using TGA and DSC. *Journal of applied polymer science*, *105*(6), 3220-3227.

173. de Bruyn, J. R., Goiko, M., Mozaffari, M., Bator, D., Dauphinee, R. L., Liao, Y.,...& Goldberg, H. A. (2013). Dynamic light scattering study of inhibition of nucleation and growth of hydroxyapetite crystals by osteopontin. *PLoS One*, *8*(2), e56764.

174. Mostafa, N. Y. (2005). Characterization, thermal stability and sintering of hydroxyapetite powders prepared by different routes. *Materials chemistry and physics*, *94*(2-3), 333-341.

175. Singh, N. E. E. R. A. (2014). *Synthesis, sintering and characterization of Al2O3-13 wt.% TiO2 composite powder prepared by polymer assisted co-precipitation route* (Doctoral dissertation).

176. Ebrahimi, M., Mobasherpour, I., Bafrooei, H. B., Bidabadi, F. S., Mansoorianfar, M., Orooji, Y., ...& Ebadzadeh, T. (2019). Taguchi design for optimization of structural and mechanical properties of hydroxyapetite-alumina-titanium nanocomposite. *Ceramics International*, *45*(8), 10097-10105.

177. Islam, M. N., & Pramanik, A. (2016). Comparison of design of experiments via traditional and Taguchi method. *Journal of Advanced Manufacturing Systems*, *15*(03), 151-160.

178. Aksoğan Korkmaz, Aydan, and Yeliz Toptaş. "Implementation of Taguchi method, ANOVA and regression analyses to enhance char yield by carbonization in lignite-biomass blended." *International Journal of Coal Preparation and Utilization* 45.2 (2025): 264-280.

179. Kumanan, S., Dhas, J., & Gowthaman, K. (2007). Determination of submerged arc welding process parameters using Taguchi method and regression analysis.

180. Adamu, M. A., Sumaila, M., Dauda, M., & Ause, T. (2023). Production and optimization of novel rice husk ash reinforced polycaprolactone/hydroxyapetite composite for bone regeneration using grey relational analysis. *Scientific African*, *19*, e01563.

181. Kim, K., Dean, D., Lu, A., Mikos, A. G., & Fisher, J. P. (2011). Early osteogenic signal expression of rat bone marrow stromal cells is influenced by both hydroxyapetite nanoparticle content and initial cell seeding density in biodegradable nanocomposite scaffolds. *Acta biomaterialia*, *7*(3), 1249-1264.

182. Deligianni, D. D., Katsala, N. D., Koutsoukos, P. G., & Missirlis, Y. F.

(2000). Effect of surface roughness of hydroxyapetite on human bone marrow cell adhesion, proliferation, differentiation and detachment strength. *Biomaterials*, *22*(1), 87-96.

183. Mourabet, M., El Rhilassi, A., El Boujaady, H., Bennani-Ziatni, M. R. E. I., El Hamri, R., & Taitai, A. (2015). Removal of fluoride from aqueous solution by adsorption on hydroxyapetite (HAp) using response surface methodology. *Journal of Saudi Chemical Society*, *19*(6), 603-615.

184. Osuchukwu, O. A., Salihi, A., Abdullahi, I., & Obada, D. O. (2022). Taguchi grey relational optimization of sol–gel derived hydroxyapetite from a novel mix of two natural biowastes for biomedical applications. *Scientific Reports*, *12*(1), 17968.

185. Ahmed, M. A., Abbas, M., & Ibrahim, M. (2021, August). Preparation and characterization of hydroxyapetite and optimizing its properties using regression model. In *Journal of Physics: Conference Series* (Vol. 1973, No. 1, p. 012141). IOP Publishing.

186. Cordell, J. M., Vogl, M. L., & Johnson, A. J. W. (2009). The influence of micropore size on the mechanical properties of bulk hydroxyapetite and hydroxyapetite scaffolds. *Journal of the mechanical behavior of biomedical materials*, *2*(5), 560-570.

187. Hing, K. A., Best, S. M., & Bonfield, W. (1999). Characterization of porous hydroxyapetite. *Journal of Materials Science: Materials in Medicine*, *10*(3), 135-145.

188. Nosrati, H., Sarraf-Mamoory, R., Le, D. Q. S., & Bünger, C. E. (2020). Enhanced fracture toughness of three dimensional graphene-hydroxyapetite nanocomposites by employing the Taguchi method. *Composites Part B: Engineering*, *190*, 107928.

189. Abifarin, J. K. (2021). Taguchi grey relational analysis on the mechanical properties of natural hydroxyapetite: effect of sintering parameters. *The International Journal of Advanced Manufacturing Technology*, *117*(1), 49-57.

190. Iji, J. O., Ibrahim, F. B., Argungu, A. S., & Obada, D. O. (2023). Development and optimization of hydroxyapetite/kaolin-based ceramic materials as potential adsorbents for water purification. *Environmental Advances*, *13*, 100419.

191. Sharma, N., Kumar, K., Raj, T., & Kumar, V. (2019). Porosity exploration of SMA by Taguchi, regression analysis and genetic programming. *Journal of Intelligent Manufacturing*, *30*(1), 139-146.

192. Hosseinzadeh, F., & Sarpoolaky, H. (2019). Optimization of mesoporous alumina sol-gel synthesis by Taguchi and response surface methodology. *International Journal of Applied Ceramic Technology*, *16*(4), 1544-1556.

193. Thakur, S. P., & Hambire, U. V. Effect of Hydroxyapetite Nanoparticles On Compressive strength and Flexural strength of Dental Composites Using Taguchi Method.

194. Prasetiyo, A. B., Sekarjati, K. A., & Tontowi, A. E. (2021). Application Of Rsm Method In Bio-composite Materials (polymethyl-methacrylatehydroxyapetite) Tension Strength Optimization By 3d Printing Machine Process. *JEMMME (Journal of Energy, Mechanical, Material, and Manufacturing Engineering)*, *6*(2), 119-126.

195. Nugraha, F. K. A., & Tontowi, A. E. (2016, June). Shrinkage of [HA/Bioplastic/Sericin] composite part printed by bioprinter.In *AIP Conference Proceedings* (Vol. 1746, No. 1).AIP Publishing.

196. Zhang, S., Miyanaji, H., Yang, L., Zandinejad, A. A., Dilip, J. J. S., & Stucker,B. (2014). An experimental study of ceramic dental porcelain materials using a 3D print (3DP) process.

197. Somani, V. (2006). Alumina-aluminum Titanate-titania Nanocomposite: Synthesis, Sintering Studies, Assessment Of Bioactivity And Its Mechanical And Electrical Properties.

198. Yates, K. (2024). *A Generalized Process Road-Map for Additive Manufacturing Ceramics Utilizing Stereolithographic Methods via Preceramic Polymers*.University of Louisiana at Lafayette.

199. Jailani, N. A. (2015). *Structure Characterization and Surface Morphology of Low Sintering Temperature Synthesized Calcium Titanate Ceramics* (Doctoral dissertation, Universiti Teknologi Malaysia).

200. Khalid, M. (2023). *Polylactic Acid/Polyhydroxyalkanoate/Eggshell Based Hydroxyapetite Biocomposites for Bone Tissue Applications* (Doctoral dissertation, Universiti Tun Hussein Onn (Malaysia)).

201. Arab, M., Behboodi, P., Khachatourian, A. M., & Nemati, A. (2024). Enhanced mechanical properties and biocompatibility of hydroxyapetite scaffolds by magnesium and titanium oxides for bone tissue applications. *Heliyon*, *10*(13).

202. Roudan, M. A. (2018). *Synthesis of Eggshell-Derived Hydroxyapetite and its Deposition on Titanium by Electrophoretic Method* (Doctoral dissertation, University of Malaya (Malaysia)).

203. Cordell, J. M., Vogl, M. L., & Johnson, A. J. W. (2009). The influence of

micropore size on the mechanical properties of bulk hydroxyapetite and hydroxyapetite scaffolds. *Journal of the mechanical behavior of biomedical materials*, *2*(5), 560-570.

204. Cui, X., Liang, T., Liu, C., Yuan, Y., & Qian, J. (2016). Correlation of particle properties with cytotoxicity and cellular uptake of hydroxyapetite nanoparticles in human gastric cancer cells. *Materials Science and Engineering: C*, *67*, 453-460.

205. Mavropoulos, E., Costa, A. M., Costa, L. T., Achete, C. A., Mello, A., Granjeiro,J. M., & Rossi, A. M. (2011). Adsorption and bioactivity studies of albumin onto hydroxyapetite surface. *Colloids and Surfaces B: Biointerfaces*, *83*(1), 1-9.

206. Demirtaş, T. T., Kaynak, G., & Gümüşderelioğlu, M. (2015). Bone-like hdroxyapatite precipitated from 10× SBF-like solution by microwave irradiation. *Materials Science and Engineering: C*, *49*, 713-719.

207. Barrère, F., van Blitterswijk, C. A., de Groot, K., Rey, C., & Layrolle, P. (1973). Calcium Phosphate interactions with titanium oxide and Aluminium oxide: AN XPS STUDY. *Biomimetic Calcium Phosphate Coatings*, 73.

208. Mehta, D., George, S., & Mondal, P. (2014). Synthesis of hydroxyapetite by chemical precipitation technique and study of its biodegradability. *International Journal of Research in Advent Technology*, *2*(4), 159-161.

209. Sivaperumal, V. R., Mani, R., Polisetti, V., Aruchamy, K., & Oh, T. (2022). Synthesis of hydroxyapetite (HAp)-zirconia nanocomposite powder and evaluation of its biocompatibility: An in vitro study. *Applied Sciences*, *12*(21), 11056.

210. Sabarish, K. V., & Pratheeba, P. (2020). An experimental analysis on structural beam with Taguchi orthogonal array. *Materials Today: Proceedings*, *22*, 874-878.

211. Ke, Y., Chen, Y., Liang, S., Hu, J., Hou, H., Quan, J., ... & Yang, J. (2023). Environmentally sound management of industrial solid waste: A paradigm of proposed bi-tetrahedron. *Resources, Conservation and Recycling*, *198*, 107212.

212. 212)Ansari, T., Chandra, G., Gupta, P. K., Joshi, G., & Rana, V. (2023). Synthesis of pine needle cyanoethyl cellulose using Taguchi L25 orthogonal array. *Industrial Crops and Products*, *191*, 115973.

213. 213) Karthikeyan, G., Elatharasan, G., & Thulasi, S. (2025, March). Characterization and milling parameter study on ZrO2 particle reinforced with LM25 aluminium alloy by using L9 Taguchi orthogonal array method. In *AIP Conference Proceedings* (Vol. 3137, No. 1, p. 050009). AIP Publishing LLC.

214. 214) Özdemir, U., Özbay, B., Özbay, İ., & Veli, S. (2014). Application of Taguchi L32 orthogonal array design to optimize copper biosorption by using

Spaghnum moss. *Ecotoxicology and Environmental Safety*, *107*, 229-235.
215. 215) Zolgharnein, J., Asanjarani, N., & Shariatmanesh, T. (2013). Taguchi L16 orthogonal array optimization for Cd (II) removal using Carpinus betulus tree leaves: adsorption characterization. *International Biodeterioration & Biodegradation*, *85*, 66-77.

List of Publications

1) Patent Granted

Title: Novel chemical conversion of carbide lime and process thereof (Granted 2024)

INTELLECTUAL PROPERTY INDIA

क्रम सं/SL No :011191444

सत्यमेव जयते

पेटेंट कार्यालय,भारत सरकार
पेटेंट प्रमाण पत्र
(पेटेंट नियमावली का नियम 74)

The Patent Office, Government Of India
Patent Certificate
(Rule 74 of The Patents Rules)

पेटेंट सं. / Patent No. : 496291

आवेदन सं. / Application No. : 202211008782

फाइल करने की तारीख / Date of Filing : 19/02/2022

पेटेंटी / Patentee : Lovely Professional University

प्रमाणित किया जाता है कि पेटेंटी को, उपरोक्त आवेदन में यथाप्रकटित *NOVEL CHEMICAL CONVERSION OF CARBIDE LIME AND PROCESS THEREOF* नामक आविष्कार के लिए, पेटेंट अधिनियम, 1970 के उपबंधों के अनुसार आज तारीख फरवरी 2022 के उन्नीसवें दिन से बीस वर्ष की अवधि के लिए पेटेंट अनुदत्त किया गया है।

It is hereby certified that a patent has been granted to the patentee for an invention entitled *NOVEL CHEMICAL CONVERSION OF CARBIDE LIME AND PROCESS THEREOF* as disclosed in the above mentioned application for the term of 20 years from the 19th day of February 2022 in accordance with the provisions of the Patents Act,1970.

अनुदान की तारीख : 09/01/2024
Date of Grant :

पेटेंट नियंत्रक
Controller of Patents

टिप्पणी - इस पेटेंट के नवीकरण के लिए फीस, यदि इसे बनाए रखा जाना है, फरवरी 2024 के उन्नीसवें दिन को और उसके पश्चात प्रत्येक वर्ष में उसी दिन देय होगी।

Note. - The fees for renewal of this patent, if it is to be maintained, will fall / has fallen due on 19th day of February 2024 and on the same day in every year thereafter.

2) **Graphical Abstract (Copyright)**

Title: Utilization of carbide lime for the synthesis of hydroxyapetite and study of its biocompatibility

प्रमाणपत्र सं. / Certificate No.: LD-20250168807

INTELLECTUAL PROPERTY INDIA

प्रतिलिप्याधिकार कार्यालय, भारत सरकार | Copyright Office, Government Of India

प्रतिलिप्याधिकार प्रमाणपत्र I Copyright Certificate

प्रतिलिप्याधिकार नियम का नियम 70 I Rule 70 of The Copyright Rules

प्रतिलिप्याधिकार रजिस्टर से उद्धरण I Extracts from the Register of Copyrights

आवेदन सं. / Application No.: 41358/2024-CO/L दाखिल करने की तिथि/ Date of Filing: 26/12/2024

एतद्वारा यह प्रमाणित किया जाता है कि प्रतिलिप्याधिकार अधिनियम, 1957 के प्रावधानों के अनुसार, उपर्युक्त आवेदन में प्रकट किए गए "Utilization Of Carbide Lime For The Synthesis Of Hydroxyapetite And Study Of Its Biocompatibility" नामक कार्य के लिए प्रतिलिप्याधिकार प्रदान किया गया है।

This is to certify that a copyright has been registered for the work titled "Utilization Of Carbide Lime For The Synthesis Of Hydroxyapetite And Study Of Its Biocompatibility" as disclosed in the below mentioned application in accordance with the provisions of the Copyright Act,1957.

रचयिता / Authors:

सं. / SNO.	नाम / Name	पता / Address
1	Navneet Kaur	Lovely Professional University Jalandhar Delhi-Gt Road Phagwara Punjab-144411
2	Dr. Anjuvan Singh	Lovely Professional University Jalandhar Delhi-Gt Road Phagwara Punjab-144411

स्वामी / Owners:

सं. / SNO.	नाम / Name	पता / Address
1	Lovely Professional University	Lovely Professional University Jalandhar Delhi-Gt Road Phagwara Punjab-144411

प्रकाशक विवरण / Publisher Details:	N.A.
कार्य की भाषा / Language of the Work:	English
कार्य का विवरण / Description of the Work:	N.A.
(शर्तें / टिप्पणियाँ, यदि कोई हो) / (Conditions/ Remarks, if any):	N.A.

आर. ओ. सी. जारी होने की तिथि / Date of ROC: 22/07/2025

Registrar of Copyrights

Research paper Published

1) Kaur, Navneet, et al. "Synthesis and characterization of nano-hydroxyapetite from carbide lime waste through a green conversion approach." *Nano- Structures & Nano-Objects* 41 (2025): 101433.

Nano-Structures & Nano-Objects 41 (2025) 101433

Contents lists available at ScienceDirect

Nano-Structures & Nano-Objects

journal homepage: www.elsevier.com/locate/nanoso

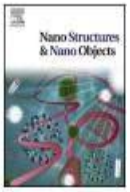

Synthesis and characterization of nano-hydroxyapatite from carbide lime waste through a green conversion approach

Navneet Kaur [a], Rohit Kumar [b], Kavindra Kumar Kesari [c,d], Piyush Kumar Gupta [b,e,*], Anjuvan Singh [a,**]

[a] Department of Biotechnology, School of Bioengineering and Biosciences, Lovely Professional University, Phagwara, Punjab 144001, India
[b] Centre for Development of Biomaterials & Department of Life Sciences, Sharda School of Basic Sciences and Research, Sharda University, Greater Noida, Uttar Pradesh 201310, India
[c] Department of Applied Physics, School of Science, Aalto University, Espoo 00076, Finland
[d] University Centre for Research and Development, Chandigarh University, Mohali, Punjab 140413, India
[e] Department of Biotechnology, Graphic Era (Deemed to be University), Dehradun, Uttarakhand 248002, India

ARTICLE INFO

Keywords:
Hydroxyapatite
Carbide lime
Acetylene gas
Biomaterial, Biocompatibility

ABSTRACT

Annually, a substantial quantity of industrial waste is generated globally, and the build-up of this waste poses a serious risk to society. The generation of carbide lime waste as a byproduct during acetylene gas production in industries has resulted in many environmental issues. This study attempts to convert carbide lime waste into nanohydroxyapatite (nHAp) that can be used to treat patients suffering from orthopaedic injuries. The synthesis of nHAp from carbide lime was carried out by chemical precipitation method using 85 % orthophosphoric acid. The resulting nHAp was physicochemically characterized by different instruments. Fourier Transform Infrared Spectroscopy (FTIR) was used to analyze the functional groups to confirm the conversion of carbide lime. The

2) Kaur, Navneet, Anjuvan Singh, and Swastik Pradhan. "Optimizing, Sintering and Mechanical Properties of Hydroxyapetite-Alumina-Tio2 Composites by Taguchi Method and its study of its biocompatibility." *Ceramics International* (2025).

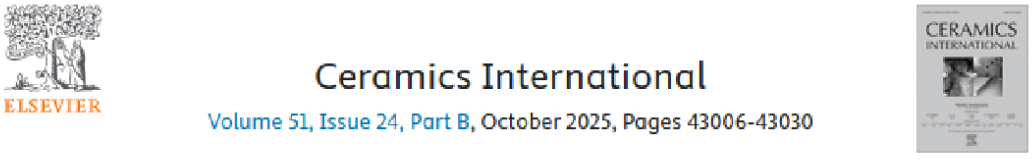

Ceramics International
Volume 51, Issue 24, Part B, October 2025, Pages 43006-43030

Optimizing, sintering and mechanical properties of hydroxyapetite-alumina-Tio_2 composites by Taguchi method and its study of its biocompatibility

Navneet Kaur [a], Anjuvan Singh [a], Swastik Pradhan [b]

Show more

+ Add to Mendeley Share Cite

https://doi.org/10.1016/j.ceramint.2025.07.045 Get rights and content

Conferences and workshops attended

1) Attended and participated in Poster Presentation on the topic entitled ―Utilization and characterization of carbide lime for the synthesis of slaked lime‖ in International Conference on Sustainability: Life on Earth 2021 (ICS- LOE 2021) held on 17-18 December 2021 organized by Department of Botany and Zoology, School of Bioengineering and Biosciences, and Institute of Forest Productivity, Ranchi, Jharkhand at Lovely Professional University, Punjab.

LOVELY PROFESSIONAL UNIVERSITY
Transforming Education Transforming India

INSTITUTE OF FOREST PRODUCTIVITY

Certificate No. 238874

Certificate of Participation

This is to certify that ***Prof./Dr./Mr./Ms. Navneet Kaur of Lovely Professional University*** *has participated in* ***Poster Presentation*** *on the topic entitled* ***Utilization and characterization of carbide lime for the synthesis of slaked lime*** *in International Conference on* ***Sustainability: Life on Earth 2021 (ICS-LOE 2021)*** *held on 17-18 December 2021 organized by Department of Botany and Zoology, School of Bio-engineering and Biosciences, and Institute of Forest Productivity, Ranchi, Jharkhand at Lovely Professional University, Punjab.*

Date of Issue: 18-02-2022
Place of Issue: Phagwara (India)

Prepared by
(Administrative Officer-Records)

Dr. Joydeep Dutta
Organizing Secretary, ICS-LOE, 2021

Dr. Neeta Raj Sharma
Convener, ICS-LOE, 2021

2) Attended and participated in oral presentation in 2 days DBT sponsored National Symposium on ―Next Generation Drug Delivery Systems (NGDDS- 2024) organized at Department of Life Science, Sharda School of Basic Science and Research, Sharda University, Greater Noida-201310, Uttar Pradesh, India from 26th to 27th December 2024.


SHARDA SCHOOL OF BASIC SCIENCES & RESEARCH

SHARDA UNIVERSITY

Certificate of Participation

The Symposium program certificate is proudly awarded to

Navneet Kaur , Lovely Professional University

for successful YSA/Oral/Poster presentation/participation in

02 Days DBT sponsored National Symposium on

"Next Generation Drug Delivery Systems (NGDDS) - 2024"

Organized at

Department of Life Sciences, Sharda School of Basic Sciences and Research

Sharda University, Greater Noida-201310, Uttar Pradesh, India

From 26th to 27th December 2024

Dr. Piyush Kumar Gupta

Dr. Ashwini Kumar

Dr. Santosh Kumar Mishra
HOD Life Sciences

Prof. Shyamal Kumar Banerjee
Dean, SSBSR

Prof. (Dr.) Sibaram Khara
Vice Chancellor

3) Attended and participated in Oral Presentation on the topic entitled ―Extraction of Precipitated Calcium Carbonate from industrial waste‖ in the International Conference on Bioengineering and Biosciences (ICBB-2022) held on 18-19 November 2022 organized by the Department of Biotechnology, School of Bioengineering and Biosciences in association with the Society of Bioinformatics for Experimenting Scientists (Bio clues) organized at Lovely Professional University, Punjab.

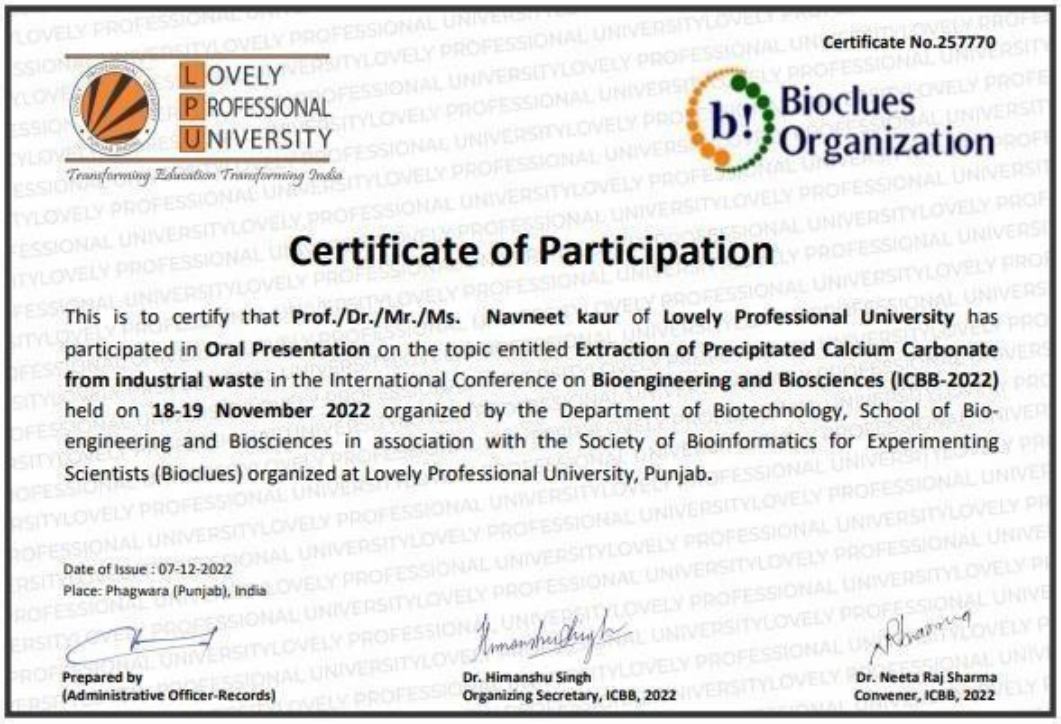

Certificate No.257770

LOVELY PROFESSIONAL UNIVERSITY

Transforming Education Transforming India

b! Bioclues Organization

Certificate of Participation

This is to certify that **Prof./Dr./Mr./Ms. Navneet kaur** of **Lovely Professional University** has participated in **Oral Presentation** on the topic entitled **Extraction of Precipitated Calcium Carbonate from industrial waste** in the International Conference on **Bioengineering and Biosciences (ICBB-2022)** held on **18-19 November 2022** organized by the Department of Biotechnology, School of Bioengineering and Biosciences in association with the Society of Bioinformatics for Experimenting Scientists (Bioclues) organized at Lovely Professional University, Punjab.

Date of Issue : 07-12-2022
Place: Phagwara (Punjab), India

Prepared by
(Administrative Officer-Records)

Dr. Himanshu Singh
Organizing Secretary, ICBB, 2022

Dr. Neeta Raj Sharma
Convener, ICBB, 2022

4) Attended and participated in oral presentation on the topic entitled ―Synthesis and Characterization of Calcium Oxide from Acetylene producing Industrial Waste‖ in the at International Conference on Recent Advances in Biotechnology (icRAB -2022) on 2nd-4th December 2022 organized by Dr. B R Ambedkar National Institute of Technology Jalandhar

EB20OP

Dr B R Ambedkar National Institute of Technology Jalandhar

CERTIFICATE OF PARTICIPATION

Is Presented to

Navneet Kaur

For Oral presentation on the title

"Synthesis and Characterization of Calcium Oxide from Acetylene producing Industrial Waste" with

Co-author/s: Anjuvan Singh

at International Conference on Recent Advances in Biotechnology (icRAB -2022)

on 2nd-4th December 2022

Dr. Sumer Singh Meena
(Conference Chair)

Dr. Nikhil G N
(Organizing Secretary)